Summer 9-15-2023

Halogen Oxidants Contribute to Organic Compound Degradation and Toxic Halogenated Byproduct Formation in Engineered Aquatic Systems

Moshan Chen
Washington University – McKelvey School of Engineering

WASHINGTON UNIVERSITY IN ST. LOUIS

McKelvey School of Engineering
Department of Energy, Environmental & Chemical Engineering

Dissertation Examination Committee:
Kimberly M. Parker, Chair
Jeffrey G. Catalano
Daniel E. Giammar
Young-Shin Jun
Elijah Thimsen

Halogen Oxidants Contribute to Organic Compound Degradation and Toxic Halogenated Byproduct Formation in Engineered Aquatic Systems

by
Moshan Chen

A dissertation presented to
the McKelvey School of Engineering
of Washington University in
partial fulfillment of the
requirements for the degree
of Doctor of Philosophy

August 2023
St. Louis, Missouri

Table of Contents

List of Figures

List of Tables

Acknowledgments

I would first like to sincerely thank my advisor Dr. Kimberly M. Parker for her guidance, patience, and encouragement throughout my doctoral study. Working with Dr. Parker has always been enjoyable and instructive. I appreciate Dr. Parker always pushing me to become a better scientist. I would like to thank Dr. Daniel E. Giammar, Dr. Young-Shin Jun, Dr. Elijah Thimsen, and Dr. Jeffrey G. Catalano for serving on my thesis committee and providing support throughout my doctoral study. I especially would like to thank Dr. Thimsen for teaching me how to work with plasma reactors in the last few years of my doctoral study.

I would like to thank Dr. Ke Zhang for being a very helpful senior student, who helped me a lot in my doctoral study. I would also like to thank current members Anamika Chatterjee, Jacqueline Rogers, Kun-Pu Ho, Anna Hartig, Jean Brownell, and former members Dr. Stephen Sharkey, Wentao Dai, Carter Rholl, Shane Persaud, and Tianchen He. I would like to thank collaborators from other labs, Zixuan Wang, Dillon Moher, Dr. Trey Oldham, Dr. Xiaoshaung Chen, Dr. Zhen He and Dr. Elijah Thimsen. I would also like to thank Dr. Shurik Yatom from Princeton Plasma Physics Laboratory for collaborating on some experiments.

This work was financially supported by Dr. Parker's funding from the International Center for Energy, Environment and Sustainability at Washington University in St. Louis, the U.S. Geological Survey (G16AP00066, Project 00069900), and National Science Foundation (ECO-CBET 2033714). The work with at Princeton Plasma Physics Laboratory was also supported by Princeton Collaborative Research Facility, which is supported by the U.S. Department of Energy (DOE) under Contract No. DE-AC02-09CH11466.

I would like to thank Dr. Daniel Giammar and Dr. Fuzhong Zhang for providing some chemicals, Dr. Yinjie Tang and Dr. Marcus Foston for access to some instruments.

Last, I would like to thank my parents, Yanhong Chen and Li Yang, for their unconditional love and support for my study in the U.S.

Moshan Chen

Washington University in St. Louis

August 2023

ABSTRACT OF THE DISSERTATION

Halogen Oxidants Contribute to Organic Compound Degradation and Toxic Halogenated Byproduct Formation in Engineered Aquatic Systems

by

Moshan Chen

Doctor of Philosophy in Energy, Environmental, and Chemical Engineering

Washington University in St. Louis, 2023

Professor Kimberly Parker, Chair

Organic contaminants are present in the aquatic environment and pose risks to human health. To address this concern, organic contaminants are degraded by oxidants in engineered aquatic systems. Halogen oxidants, including hypohalous acids and halogen radicals, are commonly used for the degradation of organic contaminants. However, one environmental concern associated with halogen oxidants is the formation of toxic halogenated byproducts. Thus, it is essential to develop effective strategies to degrade organic contaminants while mitigating the formation of halogenated byproducts. Consequently, this dissertation focused on evaluating the degradation kinetics and transformation mechanisms of organic compounds in three different engineered aquatic systems involving halogen oxidants.

The first objective examined how halogen oxidants (e.g., hypochlorous acid) led to the formation of halogenated byproducts in conventional drinking water treatment during harmful algal blooms. Specifically, multiple oxidation stages in drinking water treatment may impact the formation of halogenated byproducts from algal organic matter (AOM) that occurred at high concentrations during harmful algal blooms. I found that transformations of organic moieties in AOM through additional oxidation processes changed the potential for halogenated byproduct formation from the reactions between halogen oxidants and AOM. The potentially increased

formation of halogenated byproducts raises challenges for water treatment processes due to the escalating issue of harmful algal blooms on a global scale.

The second objective investigated the impacts of halogen oxidants on the mechanisms and kinetics of organic compound degradation in hydraulic fracturing fluids. Specifically, persulfate is commonly used to generate sulfate radicals to break down polymer-based gels during hydraulic fracturing processes. However, high concentrations of halides in hydraulic fracturing fluids may convert sulfate radicals to halogen oxidants (i.e., hypohalous acids, halogen radicals). I found that halogen radicals were the key intermediates that led to the halogenation and selective degradation of organic compounds in hydraulic fracturing fluids. In addition, while previous research primarily investigated the direct reactions between halogen radicals and organic compounds, I demonstrated that the recombination products of halogen radicals (i.e., hypohalous acids) are also important oxidants that lead to the formation of halogenated byproducts in hydraulic fracturing fluids. The unintentional formation of halogen oxidants must be considered in future hydraulic fracturing designs to minimize their adverse effect on target organic compound degradation and to mitigate halogenated byproduct formation.

The final objective evaluated how halogen oxidants contributed to organic compound degradation during brine treatment by plasma, a recently developed water treatment technology. Specifically, since hydroxyl radicals are the primary reactive species generated during plasma-based water treatment, halides in brines may convert hydroxyl radicals to halogen oxidants and thereby lead to selective degradation of organic compounds. I provided the first evidence that in contrast to the negligible effect of chloride, bromide that occurs at orders of magnitude lower concentrations significantly increased the formation of halogen oxidants during plasma treatment of brines. I also for the first time demonstrated that, via a radical-mediated pathway, halides led to the formation of hypohalous acids as the dominant oxidants during plasma treatment. The

formation of hypohalous acids altered the degradation kinetics of some organic compounds from pseudo-first order to zero order, distinguishing plasma reactors from conventional radical-based treatment processes. The dominant role of hypohalous acids suggests that halides may contribute to the formation of halogenated byproducts, which is important to consider when expanding the application of plasma-based water treatment to more complex brines.

Overall, this dissertation sheds light on the role of halogen oxidants in both conventional water treatment and emerging oxidative processes based on radicals. In conventional drinking water treatment, careful consideration of the oxidation of organic moieties is essential for effective strategies to control halogenated byproduct formation during harmful algal blooms. Moreover, in emerging oxidative treatment, it is important to acknowledge the role of hypohalous acids in assessing the degradation efficiency and halogenated byproduct formation when halides are present. These findings are necessary for future engineering designs to effectively degrade organic compounds while reducing the hazard posed by halogenated byproducts.

Chapter 1: Introduction

1.1 Background and motivation

Organic contaminants in the aquatic environment may pose risks to the ecosystem and human health. To alleviate the environmental risks posed by organic contaminants, we may degrade them through redox reactions. In engineered aquatic systems, conventional chemical oxidants (e.g., hypochlorous acid, monochloramine, ozone, permanganate) and reactive species (e.g., hydroxyl radicals (•OH), sulfate radicals ($SO_4^{\bullet-}$)) are often used to react with organic contaminants and decrease their concentrations. For example, in water treatment facilities, hypochlorous acid, monochloramine, and ozone can be used to reduce the concentrations of organic contaminants (e.g., pesticides,[1–3] pharmaceuticals).[1,4] In addition, both hydroxyl and $SO_4^{\bullet-}$ react with a wide range of organic contaminants with near-diffusion-limit rate constants[5,6] so that they have been employed in advanced oxidation processes (AOPs) during water treatment.

Among various oxidants, halogen oxidants (e.g., hypochlorous acid, halogen radicals) specifically raise concern because their reactions with organic contaminants potentially lead to the formation of toxic halogenated byproducts.[7,8] For example, in water treatment facilities, one major issue relevant to disinfection using hypochlorous acid is the formation of carcinogenic disinfection byproducts (DBPs, e.g., trihalomethanes, haloacetic acids, haloacetonitriles, nitrosamines) from the degradation of organic compounds.[9,10] Similarly, in other engineered aquatic systems involving halogen radicals, halogenated byproducts have raised particular concerns due to their toxicity.[8]

Consequently, to ensure the water quality in the aquatic environment, it is necessary to assess the formation of unwanted byproducts in the degradation of organic contaminants. Therefore, the overall objective of this dissertation is to investigate how halogen oxidants

contributed to the degradation kinetics and halogenation mechanisms of organic compounds in three specific engineered aquatic systems.

1.1.1 Conventional chemical oxidants in drinking water treatment

Chemical oxidants are added to degrade organic compounds that pose adverse effects on human health in drinking water facilities. In more than 70% of all community water systems and all surface water systems in the U.S, hypochlorous acid, monochloramine, chlorine dioxide and permanganate have been used as preoxidants in raw water.[11] In addition, in most water treatment facilities, hypochlorous acid, chloramine and ozone have been primarily used as disinfectants in post-disinfection.[11] As these chemicals may degrade organic contaminants, DBPs are often produced at levels that potentially cause risks in human health. For example, hypochlorous acid, the most commonly applied chemical oxidant,[12,13] often lead to the highest levels of halogenated disinfection byproducts such as trihalomethanes and haloacetic acids among all chemical oxidants in the treatment of freshwater,[14,15] wastewater,[16] and desalinated seawater[17]. To meet the regulatory standards of trihalomethanes and haloacetic acids by the U.S. Environmental Protection Agency (i.e., 80 μg/L and 60 μg/L, respectively),[18] ozone, monochloramine, and chlorine dioxide were considered as alternative oxidants to hypochlorous acid. However, previous literature reported that these alternative oxidants would likely lead to the formation of other DBPs (e.g., nitrosamine)[19–21] that were currently unregulated.

The formation of DBPs causes many challenges in the treatment of impaired water, including water impacted by harmful algal blooms (HABs). During HAB events, conventional oxidants such as permanganate and hypochlorous acid cause algal cells to lyse and release algal organic matter (AOM), which is a precursor for DBPs.[22–26] Moreover, because AOM is more abundant in nitrogen, one particular concern associated with HAB-impacted water is the formation

of unregulated nitrogenous DBPs (e.g., haloacetonitriles) that are more toxic than regulated trihalomethanes and haloacetic acids.[27] Consequently, the application of conventional chemical oxidants during drinking water treatment needs additional scrutiny during HAB events.

1.1.2 Radical-based AOPs used in engineered aquatic systems.

Radical-based treatments are often applied in engineered aquatic systems. In water treatment facilities, radicals are primarily generated by ultraviolet (UV) advanced oxidation processes (AOPs). In common UV AOPs, conventional chemical oxidants have also been added to improve the degradation efficiency of organic compounds. In these so-called UV-based AOPs, oxidants such as hydrogen peroxide and persulfate may undergo activation and generate $^{\bullet}OH$ and $SO_4^{\bullet-}$. Theses radicals have high oxidation-reduction potentials (e.g., 1.8-2.7 V for $^{\bullet}OH$,[5] 2.5-3.1 V for $SO_4^{\bullet-}$)[6] and react with most organic pollutants at near-diffusion-limited rate constants.[8,28] In prior reports, $^{\bullet}OH$ indiscriminately reacts with organic compounds (e.g., saturated aliphatic, olefinic, aromatic, and organosulfur compounds) at bimolecular rate constants near 10^{10} $M^{-1}s^{-1}$.[8] Also, $SO_4^{\bullet-}$ has been previously shown to react with a wide spectrum of organic compounds (e.g., aliphatic alcohols,[29] alkanes,[30] ethers,[30,31] aromatic compounds).[32,33]

In contrast to these non-selective reactive species (i.e., $^{\bullet}OH$, $SO_4^{\bullet-}$), halogen radicals (i.e., $Cl^{\bullet}$, $Br^{\bullet}$, $Cl_2^{\bullet-}$, $BrCl^{\bullet-}$, $Br_2^{\bullet-}$), except for chlorine radical, are more selective oxidants.[8] In engineered aquatic systems such as water treatment facilities, selective halogen radicals may be generated directly by the photolysis of hypochlorous acid or monochloramine or converted from primary radicals (e.g., $^{\bullet}OH$ and $SO_4^{\bullet-}$) by halides (e.g., in seawater).[8] Halogen radicals are selective because they react with certain organic compounds (e.g., alkenes, aromatics, organothiols) with high rate constants (i.e., $k = 10^6$-10^{10} $M^{-1}s^{-1}$) and react with other organic compounds (e.g., aliphatic molecules) with much lower rate constants (i.e., $k = 10^3$-10^6 $M^{-1}s^{-1}$).[8] In addition, the conversion

of radicals and other reactive species to halogen radicals in sunlit seawater has also been shown to accelerate the transformations of certain pollutants and biogeochemically relevant compounds (e.g., algal toxins,[34,35] organosulfur biomolecules,[35,36] chromophoric moieties in organic matter).[37–40] In addition to altering reaction rates, halogen radicals also alter reaction mechanisms by enabling halogenation both directly and indirectly. Directly, halogen radicals add to the structure of certain aromatic[41] and olefinic molecules.[41,42] Indirectly, halogen radicals react via termination reactions to generate other halogenating agents (i.e., hypohalous acids),[43–49] which react with organics through substitution[50–52] or addition.[50]

Although reactions between halogen radicals and organic compounds have been widely studied in seawater or brines, they have not yet been investigated more broadly in other saline engineered aquatic systems, for example, hydraulic fracturing fluid. Recent studies have demonstrated that one particular concern of hydraulic fracturing fluid is the formation of halogenated products. As a radical-based process (i.e., breaker persulfate generates $SO_4^{\bullet-}$) is involved in the hydraulic fracturing operation,[53,54] halogen radicals may be involved in the mechanism of generating halogenated products. Consequently, understanding the role of halogen radicals may help future hydraulic fracturing designs to reduce the levels of halogenated products.

1.1.3 Plasma-based water treatment

Plasma has the potential to improve water treatment systems. Plasma in liquid or gas-liquid systems generates highly reactive oxidizing species (e.g., $^{\bullet}OH$, hydrogen peroxide or H_2O_2) and reducing species (i.e., hydrated electron, superoxide).[55] In previous studies, the proposed application of plasma in water treatment is based on the formation of some reactive species (e.g., ($^{\bullet}OH$) that are non-selective toward a wide spectrum of organic compounds (e.g., pentachlorophenol,[56] tert-methyl butyl ether,[57] pesticides,[58] pharmaceuticals,[59] algal toxins).[60] In

addition, recent studies also revealed that solvated electron generated in plasma causes the reductive destruction of per- and polyfluoroalkyl substances (PFASs)).[61–64]

However, to implement plasma technology in water treatment facilities, we should also consider various treatment scenarios, including the application of plasma to high-salinity systems that contain high concentrations of halides. Due to the scavenging ability of halides on •OH, which generates halogen radicals, we suspected that halides would alter the degradation kinetics of organic compounds. Therefore, the effects of halides on organic compound degradation are necessary when expanding plasma application to more complex water matrices such as brines.

1.2 Research objectives and hypotheses

The overall objective of this study is to investigate the reaction kinetics of organic compounds and the mechanisms of halogenated byproduct formation in three different engineered aquatic systems. In the first objective (Chapter 2), I investigated the mechanisms of how conventional chemical oxidants contributed to halogenated disinfection byproduct formation during HABs. More specifically, I evaluated the impact of permanganate as a preoxidant on halogenated DBP formation during subsequent chlorination or chloramination. In the second objective (Chapter 3), I investigated the degradation kinetics and halogenation mechanism of organic additives in high-salinity hydraulic fracturing fluids. In the third objective (Chapter 4), I investigated the effects of halides on organic compound degradation during plasma treatment of brines. Specific objectives and hypotheses are given below.

Objective 1. Investigate disinfection byproduct formation in drinking water treatment during HABs.

Hypothesis 1: Permanganate preoxidation increases the formation of certain DBPs during subsequent chlorination of AOM.

Hypothesis 2: Permanganate preoxidation increases the formation of certain DBPs during subsequent chloramination of AOM.

Hypothesis 3: Permanganate preoxidation increases the overall toxicity of treated water impacted by high concentrations of AOM.

Objective 2. Elucidate the halogenation and degradation kinetics of organic additives used in hydraulic fracturing.

Hypothesis 1: Halogenation of organic additives in hydraulic fracturing fluid is mediated by halogen radicals.

Hypothesis 2: Selective halogen radicals promote the degradation rates of certain organic additives but reduce the degradation rates of others.

Objective 3. Evaluate the effects of halides on organic compound degradation during plasma treatment of brines.

Hypothesis 1: Halides lead to the selective degradation of organic compounds during plasma treatment of brines.

Hypothesis 2: High concentrations of scavengers for oxidants such as bicarbonate and organic matter in brines suppress the effect of halides on organic compound degradation during plasma treatment.

Chapter 2: Permanganate preoxidation affects the formation of disinfection byproducts from algal organic matter

This chapter is adapted from Chen, M.; Rholl, C. A.; Persaud, S. L.; Wang, Z.; He, Z.; Parker, K. M. Permanganate Preoxidation Affects the Formation of Disinfection Byproducts from Algal Organic Matter. *Water Res.* **2023**, *232*, 119691.

2.1 Abstract

During harmful algal blooms (HABs), permanganate may be used as a preoxidant to improve drinking water quality by removing algal cells and degrading algal toxins. However, permanganate also lyses algal cells, releasing intracellular algal organic matter (AOM). AOM further reacts with permanganate to alter the abundance of disinfection byproduct (DBP) precursors, which in turn affects DBP formation during disinfection. In this study, we evaluated the impacts of preoxidation by permanganate applied at commonly used doses (i.e., 1-5 mg/L) on DBP generation during chlorination and chloramination of AOM. We found that permanganate preoxidation increased trichloronitromethane (TCNM) formation by up to 3-fold and decreased dichloroacetonitrile (DCAN) formation by up to 40% during chlorination, indicating that permanganate oxidized organic amines in AOM to organic nitro compounds rather than organic nitrile compounds. To test this proposed mechanism, we demonstrated that permanganate oxidized organic amines in known DBP precursors (i.e., tyrosine, tryptophan) to favor the production of TCNM over DCAN during chlorination. Compared to the decreased formation of DCAN during chlorination, permanganate increased DCAN formation by 30-50% during chloramination of AOM. This difference likely arose from monochloramine's ability to react with non-nitrogenous

precursors (e.g., organic aldehydes) that formed during permanganate preoxidation of AOM to generate nitrogen-containing intermediates that go on to form DCAN. Our results also showed that permanganate preoxidation favored the formation of dichlorobromomethane (DCBM) over trichloromethane (TCM) during chlorination and chloramination. The increased formation of DBPs, especially nitrogenous DBPs that are more toxic than carbonaceous DBPs, may increase the overall toxicity in finished drinking water when permanganate preoxidation is implemented.

2.2 Introduction

Preoxidation is commonly used during drinking water treatment. Among surface water treatment facilities that implemented preoxidation in the U.S., permanganate was the second most commonly used preoxidant.[11] Permanganate is conventionally used to remove iron and manganese and control the taste and odor of drinking water. [11] Due to its ability to degrade moieties in natural organic matter (NOM) such as olefins, amines, and phenolic compounds,[65–67] permanganate has also been investigated for its impact on the formation of toxic disinfection byproducts (DBPs) during subsequent disinfection. For example, prior studies reported that permanganate decreased the formation of trihalomethanes (THMs) by 10-20%[68–72] and haloacetonitriles (HANs) by 50-70%[70–72] during subsequent chlorination.

Permanganate may also be used as a preoxidant during harmful algal blooms (HABs), which threaten drinking water quality worldwide by causing taste and odor problems and producing toxins.[73–76] During HABs, permanganate preoxidation has been applied to induce aggregation of algal cells for removal by coagulation-flocculation,[77–81] lyse cells to prevent membrane fouling,[26,77,82–84] and degrade certain algal toxins (e.g., microcystins, anatoxin-a).[85,86] However, algal cell lysis caused by permanganate preoxidation also leads to the release of intracellular algal organic matter (AOM) that is a precursor of DBPs.[22,23,87] To date, information

regarding the impact of permanganate preoxidation on DBP formation during disinfection of intracellular AOM remains limited. When treating algal cell suspensions, one study showed that permanganate decreased the abundance of trichloromethane (TCM) precursors by up to 40% from extracellular AOM,[88] while another one found that permanganate preoxidation did not alter DBP formation during subsequent chlorination.[82] However, the permanganate dosages applied in these studies were too low (<2 mg/L) to lyse algal cells and release intracellular AOM.[26] The impact of permanganate on intracellular AOM from lysed cells was only investigated by one study, which found that permanganate dosed at 4 mg/L did not alter DBP formation (e.g., TCM, dichloroacetonitrile (DCAN), trichloronitromethane (TCNM)) during subsequent chlorination.[89] However, this study reported the impact of permanganate only under a single pair of preoxidant/disinfectant doses,[89] which may be insufficient to account for preoxidant effects that depend on the doses of preoxidant and disinfectant.[71,72,90]

Whereas preoxidants tend to decrease DBP formation from NOM, preoxidants other than permanganate have been found to increase the formation of DBPs from AOM. For example, preoxidation using chlorine dioxide decreased the formation of TCM by 10% and DCAN by 60% during chlorination of NOM,[91] but increased the formation of these DBPs during chlorination of intracellular AOM (i.e., by 60% for TCM, 50% for DCAN).[89] Like chlorine dioxide, ozone typically decreased THM formation by 20-50% during chlorination of NOM,[71,92,93] but increased THM formation by 30-70% during chlorination of AOM.[89,94–96] The increased formation of DBPs from AOM may result from specific changes made by the preoxidants to AOM properties (e.g., decreasing its molecular weight, aromaticity, or hydrophobicity).[87,89,94] In addition, some preoxidants react with specific moieties from AOM to generate DBPs. For example, organic amines, which are more abundant in AOM than NOM,[23,87] were oxidized by ozone to generate

precursors of TCNM,[97] which could contribute to a greater extent of increase in the formation of TCNM by preozonation observed from AOM (i.e., 5- to 100-fold) than NOM (i.e., 2- to 8-fold).[89,92–96]

In this study, we hypothesized that permanganate preoxidation increases DBP formation during disinfection of AOM in contrast to NOM, which was included as a control throughout the study. Using AOM derived from cultivated *Microcystis aeruginosa*, we first tested the effects of permanganate on DBP formation during chlorination of AOM and linked some of these effects to the reaction of permanganate with specific moieties in AOM (i.e., organic amines). We next extended our work to investigate the impact of permanganate on DBP formation during chloramination of AOM, which we hypothesized would differ from chlorination due to monochloramine acting as a weaker oxidant that can also participate in unique reactions that generate new DBP precursors, particularly for nitrogenous DBPs.[23,27,98] Finally, we evaluated the impact of permanganate preoxidation on calculated toxicity associated with DBP formation.[99–101] In contrast to prior findings under limited conditions,[89] our work demonstrated that permanganate preoxidation increased the formation of some DBPs specifically from AOM under relevant doses of permanganate and disinfectant.

2.3 Materials and Methods

2.3.1 Chemicals and reagents

All chemicals (**Table S2.1**) were used as received. Oxidant solutions were prepared in Milli-Q water as described in **Section 2.5.1**. We obtained AOM from *Microcystis aeruginosa* following the method described in **Section 2.5.2**. For experiments, AOM was added to Milli-Q water at a concentration of 5 mg-C/L, which is approximately equivalent to the concentration of

AOM that would be released by algal cells present at 10^6 cells/mL [22,82]. We obtained NOM from natural water samples that were collected from the Mississippi River at a location near the Chain of Rocks Water Treatment Plant in St. Louis, Missouri, where no HAB was reported at the time of collection. The water samples were filtered through 0.7 µm glass fiber filters (Fisher) that were pre-baked in an oven at 450°C for 4 h. These water samples were directly used for experiments requiring NOM and contained total organic carbon (TOC) measured to be 3 mg-C/L. Water quality parameters including TOC, specific UV absorbance at 254 nm ($SUVA_{254nm}$), and concentrations of inorganic ions were measured for solutions containing AOM and NOM as described in **Section 2.5.3** and are shown in **Table S2.2**. All solutions containing either AOM or NOM were stored at 4 °C.

2.3.2 Experimental procedure

Experiments were conducted to measure the concentrations of DBPs generated during permanganate preoxidation and disinfection of AOM and NOM. All solutions contain 5 mg-C/L AOM or 3 mg-C/L NOM, 10 mM phosphate buffer (pH 7), and permanganate at concentrations commonly used during preoxidation (i.e., 1-5 mg/L as potassium permanganate, $KMnO_4$).[11,77,87] The solutions were prepared in 40 mL amber glass vials that were headspace-free and reacted at room temperature in the dark for 3 d to allow sufficient time for reactions between permanganate and moieties in organic matter.[102] After 3 d, residual permanganate in solutions was measured. To terminate the reaction, a quencher was applied at >10-fold molar excess relative to permanganate concentrations in a 100 µL aliquot. Sodium thiosulfate was used to quench permanganate in an early experiment (i.e., **Figure 2.1a-d**), but was replaced with ascorbic acid in all later experiments including **Figure 2.3a-d** that replicated identical experimental conditions to achieve the same results after permanganate preoxidation alone. These quenched solutions were extracted into

methyl tert-butyl ether (MtBE) within 30 min as described in **Section 2.5.4**. Then, DBP concentrations in the MtBE extracts were analyzed to determine the amount generated during permanganate preoxidation.

To a separate set of unquenched solutions after permanganate preoxidation, small volumes (i.e., <100 µL) of disinfectant stock solutions were added into each vial to achieve a targeted concentration (i.e., 15 mg/L chlorine or 4 mg/L monochloramine as chlorine, Cl_2) for disinfection carried out over 3 d. The disinfection time was selected to align with other studies investigating DBP formation from AOM,[22,23,82,88] while oxidant concentrations were selected to maintain residuals after the disinfection period (**Figure S2.1**). Subsequently, solutions were quenched with ascorbic acid, extracted, and analyzed for DBP concentrations generated during disinfection.

For experiments investigating the impact of permanganate preoxidation on DBP formation during chlorination of model organic amines (i.e., tyrosine and tryptophan), 3.2 mg-C/L tyrosine or 4.0 mg-C/L tryptophan (i.e., 30 µM) were treated with 1-50 mg/L permanganate (as $KMnO_4$, i.e., 6-320 µM) during preoxidation. These concentrations spanned values above and below permanganate demand in these experiments. After 3 d, solutions were measured for residual permanganate concentrations or treated with chlorine as described above.

2.3.3 Analytical procedures

Concentrations of residual oxidants were measured as described in **Section 2.5.5**. Residual chlorine and monochloramine concentrations were measured after disinfection for 3 d without preoxidation (**Figure S2.1**). Residual permanganate concentrations were measured after preoxidation of AOM and NOM (**Figure S2.2**) and model amino acids (**Figure S2.3**), each for 3 d.

Four THMs (i.e., TCM, dichlorobromomethane (DCBM), dibromochloromethane (DBCM), tribromomethane (TBM)), three haloacetonitriles (i.e., DCAN, bromochloroacetonitrile (BCAN), dibromoacetonitrile (DBAN)), and TCNM were measured on gas chromatography-mass spectrometry (GC-MS, **Section 2.5.4**). In all of our experiments, we only detected four of these DBPs above the levels of their method detection limit: TCM (0.1 μg/L), DCBM (0.1 μg/L), DCAN (0.1 μg/L), and TCNM (0.1 μg/L). All other measured DBPs never occurred at concentrations above the levels of their detection limit: DBCM (0.1 μg/L), TBM (0.1 μg/L), BCAN (0.2 μg/L), DBAN (0.1 μg/L).

The toxicity associated with detected DBPs was calculated by dividing the molar concentration of each DBP by their corresponding LC_{50} cytotoxicity values (i.e., the DBP concentration that results in 50% reduction in growth of Chinese hamster ovary cells compared to the untreated control), which facilitates quantitative comparison of DBP toxicities determined using a common assay.[99–101] The calculated toxicity aggregates the contributions of several DBPs measured on a consistent basis, though notably it does not account for toxicity contributed by other DBPs occurring below method detect limits nor excluded from the analytical method.[103]

2.3.4 Statistical analysis

All experiments were conducted in triplicate. Error bars represent the standard deviations of the data obtained from triplicate experiments. The significance of differences between DBP formation with and without preoxidation was assessed by two-tail t-tests in GraphPad Prism with a confidence level set to be ≤ 0.05.

2.4 Results and Discussion

2.4.1 DBP formation from disinfection without preoxidation

Before investigating the impact of preoxidation on the abundance of DBP precursors, we first measured the production of DBPs from AOM during chlorination or chloramination in the absence of preoxidation as a control. During chlorination and chloramination, we found that TCM, DCBM, DCAN, and TCNM were generated from AOM, while other four DBPs included in our method were below their detection limits (**Table S2.3**). The yields of measurable DBPs (μg per mg-C) were comparable to those reported in previous literature during chlorination of AOM, indicating that our AOM behaved similarly to AOM used in other studies (**Table S2.4**).[22,23,25,82,88,94,96,104–112] Similarly, our results showed that the yields of TCM, DCAN, and TCNM from chloramination of AOM were also comparable to the previously reported ranges from AOM (**Table S2.5**)[23,96,105,108] Among the four DBPs that formed at measurable quantities, we found that DCBM formed at the lowest yield, which was 30- to 80-fold lower than the previously reported yields (**Table S2.5**) obtained from AOM samples amended with bromide (i.e., 0.05-1 mg/L).[108]

To enable a comparison between AOM and NOM, we also measured the production of DBPs from NOM during chlorination and chloramination. Similar to AOM, only four among eight DBPs (i.e., TCM, DCBM, DCAN, TCNM) were detectable during disinfection of NOM. Similar to the yields of DBPs from AOM, the yields of these four DBPs from NOM were comparable to previously reported ranges during chlorination (**Table S2.4**).[22,23,71,91,93,105,113–119] and chloramination (**Table S2.5**).[23,91,93,113,114,118] Compared to AOM, NOM yielded more carbonaceous DBPs (C-DBPs) during chlorination (i.e., ~2-fold more TCM and ~10-fold more DCBM, **Table S2.4)** and chloramination (i.e., ~30-fold more DCBM, **Table S2.5**). The higher

yields of C-DBPs, particularly TCM, may be attributed to a higher content of aromatic organic carbon from NOM than AOM[23] that is correlated with a higher value of $SUVA_{254\ nm}$[120] from NOM (i.e., 3.5 L/(mg-C•m)) than AOM (i.e., 1.0 L/(mg-C•m), **Table S2.2**). NOM also yielded ~3-fold less DCAN and ~2-fold more TCNM than AOM during chlorination (**Table S2.4**). The total N-DBP yield (dominated by DCAN) from NOM was less than from AOM, likely because AOM has been reported to have ~20-fold higher abundance of organic nitrogen relative to organic carbon than NOM.[23]

2.4.2 DBP formation from permanganate preoxidation followed by chlorination

To investigate the effects of permanganate preoxidation on the abundance of DBP precursors from AOM and NOM, we next added 1-5 mg/L permanganate before chlorination. Measured DBPs were never detected after permanganate preoxidation of AOM (**Figure 2.1a-d**) and NOM (**Figure 2.1e-h**) for 3 d. Therefore, the effects of permanganate on DBP formation after chlorination were entirely attributable to the effects of permanganate on precursors that subsequently reacted with chlorine rather than DBP formed from permanganate itself.

When we used 1 mg/L initial permanganate during preoxidation, the production of TCM during subsequent chlorination of AOM was comparable to the control (**Figure 2.1a**). When the concentration of permanganate was increased to 3 and 5 mg/L, the yield of TCM decreased by 20±10% and 42±4%, respectively, relative to the control (**Figure 2.1a**). Compared to AOM, we found similar effects of permanganate preoxidation on TCM yield from NOM (**Figure 2.1e**). Our results showed marginally greater decreases in TCM yield from AOM and NOM than the slight decrease reported in a prior report (i.e., by <5%) during chlorination of NOM under similar experimental conditions.[71] The decreased TCM formation indicates that permanganate degrades TCM precursors from AOM and NOM.

In addition to TCM, DCBM was also detected after chlorination of both AOM and NOM (**Figure 2.1b,f**). Although we found low concentrations of bromide in solutions containing AOM (i.e., <0.01 mg/L, below the detection limit) and NOM (i.e., 0.02 mg/L) (**Table S2.2**), oxidation of trace bromide may still have led to the formation of hypobromous acid[51,121] or other brominating oxidants[122–124] that react with organic matter to generate brominated DBPs like DCBM. In contrast to the decreased yield of TCM after permanganate preoxidation (**Figure 2.1a,e**), the yield of DCBM during chlorination was either unchanged or increased upon preoxidation of NOM or AOM, respectively (**Figure 2.1b, f**). While the exact causes of the different effects of permanganate preoxidation on DCBM formation relative to TCM are unknown, it is possible that permanganate reacts differently with their respective precursors, which are somewhat distinct. For example, DBPs with more brominated substituents were found to be preferentially generated from more hydrophilic organic matter fractions relative to their chlorinated analogues,[15,115] suggesting possible differences in the precursors of TCM and DCBM alter the effects of preoxidation on their eventual formation.

We next investigated the impact of permanganate preoxidation on the formation of N-DBPs including DCAN. We found that preoxidation by 1-5 mg/L permanganate decreased the yield of DCAN from AOM by up to 40% relative to the control (**Figure 2.1c**). Similarly, permanganate decreased the yield of DCAN from NOM (**Figure 2.1g**). The decrease in DCAN yield from NOM was comparable to the previously reported decrease during chlorination of NOM (i.e., by ~40%) under similar experimental conditions.[71] Our results indicate that, like its impact on DCAN precursors from NOM, permanganate also degrades DCAN precursors from AOM during preoxidation.

Although permanganate preoxidation decreased the formation of DCAN, it increased the formation of the other detected N-DBP, TCNM, from both AOM and NOM. Specifically, permanganate at 1 and 3 mg/L increased the yield of TCNM from AOM by ~3-fold relative to the control (**Figure 2.1d**). A moderate decrease in TCNM yield was observed when permanganate was increased to 5 mg/L (**Figure 2.1d**), possibly due to further oxidation of TCNM precursors similar to TCM precursors (**Figure 2.1a**). Compared to the large increase in TCNM yield from AOM, permanganate preoxidation only slightly increased the yield from NOM by ~20% relative to the control (**Figure 2.1h**). The greater increase in TCNM yield from AOM than NOM may be explained by the higher amount of organic nitrogen in AOM than NOM,[23] which makes AOM more susceptible to react with permanganate to form TCNM precursors.

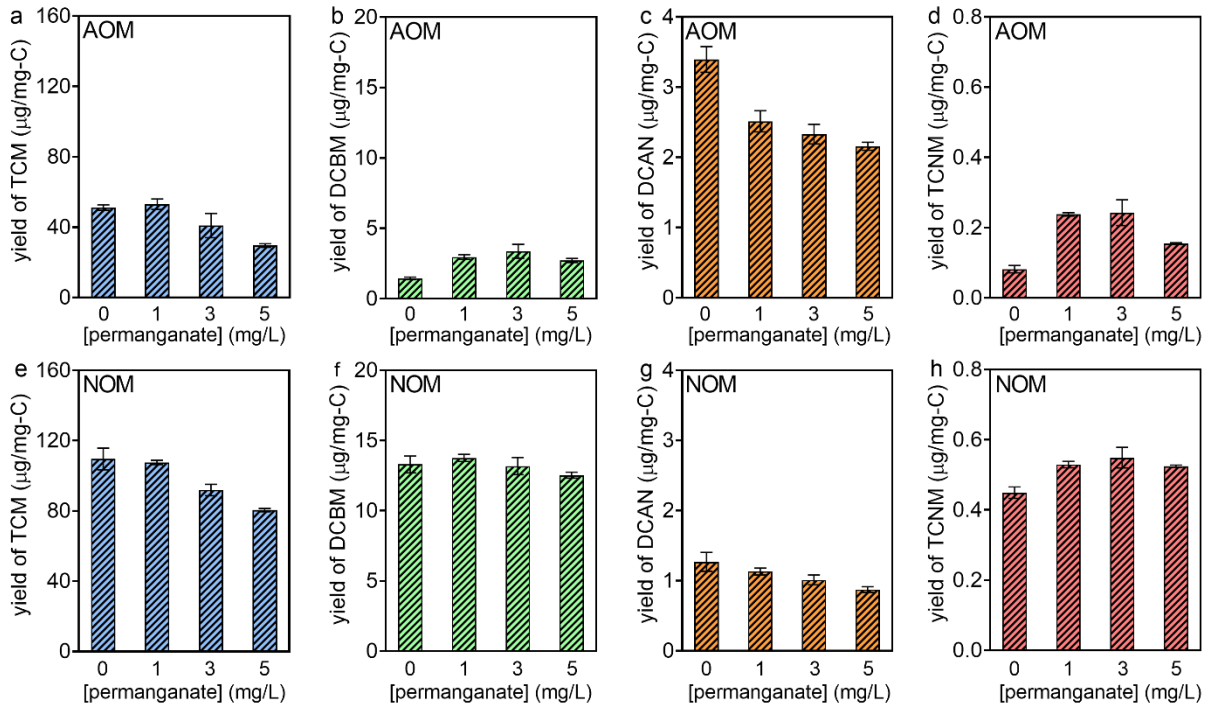

Figure 2.1. Formation of trichloromethane (TCM), dichlorobromomethane (DCBM), dichloroacetonitrile (DCAN), and trichloronitromethane (TCNM) during preoxidation by permanganate (as $KMnO_4$) for 3 d followed by chlorination of AOM (**a-d**) or NOM (**e-h**) for 3 d.

All solutions are prepared in headspace-free amber vials initially containing 5 mg-C/L AOM (**a-d**) or 3 mg-C/L NOM (**e-h**), permanganate at the indicated concentration, and 10 mM phosphate buffer (pH 7). After 3 d, 15 mg/L chlorine (as Cl_2) was added as the disinfectant to all solutions. DBP yields after permanganate preoxidation without chlorination were below the method detection limits (i.e., 0.1 µg/L: 0.02 µg/mg-C for AOM, 0.03 µg/mg-C for NOM).

The different effects of permanganate on the formation of DCAN and TCNM from AOM in our experiments might result from the fact that they are both proposed to be generated from organic amine precursors (e.g., amino acids, proteins) during the chlorination of AOM.[23] One key difference in their formation mechanisms is the transformation from organic amines to organic nitrile compounds (i.e., R-C≡N) or organic nitro compounds (i.e., R-NO_2), which leads to the formation of DCAN or TCNM, respectively.[23,27,102] We hypothesized that permanganate oxidizes organic amines from AOM to form organic nitro compounds (**Scheme 2.1,** step 1),[102,125,126] which contributes to the increased formation of TCNM during subsequent chlorination (step 2).[23,27] However, oxidation of amines to nitro groups may reduce the abundance of precursors that go on to form organic nitrile compounds (step 3) and subsequently DCAN (step 4) during chlorination.[23,27]

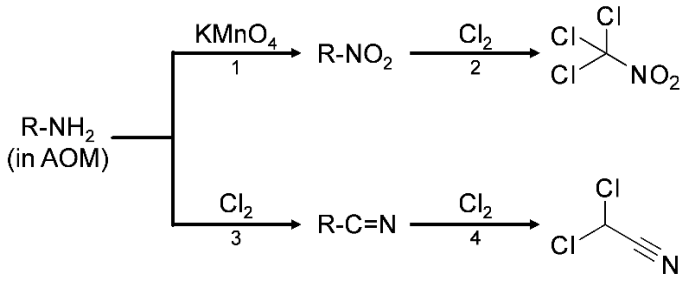

Scheme 2.1. Formation pathways of dichloroacetonitrile (DCAN) and trichloronitromethane (TCNM) from organic amines of AOM during permanganate preoxidation and chlorination. Oxidation of organic amines by permanganate to form organic nitro compounds (step 1),[102,125,126]

followed by formation of TCNM during chlorination (step 2).[23,27] Transformation of organic amines to form organic nitrile compounds during chlorination (step 3),[23,27] followed by formation of DCAN (step 4).[23,27]

To test our hypothesis regarding the effect of permanganate preoxidation on N-DBP precursors from organic amines, we measured the formation of both DCAN and TCNM from two known amine-containing precursors, namely, the amino acids tyrosine and tryptophan.[127,128] Notably, even though the carbon-based concentration of 30 µM solutions of tyrosine and tryptophan were similar to AOM and NOM (i.e., 3-4 mg-C/L relative to 3-5 mg-C/L, respectively), the permanganate demands of the model compounds were much higher (**Figure S2.3**), likely due to a greater abundance of reactive sites present relative to carbon mass. Consequently, for this mechanistic experiment, permanganate was applied at both a lower concentration range (1-5 mg/L) – corresponding to that used for AOM and NOM experiments – and a higher concentration range (10-50 mg/L) – spanning the measured permanganate demand of 3.2 mg-C/L tyrosine (i.e., 27.6±0.7 mg/L) and 4.0 mg-C/L tryptophan (i.e., 41.2±0.4 mg/L) (**Figure S2.3**). The greater permanganate demand by tryptophan than tyrosine likely resulted from permanganate selectively reacting with the indoleamine in tryptophan (**Figure 2.2**),[102] though tyrosine and tryptophan exert similar demands for other common preoxidants (e.g., chlorine, ozone).[129,130]

The effect of permanganate preoxidation on DCAN and TCNM formation during chlorination of tyrosine and tryptophan differed when permanganate was below or above the permanganate demand of the amino acid precursors. In all cases where permanganate was applied below the permanganate demand of the amino acids (i.e., 20 mg/L or lower), DCAN yield tended to increase with increasing permanganate doses (**Figure 2.2a,b**). Notably, whereas DCAN yield

from tryptophan increased continuously as the permanganate dose was increased from 1 to 20 mg/L permanganate dose (**Figure 2.2b**), DCAN yield from tyrosine plateaued when permanganate dose was increased from 5 to 20 mg/L (**Figure 2.2a**), which may be related to tryptophan's greater permanganate demand relative to tyrosine (**Figure S2.3**). When permanganate dose was applied in excess of the demand (i.e., when permanganate dose was increased from 20 to 50 mg/L), DCAN yield from both tyrosine and tryptophan decreased. In contrast to the dose-dependent effect of permanganate on DCAN yield, TCNM increased consistently with increasing permanganate doses above 3 mg/L (**Figure 2.2c,d**). The greatest increase in TCNM occurred when permanganate dose approached or exceeded the demand of the two amino acids.

Overall, our results using amino acids suggest that the effect of permanganate on DCAN and TCNM formation from organic amine precursors depends on the amount of permanganate applied relative to the demand exerted by the precursors. We found that higher doses of permanganate decreased DCAN formation and increased TCNM, but only under the condition where permanganate was applied in excess of the precursor's demand. Notably, this condition was met during our experiments using AOM, wherein all permanganate doses (1-5 mg/L) exceeded the demand (i.e., <1 mg/L, **Figure S2.2**). At lower permanganate doses, DCAN formation from amino acids increased, which suggests that partially oxidized intermediates generated from the reaction of the amino acids with permanganate serve as better precursors for DCAN than the parent molecules. This finding is in stark contrast to a prior study that reported preoxidation of amino acids by permanganate at doses ranging from 1-5 mg/L resulted in decreased formation of both DCAN and TCNM.[131] A possible cause for this difference is the elevated chlorine dose (i.e., 213 mg/L as Cl_2) employed by the prior study,[131] which may have sufficiently oxidized the amino acids in the absence of permanganate to mask the effect of preoxidation on N-DBP precursors detectable

under the more relevant conditions applied in our experiments using AOM. Together, results from both our study and the prior study point to important effects of both preoxidant and disinfectant concentrations in determining the overall effect of preoxidation on DBP formation.

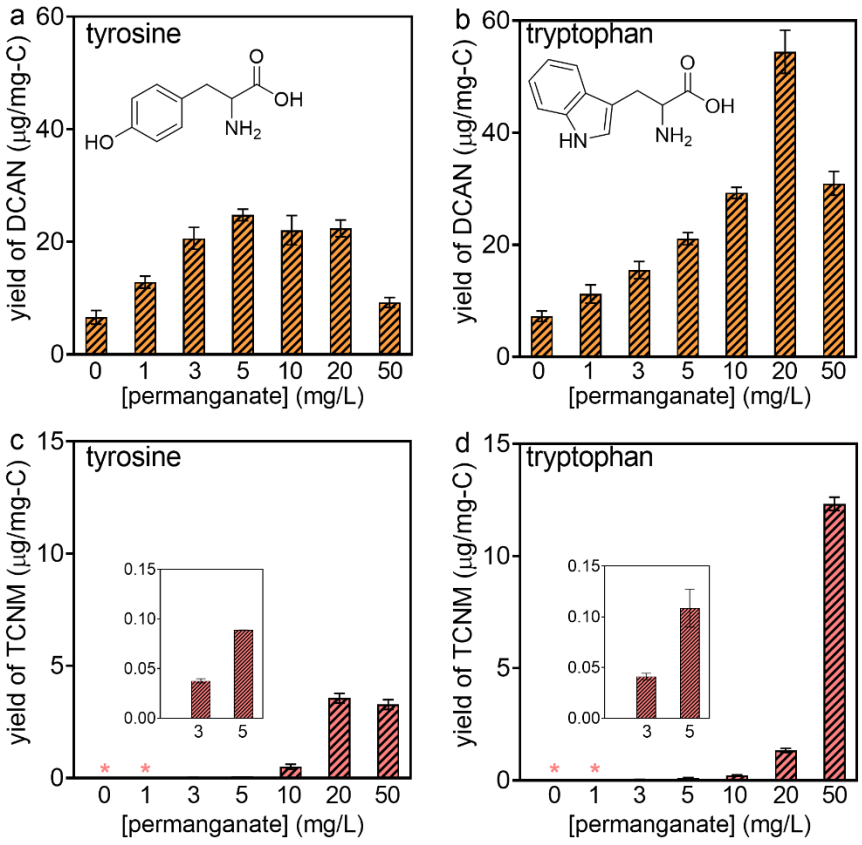

Figure 2.2. Formation of dichloroacetonitrile (DCAN) and trichloronitromethane (TCNM) during preoxidation by permanganate (as $KMnO_4$) for 3 d followed by chlorination of tyrosine (**a**,**c**) or tryptophan (**b**,**d**) for 3 d. All solutions are prepared in headspace-free amber vials initially containing 3.2 mg-C/L tyrosine (**a**,**c**) or 4.0 mg-C/L tryptophan (**b**,**d**) (i.e., both 30 μM), permanganate at the indicated concentration, and 10 mM phosphate buffer (pH 7). After 3 d, 15 mg/L chlorine (as Cl_2) was added as the disinfectant to all solutions. DBP yields after permanganate preoxidation without chlorination were below the method detection limits (i.e., 0.1

µg/L: ~0.033 µg/mg-C for tyrosine, ~0.025 µg/mg-C for tryptophan). The asterisks (*) in (**c**) and (**d**) indicate TCNM occurred at concentrations below its method detection limit.

2.4.3 DBP formation from permanganate preoxidation followed by chloramination

We next investigated the impact of permanganate on the abundance of DBP precursors from AOM when monochloramine was applied during disinfection. We hypothesized that DBP formation during chloramination is more sensitive to permanganate preoxidation because monochloramine is a weaker oxidant than chlorine and therefore reacts with a smaller pool of precursors. The ability of monochloramine to react with fewer DBP precursors in both AOM and NOM relative to chlorine was further evidenced by both lower DBP yields (i.e., **Figure 2.3** vs. **Figure 2.1**) and disinfectant demand (**Figure S2.4**). This difference between the reactivities of monochloramine and chlorine therefore may translate to differences in the effect of permanganate preoxidation on ultimate DBP formation.

Whereas TCM formation during chlorination decreased after preoxidation by higher levels of permanganate (**Figure 2.1a**), the impact of permanganate on TCM formation during chloramination of AOM varied depending on permanganate concentration (**Figure 2.3a**). Surprisingly, at the lowest dose of permanganate (i.e., 1 mg/L), TCM yield increased by 70% (**Figure 2.3a**), which suggests that permanganate at a relatively low concentration reacts with AOM to form TCM precursors that more readily react with monochloramine but not chlorine. However, at higher permanganate doses (i.e., 3 and 5 mg/L), TCM yield decreased to 50% of the control (**Figure 2.3a**), in closer alignment to decreasing yields observed from NOM upon permanganate preoxidation (**Figure 2.3e**). Notably, TCM yield during chloramination of NOM

was highly sensitive to permanganate preoxidation, decreasing to below the method detection limit when permanganate was applied at its highest dose (**Figure 2.3e**). Consequently, permanganate preoxidation appears capable of dramatically eliminating the relatively small pool of TCM precursors from NOM that react with monochloramine, but is less effective at degrading TCM precursors from AOM.

In contrast to TCM, the effects of permanganate preoxidation on the formation of DCBM during chloramination of both AOM (**Figure 2.3b**) and NOM (**Figure 2.3f**) were more similar to the effect observed during chlorination (**Figure 2.1b,f**). We again observed that permanganate preoxidation increased the yield of DCBM during chloramination of AOM, in this case by up to ~3-fold (**Figure 2.3b**), while the yield of DCAN during chloramination of NOM remained unchanged or slightly decreased (**Figure 2.3f**). As observed for TCM, the greatest increase in DCBM yield from AOM was found at the lowest permanganate dose (i.e., 1 mg/L); however, DCBM yields remained above the control even at higher permanganate doses. Together, our results from both chlorination and chloramination suggest that AOM, but not NOM, specifically reacts with permanganate to generate DCBM precursors.

Another key difference between chlorination and chloramination was observed when comparing the impact of permanganate on DCAN formation. Unlike the decreased yield of DCAN during chlorination of both AOM and NOM (**Figure 2.1c,g**), the impact of permanganate preoxidation on DCAN yield during chloramination differed between AOM and NOM (**Figure 2.3c,g**). While we still found a decreased yield of DCAN during chloramination of NOM (i.e., up to 50%, **Figure 2.3g**), permanganate preoxidation surprisingly increased the yield of DCAN during chloramination of AOM (i.e., by 30-50%, **Figure 2.3c**). When considering DCAN formation during chlorination, we proposed that permanganate preoxidation shifts N-DBP formation from

organic amines towards TCNM instead of DCAN (**Figure 2.2**), possibly due to oxidation of amines to nitro compounds (**Scheme 2.1**). While permanganate may still convert organic amines to organic nitro compounds over organic nitrile compounds before chloramination, monochloramine serves as an additional source of nitrogen for DCAN formation.[23,27,98] In this case, permanganate may have reacted with AOM to form other DCAN precursors such as organic aldehydes.[125,126,132–134] The nucleophilic attack of monochloramine on the aldehyde leads to the formation of organic nitrile compounds,[23,27,98] which in turn increase the formation of DCAN during chloramination (**Scheme 2.2**).

Similar to DCAN, the impact of permanganate preoxidation on the formation of TCNM also differed between chlorination and chloramination of AOM. While permanganate increased the yield of TCNM during chlorination (**Figure 2.1d**), the yield of TCNM was comparable to the control except when we used 3 mg/L permanganate (i.e., the yield increased by 170±30% relative to the control, **Figure 2.3d**). Our results indicate that permanganate at an intermediate concentration (i.e., 3 mg/L) oxidizes organic amines to organic nitro compounds that are reactive with monochloramine. However, these precursors may also contain other organic moieties (e.g., aromatic groups) that further react with permanganate.[65] Therefore, a higher permanganate concentration (i.e., 5 mg/L) may also oxidize these TCNM precursors to become less reactive with monochloramine. Compared to AOM, the yield of TCNM during chloramination of NOM was either unchanged or slightly decreased (**Figure 2.3h**). The increased formation of TCNM from only AOM suggests that organic amines from AOM are more susceptible than NOM to react with permanganate to produce organic nitro compounds that go on to generate TCNM.

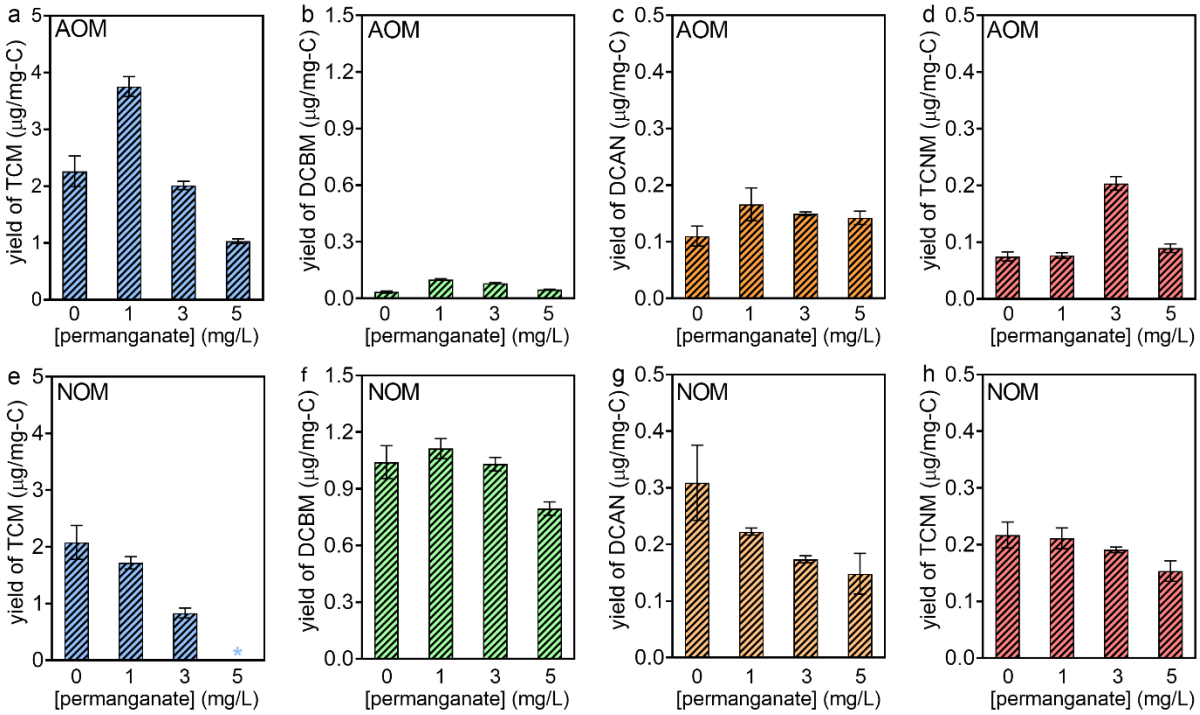

Figure 2.3. Formation of trichloromethane (TCM), dichlorobromomethane (DCBM), dichloroacetonitrile (DCAN), and trichloronitromethane (TCNM) during preoxidation by permanganate (as $KMnO_4$) for 3 d followed by chloramination of AOM (**a-d**) or NOM (**e-h**) for 3 d. All solutions are prepared in headspace-free amber vials initially containing 5 mg-C/L AOM (**a-d**) or 3 mg-C/L NOM (**e-h**), permanganate at the indicated concentration, and 10 mM phosphate buffer (pH 7). After 3 d, 4 mg/L monochloramine (as Cl_2) was added as the disinfectant to all solutions. DBP yields after permanganate preoxidation without chloramination were below the method detection limits (i.e., 0.1 µg/L: 0.02 µg/mg-C for AOM, 0.03 µg/mg-C for NOM), except TCM that was yielded at 0.029±0.007 and 0.04±0.01 µg/mg-C after preoxidation of AOM by 1 and 3 mg/L permanganate, respectively. The asterisk (*) in (**e**) indicates TCM occurred at concentrations below its method detection limit.

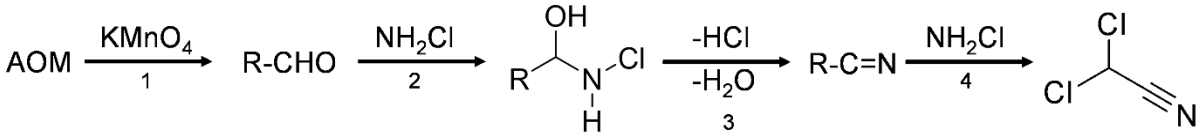

Scheme 2.2. Formation pathway of dichloroacetonitrile (DCAN) during permanganate preoxidation and chloramination of AOM. Oxidation of AOM to organic aldehyde compounds (step 1);[125,126,132–134] contribution of monochloramine nitrogen to organic aldehyde compounds to produce N-chloroaminomethanol (step 2);[27,98] formation of organic nitrile compounds through elimination of hydrochloric acid and dehydration (step 3);[23,27,98] and transformation of organic nitrile compounds to DCAN during chloramination (step 4).[23,27,98]

2.4.4 Impact of preoxidation on the toxicity of treated water

Because permanganate preoxidation had different effects on the formation of each DBP, we next calculated the summed toxicity associated with detected DBPs[99–101] to estimate the overall impact of preoxidation on the toxicity of treated water. After permanganate preoxidation, we found that subsequent chlorination led to weighted toxicity an order of magnitude higher than subsequent chloramination, which was attributed to the orders of magnitude higher concentrations of DBPs generated by chlorination (**Figure 2.1**) than chloramination (**Figure 2.3**). In addition, although DCAN occurred at 1-2 orders of magnitude lower concentrations than the most abundant DBP TCM, it contributed to 60-100% of the overall toxicity in all solutions (**Figure 2.4**). This observation was consistent with previous studies that identified haloacetonitriles as the primary contributors to the toxicity of treated AOM and NOM among DBPs considered across these studies.[111,135–137]

Because DCAN was found to be the primary toxicity driver from AOM, the changes in the overall toxicity were most closely related to the changes in DCAN concentrations. For example, permanganate preoxidation decreased the formation of DCAN from chlorination of AOM (relative to the control, **Figure 2.1c**), leading to decreased toxicity relative to the control (**Figure 2.4a**). However, as the formation of DCAN during the chloramination of AOM increased (**Figure 2.2c**), the estimated toxicity increased (**Figure 2.4b**). Although permanganate preoxidation increased the toxicity from chloramination of AOM at all permanganate doses relative to the control, the estimated toxicity after chloramination of AOM was decreased as the initial permanganate concentration was increased from 1 to 5 mg/L (**Figure 2.4b**). Therefore, higher doses of permanganate reduced the toxicity after chloramination relative to lower doses.

Our results showed that permanganate preoxidation decreased the estimated toxicity from NOM after chlorination or chloramination (**Figure 2.4c-d**). Similar to AOM, DCAN was a primary contributor to the toxicity from NOM. However, because chlorination of NOM also yielded greater TCM and less DCAN than AOM, TCM also contributed to a larger portion of the overall toxicity after chlorination of NOM (i.e., 30-40%, **Figure 2.4c**) than AOM (i.e., ~10%, **Figure 2.4a**). As permanganate preoxidation decreased the formation of both TCM and DCAN, the estimated toxicity after chlorination of NOM decreased (**Figure 2.4c**).

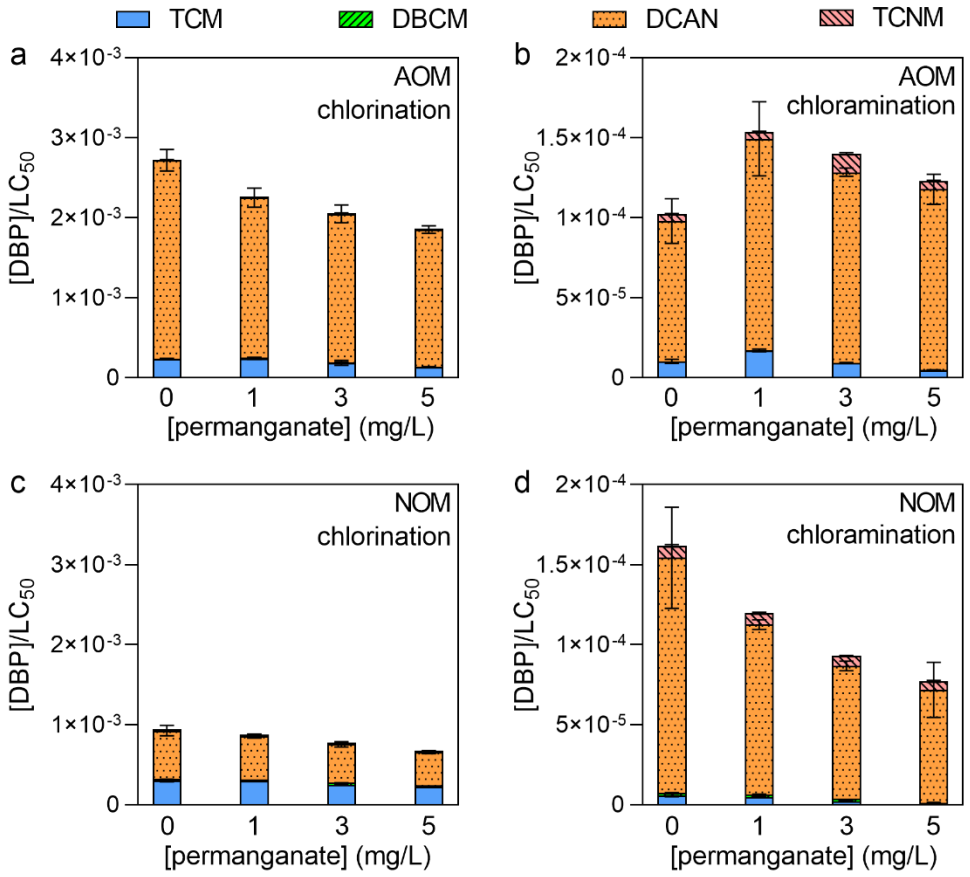

Figure 2.4. The impact of permanganate preoxidation on summed toxicity associated with detected DBPs[99–101] from (**a-b**) AOM or (**c-d**) NOM. All solutions are prepared in headspace-free amber vials initially containing 5 mg-C/L AOM (**a-b**) or 3 mg-C/L NOM (**c-d**) and 10 mM phosphate buffer (pH 7). After 3 d, 15 mg/L chlorine (as Cl_2, a and c) or 4 mg/L monochloramine (as Cl_2, **b** and **d**) was added as the disinfectant to all solutions.

2.4.5 Environmental Implications

While our work agrees with prior studies that consistently demonstrated that preoxidation decreased the DBP formation from NOM,[69,71,91,93] permanganate preoxidation increased the formation of certain DBPs during chlorination and chloramination of AOM. When followed by

chlorination, permanganate preoxidation specifically increased the formation of dichlorobromomethane and trichloronitromethane. In addition to these two DBPs, permanganate preoxidation also increased the formation of dichloroacetonitrile when followed by chloramination of AOM. Therefore, strategies involving permanganate preoxidation may require additional scrutiny during HABs.

Among DBPs considered in our study, DCAN was the primary toxicity driver in AOM-impacted water, suggesting that the formation of DCAN must be controlled to mitigate the toxicity of drinking water during HABs. While permanganate preoxidation consistently decreased the formation of dichloroacetonitrile during both chlorination and chloramination of NOM, its effect on dichloroacetonitrile formation from AOM was more variable. We found that dichloroacetonitrile formation during chlorination was decreased by permanganate preoxidation, which we tentatively attributed to oxidation of organic amine moieties under excess permanganate conditions that reduce their availability to form organic nitrile compounds during chlorination (**Scheme 2.1**). In contrast, dichloroacetonitrile formation during chloramination was increased by permanganate preoxidation; this distinction may relate to the ability of monochloramine to contribute its nitrogen when reacting with non-nitrogenous precursors (i.e., organic aldehydes) generated during permanganate preoxidation of AOM that can then become new precursors of dichloroacetonitrile (**Scheme 2.2**). Consequently, both the abundance of AOM relative to NOM and the type of disinfectant used, as well as concentrations of the preoxidant and disinfectant, may contribute to determining the impact of preoxidation on dichloroacetonitrile formation and therefore a significant fraction of DBP-associated toxicity in treated water.

Beyond DCAN, permanganate preoxidation also altered the formation of other DBPs, most notably by increasing the formation of TCNM from AOM during both chlorination and

chloramination at certain doses. Like DCAN, TCNM formation might also be related to the reaction of permanganate with organic amines, which were oxidized to nitro groups[102,125,126] that led to increased TCNM formation (**Scheme 2.1**). In addition to TCNM, permanganate preoxidation also increased the formation of DCBM – particularly in contrast to the decreased formation of its chlorinated analogue, TCM – during both chlorination and chloramination of AOM. The origin of the increased formation of DCBM from AOM preoxidized by permanganate is less clear, particularly in light of the tendency for permanganate preoxidation to decrease the formation of its chlorinated analogue, trichloromethane. However, prior studies demonstrating that more hydrophilic organic matter fractions preferentially form brominated DBPs over chlorinated DBPs[15,115] point to possible differences in their precursors that may contribute to this effect.

Our work contributed new insights into the impact of permanganate preoxidation on DBP formation during HABs. While a previous study showed that permanganate at a low concentration did not increase the formation of DBPs during chlorination of algal cell suspensions,[82] our study found that permanganate increased the formation of certain DBPs during chlorination of AOM from lysed algal cells. These differences may be explained by the permanganate concentration (i.e., 2 mg/L) used in the prior study,[82] which was lower than the level required to cause algal cell lysis (i.e., 3 mg/L).[26] However, higher permanganate concentrations (i.e., > 3 mg/L)[26] may be needed to lyse algal cells during water treatment operations to avoid other problems such as filter fouling.[84] Consequently, our findings regarding the impact of permanganate on DBP formation during HABs will be applicable to this condition under which AOM is released from lysed algal cells.

2.5 Supporting information

2.5.1 Preparation of oxidant solutions

Oxidant solutions were prepared daily before use. A chlorine stock solution was prepared from a sodium hypochlorite solution (5%) and standardized spectrophotometrically at 292 nm[138] by a UV-vis spectrophotometer (Varian Cary 50) or a NanoDrop One (Fisher). Monochloramine stock solutions were prepared daily by mixing equal volumes of ammonium chloride and chlorine solutions to achieve a chlorine to nitrogen molar ratio of 0.8[139] and standardized spectrophotometrically at 245 nm[139]. Permanganate stock solutions were prepared by dissolving solid potassium permanganate in water and standardized spectrophotometrically at 526 nm.[140]

2.5.2 Procedures to obtain AOM for DBP experiments

A culture of *Microcystis aeruginosa* (UTEX 2385) was purchased from the Culture Collection of Algae at the University of Texas at Austin. The algal cells were cultivated under a 12 h/12 h light/dark cycle at room temperature in BG-11 media.[23] After cultivation for 28 d, algal cell suspensions were centrifuged at 10,000 g for 10 min to separate algal cells and the supernatant. The collected algal cells were rinsed in Milli-Q water followed by centrifugation three times. To obtain AOM, algal cells were re-suspended in Milli-Q water, then frozen and thawed three times, and finally filtered through pre-baked 0.7 μm glass fiber filters.

2.5.3 Water quality analysis

The concentrations of total organic carbon (TOC) in solutions containing AOM and NOM were measured using a Shimadzu TOC analyzer. The UV_{254nm} absorbance was measured on a UV-vis spectrophotometer (Varian Cary 50). Nitrate (NO_3^--N), nitrite (NO_2^--N), chloride (Cl^-), and bromide (Br^-) concentrations were measured using an ion chromatography system equipped with

an IonPac AS18 column (Dionex, Thermo Fisher Scientific). The concentration of ammonium (NH_4^+-N) was measured by a salicylate colorimetric method[141] using a spectrophotometer (DR 890, Hach Company). The measured parameters were shown in **Table S2.2**.

2.5.4 Quantification of disinfection byproducts on gas chromatography – mass spectrometry

Four trihalomethanes (i.e., TCM, DCBM, DBCM, TBM), three haloacetonitriles (i.e., DCAN, BCAN, DBAN), and TCNM were measured by gas chromatography–mass spectrometry (GC-MS). As detailed in the method section in **Section 2.3.2**, we prepared quenched solutions after preoxidation and disinfection. Then, quenched solutions (20-mL) were spiked with 60 µg/L 1,2-dibromopropane as an internal standard and mixed with anhydrous sodium sulfate in excess and 3 mL tert-butyl methyl ether (MtBE). Then the solutions were vigorously shaken by hand for 2 min and allowed to sit for 20 min for separation. The MtBE extracts were further dried by ~2 g sodium sulfate and then analyzed using an Agilent 7820-5922 GC-MS equipped with an HP-5ms fused silica column (30 m × 0.25 mm × 0.25 µm). The injection volume was 5 µL in splitless mode with an inlet temperature of 90°C. The oven temperature was held at 28°C for 16 min, 40°C/min to 139°C, 60°C/min to 274°C and was held for 1 min. The quantification ions, retention times, limit of detection (LOD) levels, and recoveries of all DBPs are reported in **Table S2.3**.

2.5.5 Residual oxidant measurement

Residual chlorine and monochloramine concentrations were measured by DPD (N,N-diethyl-p-phenylendiamine) colorimetric method or DPD/potassium iodide colorimetric method, respectively.[142] Concentrations of residual permanganate were determined by measuring absorbance at 526 nm[140] after preoxidation of AOM or model amino acids. Consistent with prior literature,[82,143] in samples in which permanganate was applied as a preoxidant, we did not

subsequently measure residual chlorine and monochloramine concentrations because residual permanganate interfered with the DPD colorimetric methods.[144]

2.5.6 Supplementary tables

Table S2.1. Chemicals used in this chapter.

Vendor	Chemicals
Millipore-Sigma	ascorbic acid (ACS grade) (>99.5%) ammonium chloride (>99%) EPA 501/601 trihalomethane calibration mix L-tyrosine (99.0%) L-tryptophan (99.0%)
Fisher Scientific	monobasic sodium phosphate (>99%) dibasic sodium phosphate (>99%) sodium hydroxide (98.7%) hydrochloric acid solution (36.5-38.0%) sodium hypochlorite solution (5.65-6%)
Agilent	EPA 551B-1 disinfection byproducts standard
TCI America	1,2-dibromopropane (98.0%)
Acros	ammonium chloride (>99%)

Table S2.2. Total organic carbon (TOC), specific UV absorbance at 254 nm (SUVA254nm), and concentrations of inorganic ions in solutions containing algal organic matter (AOM) and natural organic matter (NOM).

Solutions	TOC (mg-C/L)	$SUVA_{254nm}$ L/(mg-C•m)	Cl^- (mg/L)	Br^- (mg/L)	NO_3^--N (mg-N/L)	NO_2^--N (mg-N/L)	NH_4^+-N (mg-N/L)

AOM	5.0	1.0	<0.5[a]	<0.01[a]	<0.5[a]	<0.5[a]	0.63
NOM	3.0	3.5	23	0.02[b]	2.3	<0.5[a]	0.10

[a] These values were below the lowest standard concentration of each anion.

[b] This value was measured by standard addition due to the interference by another constituent specifically in the NOM sample.

Table S2.3. Quantification ions, retention times, method detection limits, and recoveries of analytes.

analyte	quantification ions [a]	retention times (min)	method detection limits (µg/L)	recoveries (%)
TCM	83, 85	4.4	0.1	90±20
DCBM	83, 85, 129	5.7	0.1[b]	80±10
DCBM	127, 129, 131	9.6	0.1[b]	88±8
TBM	171, 173, 175	16.9	0.1[b]	98±9
DCAN	74, 76, 82, 84	6.2	0.1[b]	109±3
BCAN	74, 75, 155	11.6	0.2	90±10
DBAN	18, 120, 199	16.9	0.1[b]	100±20
TCNM	117, 119, 121	8.8	0.1[b]	80±20
1,2-dibromopropane	41, 121, 123	11.18	NA[c]	NA[c]

[a] All listed ions were used for quantification of analytes.

[b] These values are the concentrations of the lowest standard analyzed, which are higher than the calculated values of LOD based on standard curves.

[b] NA = not applicable

Table S2.4. DBP formation from chlorination of AOM and NOM. All solutions are prepared in headspace-free amber vials, initially containing 5 mg-C/L AOM or 3 mg-C/L NOM, 15 mg/L chlorine (as Cl2), and 10 mM phosphate buffer (pH 7).

DBP		yield in this study (µg/mg-C)	literature range (µg/mg-C)
TCM	AOM	51±2	10-50[a]
	NOM	110±10	40-130[b]
DCBM	AOM	1.46±0.08	2-5[c]
	NOM	13±1	8-26[d]
DCAN	AOM	3.40±0.02	0.4-5[e]
	NOM	1.3±0.1	0.5-5[f]
TCNM	AOM	0.08±0.05	0.04-0.2[g]
	NOM	0.45±0.02	0.06-0.6[h]

References:

a. 22,23,25,82,88,96,104–107,110–112
b. 22,23,71,91,93,105,113–119
c. 108,110
d. 93,118
e. 22,23,82,108,109,111
f. 23,71,91,93,113,114
g. 22,23,82,94
h. 23,93,114

Table S2.5. DBP formation from chloramination of AOM and NOM. All solutions are prepared in headspace-free amber vials, initially containing 5 mg-C/L AOM or 3 mg-C/L NOM, 4 mg/L monochloramine (as Cl2), and 10 mM phosphate buffer (pH 7).

DBP		yield in this study (µg/mg-C)	literature range (µg/mg-C)
TCM	AOM	2.2±0.2	1-4[a]
	NOM	2.1±0.3	1-10[b]
DCBM	AOM	0.034±0.006	~1-2.7[c]
	NOM	1.0±0.1	0.2-1[d]
DCAN	AOM	0.11±0.02	0.2-1.5[e]
	NOM	0.3±0.1	0.1-5[f]
TCNM	AOM	0.074±0.008	~0.1[g]
	NOM	0.21±0.01	0.06-0.3[h]

References:

a. 23,96,105,108
b. 23,91,93,113,114,118
c. 108
d. 93,118
e. 23,96,105,108
f. 23,91,93,113,114
g. 23,96
h. 23,93

2.5.7 Supplementary figures

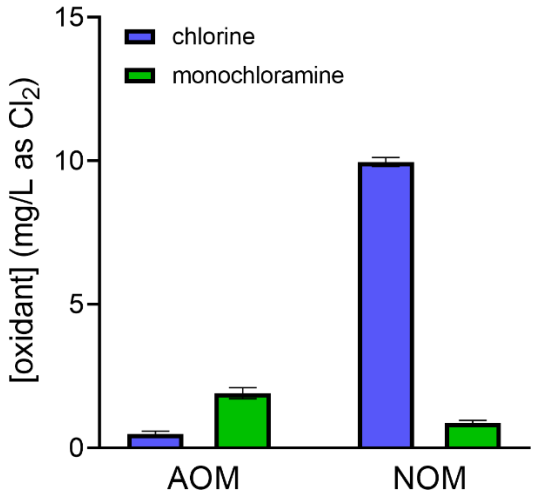

Figure S2.1. Residual chlorine and monochloramine concentrations (both mg/L as Cl2) after disinfection of (a) AOM or (b) NOM for 3-d. All solutions are prepared in headspace free amber vials, initially containing 5 mg-C/L AOM or 3 mg-C/L NOM and 10 mM phosphate buffer (pH 7). The initial chlorine concentration was 15 mg/L and the initial monochloramine concentration was 4 mg/L.

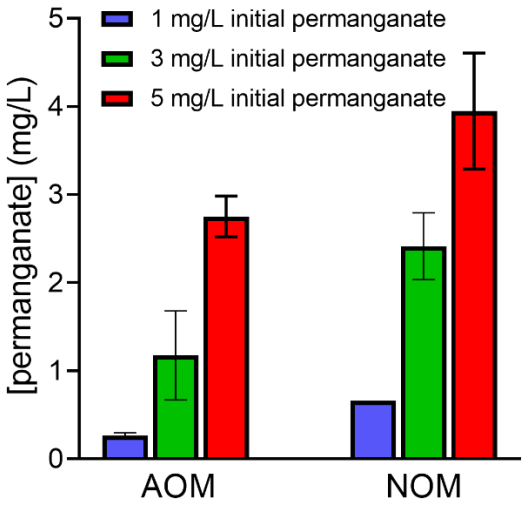

Figure S2.2. Residual permanganate concentrations (mg/L as KMnO4) after preoxidation of AOM or NOM for 3-d. All solutions are prepared in headspace-free amber vials, initially containing 5 mg-C/L AOM or 3 mg-C/L NOM and 10 mM phosphate buffer (pH 7).

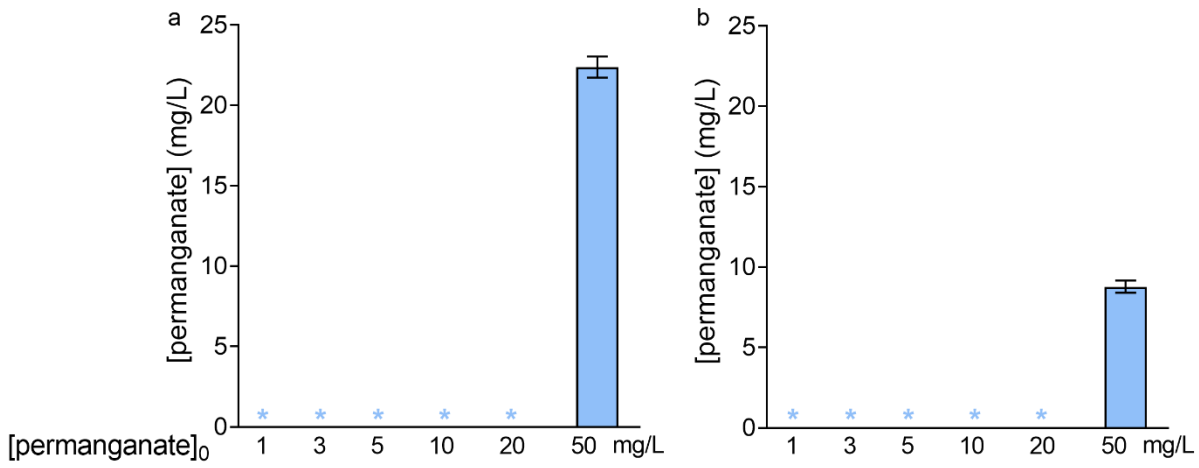

Figure S2.3. Residual permanganate concentrations (mg/L as KMnO4) after preoxidation of (a) tyrosine or (b) tryptophan for 3-d. All solutions are prepared in headspace-free amber vials, initially containing (a) 3.2 mg-C/L tyrosine or (b) 4.0 mg-C/L tryptophan (i.e., both 30 µM) and 10 mM phosphate buffer (pH 7). Data labeled with asterisks (*) indicates permanganate at concentrations below the level of the method detection limit (i.e., 0.14 mg/L).

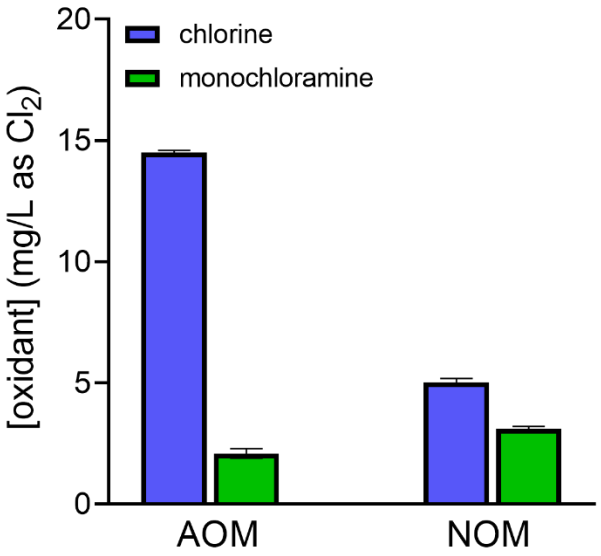

Figure S2.4. Consumption of chlorine or monochloramine concentrations (both mg/L as Cl2) during disinfection of AOM or NOM (no preoxidation). All solutions are prepared in headspace-free amber vials, initially containing 5 mg-C/L AOM or 3 mg-C/L NOM and 10 mM phosphate buffer (pH 7). The initial chlorine concentration was 15 mg/L and the initial monochloramine concentration was 4 mg/L. Error bars represent the standard deviation of triplicate experiments.

Chapter 3: Halogen radicals contribute to the halogenation and degradation of chemical additives used in hydraulic fracturing

This chapter is adapted from Chen, M.; Rholl, C. A.; He, T.; Sharma, A.; Parker, K. M. Halogen Radicals Contribute to the Halogenation and Degradation of Chemical Additives Used in Hydraulic Fracturing. *Environ. Sci. Technol.* **2021**, 55(3) 1545–1554.

3.1 Abstract

In hydraulic fracturing fluids, the oxidant persulfate is used to generate sulfate radicals to break down polymer-based gels. However, sulfate radicals may be scavenged by high concentrations of halides in hydraulic fracturing fluids, producing halogen radicals (e.g., $Cl^{\bullet}$, $Cl_2^{\bullet-}$, $Br^{\bullet}$, $Br_2^{\bullet-}$, $BrCl^{\bullet-}$). In this study, we investigated how halogen radicals alter the mechanisms and kinetics of the degradation of organic chemicals in hydraulic fracturing fluid. Using a radical scavenger (i.e., isopropanol), we determined that halogenated products of additives cinnamaldehyde (i.e., α-chlorocinnamaldehyde and α-bromocinnamaldehyde) and citrate (i.e., trihalomethanes) were generated via a pathway involving halogen radicals. We next investigated the impact of halogen radicals on cinnamaldehyde degradation rates. The conversion of sulfate radicals to halogen radicals may result in selective degradation of organic compounds. Surprisingly, we found that addition of halides to convert sulfate radicals to halogen radicals did not result in selective degradation of cinnamaldehyde over other compounds (i.e., benzoate, guar), which may challenge the application of radical selectivity experiments to more complex molecules. Overall, we find that halogen radicals, known to react in advanced oxidative treatment

and sunlight photochemistry, also contribute to the unintended degradation and halogenation of additives in hydraulic fracturing fluids.

3.2 Introduction

Hydraulic fracturing currently accounts for a major fraction of U.S. domestic natural gas extraction and is projected to account for greater than 75% of natural gas production by 2050.[145] One environmental risk associated with energy production from hydraulic fracturing is the formation of hazardous waste fluids (e.g., flowback and produced water) containing the chemical additives used in hydraulic fracturing operations, the chemical species originating from the shale itself (e.g., halides), and the products of chemical transformation occurring downhole.[146–149] Halogenated transformation products have raised particular concern due to their toxicity and persistence.[14,150–153] Recent studies have revealed dozens of halogenated organic compounds in hydraulic fracturing flowback and produced water, including halogenated benzenes, pyrans, alkanes, acetones, alcohols, and carboxylic acids.[154–157] Laboratory experiments simulating hydraulic fracturing conditions also demonstrated the halogenation of cinnamaldehyde, a commonly used corrosion inhibitor in hydraulic fracturing operation,[158,159] and citrate,[159] a known trihalomethane precursor[159–161] and widely used complexing agent in hydraulic fracturing fluid.[149,162] However, remaining uncertainties in the mechanisms contributing to the formation of halogenated compounds in hydraulic fracturing fluids challenge direct action to reduce this hazard.

In saline waters in the natural and engineered environment, halogen radicals (i.e., $Cl^{\bullet}$, $Br^{\bullet}$, $Cl_2^{\bullet-}$, $BrCl^{\bullet-}$, $Br_2^{\bullet-}$) are important oxidants that may contribute to halogenation.[8] Halogen radicals are produced when other radicals (e.g., hydroxyl radical or $^{\bullet}OH$; sulfate radical or $SO_4^{\bullet-}$) are scavenged by halides (e.g., Cl^-, Br^-).[8] This so-called conversion of $^{\bullet}OH$ and $SO_4^{\bullet-}$ to halogen radicals alters both reaction kinetics and mechanisms.[8] Both $^{\bullet}OH$ and $SO_4^{\bullet-}$ are relatively non-

selective oxidants, reacting with most organic compounds with near-diffusion-limited rate constants.[5,6] In contrast, halogen radicals (except for $Cl^{\bullet}$) are more selective oxidants.[8] They react with certain organic compounds (e.g., alkenes, aromatics, organothiols) with high rate constants (i.e., k=10^6-10^{10} $M^{-1}s^{-1}$) and react with other organic compounds (e.g., aliphatic molecules) with much lower rate constants (i.e., k=10^3-10^6 $M^{-1}s^{-1}$).[8] Consequently, the conversion of $^{\bullet}OH$ or $SO_4^{\bullet-}$ to halogen radicals decreases the degradation rate of certain organic compounds[163–165] and increases the degradation rate of others[163,166,167] in advanced oxidative treatment of brines and other saline waters. In sunlit seawater, the presence of halogen radicals accelerates the transformations of certain pollutants and biogeochemically relevant compounds.[34–40] In addition to altering reaction rates, halogen radicals also alter reaction mechanisms by enabling halogenation both directly and indirectly. Directly, halogen radicals add to the structure of certain aromatic[41] and olefinic molecules.[41,42] Indirectly, halogen radicals react via termination reactions to generate other halogenating agents (i.e., hypohalous acid),[43–49,124,168,169] which react with organics through substitution[50–52] or addition.[50]

Although the role of halogen radicals in the degradation and halogenation of additives in hydraulic fracturing fluid has not yet been investigated, there are two primary reasons to suspect that they may be involved in these reactions. Firstly, hydraulic fracturing fluids frequently have even higher halide concentrations (e.g. median Cl^- and Br^- concentrations up to 4.6 M and 5.0 mM, respectively)[170] than seawater or brines previously shown to be conducive to halogen radical formation.[34,38,163–165,167] Secondly, oxidative breakers (e.g., persulfate, $S_2O_8^{2-}$) are widely used to generate radicals (in particular $SO_4^{\bullet-}$) at high temperatures (i.e., 40-100°*C)*[170] to break down polymer gels (i.e., guar).[53,54] The use of persulfate as an oxidative breaker is associated with the formation of halogenated products in hydraulic fracturing fluids,[156–159] and water treatment with

$SO_4^{\bullet-}$ in the presence of halides can lead to the halogenation of organic compounds.[171–174] Notably, $SO_4^{\bullet-}$ generated from thermally activated persulfate is likely to generate halogen radicals because it can be scavenged directly by either Cl^- or Br^- (Eq. 3.1-3.2[175,176]). In comparison, halogen radical formation from $^{\bullet}OH$ is limited by the rapid reverse reaction of the intermediate $ClOH^{\bullet-}$ (Eq. 3.3-3.4), which limits its accumulation.[177] Consequently, the formation of halogen radicals from $^{\bullet}OH$ scavenging is dependent on reactions with Br^- in most environmental systems (Eq. 3.5-3.6).[8,178–180] As Cl^- is much more abundant than Br^- in most environmental waters including hydraulic fracturing fluids, radical reactions involving $SO_4^{\bullet-}$, including reactions resulting from the use of persulfate in hydraulic fracturing fluids, are more susceptible to halide scavenging than those involving $^{\bullet}OH$.[164]

$$SO_4^{\bullet-} + Cl^- \rightarrow Cl^{\bullet} + SO_4^{2-} \qquad k_1 = 2.5\times10^8\ M^{-1}s^{-1}\ [175] \tag{3.1}$$

$$SO_4^{\bullet-} + Br^- \rightarrow Br^{\bullet} + SO_4^{2-} \qquad k_2 = 3.5\times10^9\ M^{-1}s^{-1}\ [176] \tag{3.2}$$

$$^{\bullet}OH + Cl^- \rightarrow ClOH^{\bullet-} \qquad k_{3,f} = 4.3\times10^9\ M^{-1}s^{-1}, [177]\ k_{3,r} = 6.1\times10^9\ s^{-1} [177] \tag{3.3}$$

$$ClOH^{\bullet-} + H^+ (+ Cl^-,\ Br^-) \rightarrow Cl^{\bullet}\ (\text{or } Cl_2^{\bullet-},\ BrCl^{\bullet-}) + H_2O \tag{3.5}$$

$$^{\bullet}OH + Br^- \rightarrow BrOH^{\bullet-} \qquad k_{4,f} = 1.1\times10^{10}\ M^{-1}s^{-1}, [178]\ k_{4,r} = 3.3\times10^7\ s^{-1} [178] \tag{3.4}$$

$$BrOH^{\bullet-} + H^+ (+ Cl^-,\ Br^-) \rightarrow Br^{\bullet}\ (\text{or } BrCl^{\bullet-},\ Br_2^{\bullet-}) + H_2O \tag{3.6}$$

The goal of this work was to evaluate the processes that contribute to the degradation and potential halogenation of chemical additives in hydraulic fracturing fluids. Specifically, we investigated the halogenation of additives including cinnamaldehyde and citrate, which were previously shown to be the precursors of halogenated compounds in simulated hydraulic fracturing fluid.[158,159] We firstly hypothesized that the halogenation of cinnamaldehyde and citrate occurs through a radical-mediated pathway in the presence of halides and persulfate.[8] After testing the involvement of radicals in halogenation, we next investigated the radical initiation and propagation

mechanisms that dominate under conditions relevant to hydraulic fracturing. Finally, we tested how the conversion of $SO_4^{\bullet-}$ to halogen radicals impacted radical selectivity. We hypothesized that the generation of halogen radicals would result in rapid degradation of cinnamaldehyde due to their apparent role in its halogenation, while reducing the rate of reactions between radicals and other solution components (i.e., guar). We discussed the implications of expanding the role of halogen radicals beyond reactions in other high salinity waters to halogenation and degradation reactions in hydraulic fracturing.

3.3 Materials and Methods

3.3.1 Chemicals and reagents

In this work, all chemicals were used as received (**Table S3.1).** All experimental solutions were prepared in Milli-Q^R water.

3.3.2 Investigation of additive halogenation mechanisms

To investigate the halogenation of organic additives under physicochemical conditions relevant to hydraulic fracturing, we measured the formation of halogenated products of cinnamaldehyde (α-chlorocinnamaldehyde and α-bromocinnamaldehyde)[158,159] by high pressure liquid chromatography (HPLC) and citrate (four trihalomethanes)[159] by gas chromatography – mass spectrometry (GC-MS). In a typical experiment, solutions were prepared with halides, organic substrates, and phosphate buffer at indicated concentrations. Indicated experiments also included additional chemicals common to hydraulic fracturing fluid (**Table S3.2**). All experiments were performed in a water bath that was preheated to 80 °C to match the temperature commonly occurring in actual hydraulic fracturing practice (median temperature 77 °C).[170] Specific

experimental and analytical procedures of experiments with cinnamaldehyde or citrate are described in **Section 3.5.1** and **Section 3.5.2**, respectively.

3.3.3 Persulfate loss rate constant determination

To investigate the radical initiation process under conditions relevant to hydraulic fracturing, we determined the first order rate constant of persulfate loss by measuring the decreasing persulfate concentration over the experimental time. Solutions (10 mL) containing 10 mM phosphate buffer (at the experimental pH) and any additional constituents (e.g., salts, organic compounds) were first heated until the temperature was stabilized. A small volume (0.1 mL) of 0.1 M persulfate stock was spiked in the sample to achieve an initial concentration of 1 mM persulfate. The persulfate concentration was measured periodically using a version of a previous method modified to accommodate smaller volumes.[181] Specifically, a 25 µL aliquot of the sample was transferred to 2 mL 100 mM phosphate buffer (pH 6.85) followed by the addition of 0.5 mL potassium iodide (6 M) solution. The remaining persulfate concentration was then calculated from a standard curve using absorption at 352 nm measured on a Varian Cary 50 Bio UV-Vis Spectrophotometer. Additional constituents were confirmed to not interfere with the persulfate measurement (**Figure S3.1**). The limit of detection (LOD) of persulfate detected by this method is 0.03 mM.

3.3.4 Effect of radical speciation on the kinetics of organic degradation

To investigate the kinetics of additive degradation in hydraulic fracturing fluids, we first measured the degradation rates of organic compounds mixed together in solutions under conditions relevant to hydraulic fracturing. Solutions (25 mL) were prepared in 40 mL amber vials with 50 µM of each organic compound (i.e., *para*-hydroxybenzoate and benzoate, cinnamaldehyde and benzoate), salts selected for the experiment condition, and 10 mM phosphate buffer (pH 7).

The reaction was initiated and quenched as described in experiments investigating cinnamaldehyde halogenation. Over the duration of 10 min, 6 aliquots (each 0.5 mL) were collected every 2 min into 2 mL amber vial and analyzed by HPLC (**Section 3.5.3**). Additional experimental procedures for the measurement of cinnamaldehyde degradation in the presence of guar are shown in **Section 3.5.4**.

3.3.5 Statistical analysis

All experiments were conducted in two replicates. Errors in concentrations represent the range of two replicate measurements. Errors in degradation rate constants represent the standard error of the slope obtained from linear regression.

3.4 Results and Discussion

3.4.1 Radical involvement in halogenation of cinnamaldehyde

We used cinnamaldehyde to investigate the mechanisms leading to halogenation in the presence of persulfate under physicochemical conditions relevant to hydraulic fracturing (i.e., pH 7, 80°C, 1.4 M Cl^-, 6 mM Br^-). We selected cinnamaldehyde because it had previously been shown to produce halogenated products, α-chlorocinnamaldehyde and α-bromocinnamaldehyde, in simulated hydraulic fracturing fluid.[158]

In our experiments, cinnamaldehyde (initially present at 500 μM) was degraded with a pseudo-first order rate constant of $7.7(\pm0.3)\times10^{-5}$ s^{-1} (**Figure 3.1a**). After 2 h, 220±30 μM of cinnamaldehyde was degraded, while 1.6±0.1 μM α-chlorocinnamaldehyde was produced over the same period (**Figure 3.1b**). The resultant molar product yield of α-chlorocinnamaldehyde (0.7±0.2%, **Figure S3.2**) is about 2-fold lower than that previously reported to occur (1.2±0.1%) at similar conditions (pH 7, 60°*C*, 1.4 M Cl^-, 6 mM Br^-*)*.[158] In addition, in our experiments, α-

bromocinnamaldehyde concentration remained below the LOD (0.07 μM, **Figure 3.1b**) over the 2 h time frame, whereas the molar yield of α-bromocinnamaldehyde had been previously reported as 6.4±0.4% (pH 7).[158] We hypothesized that the lower product yield in our experiment resulted from the lower initial concentration of cinnamaldehyde in our study (0.5 mM) in comparison to the prior study (5 mM).[158] The lower initial concentration of cinnamaldehyde may have favored product degradation by oxidants during the experiment. To investigate the impact of initial cinnamaldehyde concentration on halogenation yield, we decreased the initial cinnamaldehyde concentration in our experiment by 10-fold to 0.05 mM. Our results showed that the α-chlorocinnamaldehyde concentration reached a maximum after 30 min, but then decreased to below the LOD (0.08 μM) after 2 h (**Figure S3.3**). After 30 min, reactions appeared to degrade α-chlorocinnamaldehyde faster than it could be generated since less than 20% of the initial cinnamaldehyde concentration remained (**Figure S3.3**). In this experiment, α-bromocinnamaldehyde was never detected (**Figure S3.3**). Because bromo-substituted molecules may react more quickly with key oxidants (e.g., halogen radicals) than chloro-substituted molecules,[8] the rapid degradation of α-bromocinnamaldehyde under our experimental conditions may account for our inability to detect it.

Because we sought to evaluate the mechanisms leading to both α-chlorocinnamaldehyde and α-bromocinnamaldehyde simultaneously, we selected to increase Br^- concentration to favor α-bromocinnamaldehyde formation from cinnamaldehyde. When the Br^- concentration was increased 10-fold to 60 mM, the rate constant of cinnamaldehyde degradation increased by ~50% to $1.12(\pm0.04)\times10^{-4}$ s^{-1} (**Figure 3.1a**). As cinnamaldehyde degraded, both α-chlorocinnamaldehyde and α-bromocinnamaldehyde were produced, resulting in final concentrations of 1.5±0.3 μM and 2.1±0.2 μM, respectively, over the 2 h experiment (**Figure**

3.1b). Overall, the molar yield of α-chlorocinnamaldehyde at 2 h slightly decreased from 0.7±0.2% in the presence of 6 mM Br^- to 0.5±0.1% in the presence of 60 mM Br^- (**Figure S3.2**). In the 60 mM Br^- solution, α-bromocinnamaldehyde formed at a similar yield (0.7±0.1% after 2 h) (**Figure S3.2**).

To investigate the involvement of radicals in the halogenation of cinnamaldehyde, we next evaluated α-chloro- and α-bromocinnamaldehyde formation in the presence of isopropanol. Isopropanol effectively scavenges both $SO_4^{\bullet-}$ (i.e., $k_{isopropanol,SO4^{\bullet-}}=8.0\times10^7\ M^{-1}s^{-1}$)[6] and halogen radicals (e.g., $k_{isopropanol,Cl2^{\bullet-}}=1.2\times10^5\ M^{-1}s^{-1}$,[41] $k_{isopropanol,Br^{\bullet}}=6.6\times10^6\ M^{-1}s^{-1}$).[179] Our results showed that, in the presence of 50 mM isopropanol, the concentrations of both α-chlorocinnamaldehyde and α-bromocinnamaldehyde were below their respective LOD throughout the 2 h experiment (**Figure 3.1b**). The complete reduction in measurable halogenation indicated that radicals are intermediates in the halogenation of cinnamaldehyde.

We hypothesized that the radical intermediates involved in cinnamaldehyde halogenation were halogen radicals. Therefore, we calculated the expected fraction of $SO_4^{\bullet-}$ converted to halogen radicals in the above experimental solutions. The calculation showed that, at both halide concentrations (i.e., 1.4 M Cl^-, 6 or 60 mM Br^-) and with or without 50 mM isopropanol, almost all (> 99%) of the $SO_4^{\bullet-}$ is scavenged by halides rather than other constituents (**Tables S3.3-S3.5**). Although bimolecular rate constants between halogen radicals and cinnamaldehyde are unavailable in literature, available rate constants for reactions of halogen radicals with other aromatic and olefinic molecules span the same range as those for reactions with isopropanol (i.e., 10^5-$10^{10}\ M^{-1}s^{-1}$).[8] Consequently, it is feasible that 50 mM isopropanol (two orders of magnitude higher in concentration than cinnamaldehyde) could scavenge halogen radicals under these conditions.

Although the production of both α-chlorocinnamaldehyde and α-bromocinnamaldehyde was prevented by the addition of 50 mM isopropanol, the pseudo-first order rate constant of cinnamaldehyde degradation only decreased by about 50% relative to the isopropanol-free control (**Figure 3.1a**) and was not decreased further by the addition of a 5-fold higher isopropanol concentration (**Figure S3.4**). Consequently, the remaining degradation of cinnamaldehyde was attributed to other oxidants that were not scavenged by isopropanol. We evaluated the potential for non-radical reactions to contribute to cinnamaldehyde loss in subsequent experiments.

To provide additional evidence that the halogenation of cinnamaldehyde proceeded through a radical-mediated pathway, we evaluated the potential contribution of an alternative non-radical pathway to halogenation (**Section 3.5.5**). Specifically, since persulfate oxidizes I^- to produce I_2/HOI,[181] we investigated whether HOCl and HOBr[8] were generated by persulfate directly oxidizing Cl^- or Br^- and subsequently contribute to organic halogenation. Our experiments showed that while no HOCl was detected above its LOD (23 μM) upon the addition of 1.4 M Cl^- to 1 mM persulfate, 120±4 μM HOBr was produced when 60 mM Br^- was added to 1 mM persulfate (pH 7, 2 h, 80°C, **Figure S3.5**). However, when 50 mM isopropanol was added, no HOBr was detected above its lowest standard concentration (13 μM) (pH 7, 2 h, 80°C, **Figure S3.5**). Since isopropanol reacts very slowly with HOBr (i.e., $k_{HOBr,isopropanol}<3.9\times10^{-4}$ $M^{-1}s^{-1}$),[182] HOBr generated in the absence of isopropanol was attributed to halogen radical recombination rather than the non-radical pathway. Consequently, halogenation of cinnamaldehyde is most likely to occur only via a radical-mediated pathway under physicochemical conditions relevant to hydraulic fracturing.

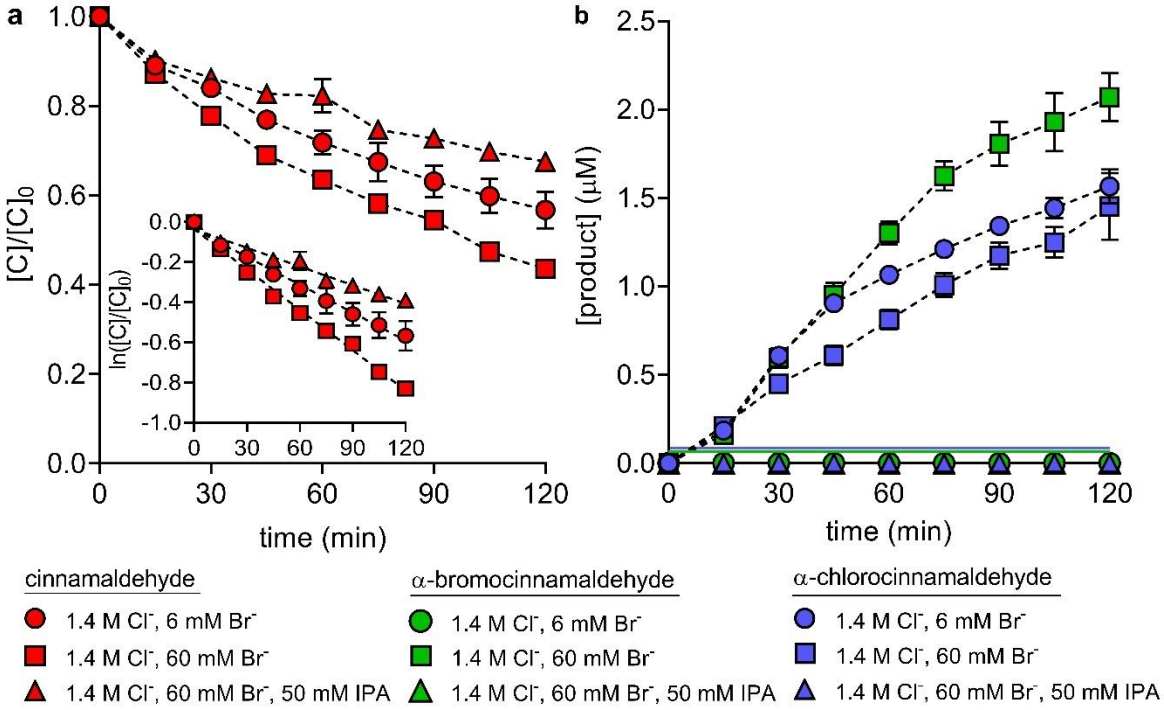

Figure 3.1. (**a**) Cinnamaldehyde degradation and (**b**) formation of α-bromocinnamaldehyde and α-chlorocinnamaldehyde in the presence of persulfate, halides and isopropanol (IPA). Experiments were conducted at 80°C in solutions initially containing 1 mM persulfate and 0.5 mM cinnamaldehyde at pH 7 buffered with 10 mM phosphate buffer. Green and blue lines in (**b**) represent the limit of detection of α-bromocinnamaldehyde (0.07 μM) and α-chlorocinnamaldehyde (0.08 μM), respectively.

3.4.2 Radical involvement in formation of trihalomethanes

We also hypothesized that halogenation of citrate to generate trihalomethanes[159–161] is mediated by halogen radicals in hydraulic fracturing fluid. Thus, we next investigated the role of halogen radicals in the halogenation of citrate under physicochemical conditions relevant to hydraulic fracturing.[159] Our results showed that in the presence of 1.4 M Cl^- and 60 mM Br^-,

$2.4(\pm0.3)\times10^{-4}$ μM dichlorobromomethane, $3.7(\pm0.4)\times10^{-3}$ μM dibromochloromethane, and $9.3(\pm0.2)\times10^{-3}$ μM tribromomethane were produced from 0.05 mM citrate over 2 h (pH 7, 80°C, **Figure 3.2a**). Moreover, the addition of 50 mM isopropanol reduced the levels of dichlorobromomethane and dibromochloromethane to below their lowest standard concentrations (**Table S3.6**) and reduced the level of tribromomethane more than 99% to 5.3×10^{-5} μM (**Figure 3.2a**), indicating that the formation of trihalomethanes depends on halogen radicals as intermediates.

Next, we tested whether halogen radicals contribute to the formation of trihalomethanes in solutions including additional common chemical components used in hydraulic fracturing fluids (**Table S3.2**). We observed that $2.2(\pm0.3)\times10^{-4}$ μM dichlorobromomethane, $2.8(\pm0.4)\times10^{-4}$ μM dibromochloromethane, and $2.4(\pm0.4)\times10^{-4}$ μM tribromomethane were produced over 2 h (**Figure 3.2b**). Compared to trihalomethane levels produced in the absence of major hydraulic fracturing fluid components (**Figure 3.2a**), the concentrations of dibromochloromethane and tribromomethane formed in the presence of major hydraulic fracturing components were orders of magnitude lower, likely due to the scavenging of halogen radicals by these components. Furthermore, when 50 mM isopropanol was added to the mixture, all trihalomethanes were not measurable (**Figure 3.2b**). The elimination of measurable trihalomethanes indicate that halogen radicals are the key intermediates in the halogenation of citrate even in the presence of major hydraulic fracturing fluid components.

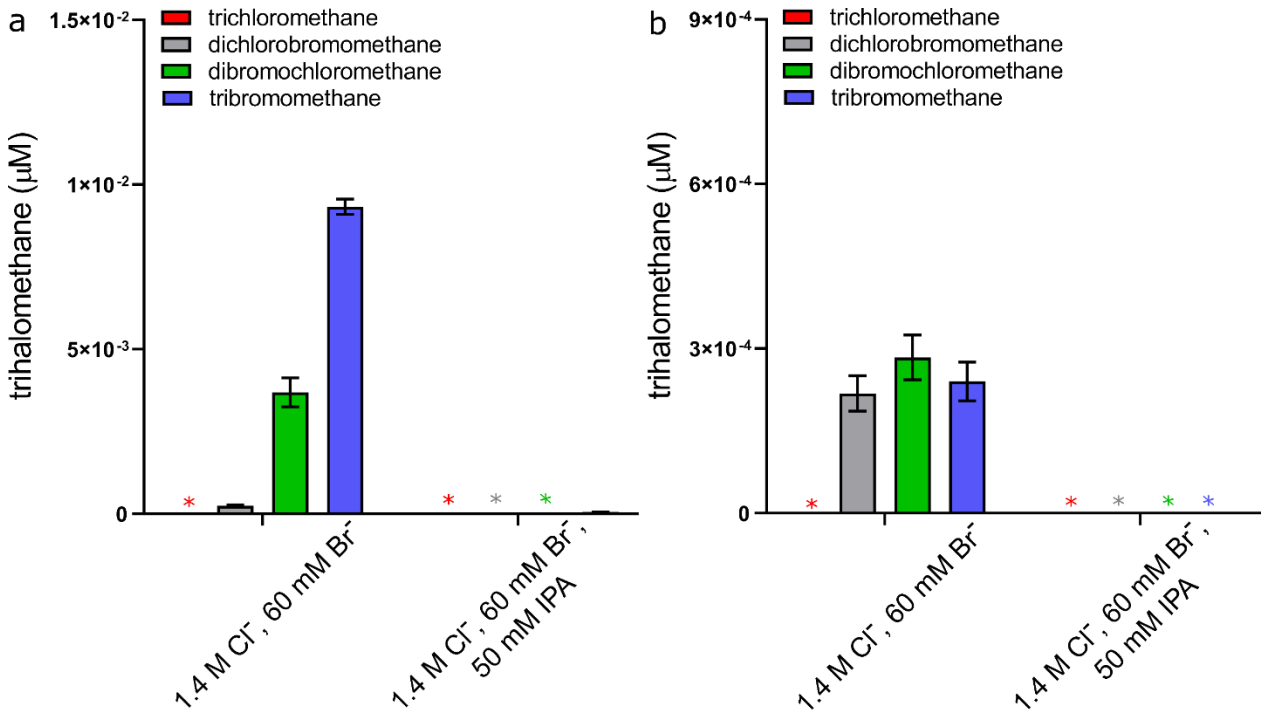

Figure 3.2. Trihalomethane formation from citric acid for 2 h at 80°C. (a) Solutions initially contained 200 mg/L guar, 5 mM persulfate and 0.05 mM citrate at pH 7 buffered with 10 mM phosphate buffer in MilliQ water. (b) In addition to the constituents included in experiments presented in (a), these solutions also contained 200 mg/L guar, 212 mg/L petroleum distillate, 47.2 mg/L citrus terpenes, 280 mg/L propylene glycol, 9.6 mg/L, 400 mg/L borate and 200 mg/L sodium carbonate. Halide and isopropanol (IPA) concentrations are as indicated. Red, grey, green, and blue asterisk signs (*) represent below the lowest standard concentrations of trichloromethane (8.4×10^{-5} µM), dichlorobromomethane (6.1×10^{-5} µM), dibromochloromethane (4.8×10^{-5} µM) and tribromomethane (4.0×10^{-5} µM).

3.4.3 Initiation and Propagation of Radical Species.

Our above results demonstrate that halogen radicals are likely intermediates in organic chemical halogenation in hydraulic fracturing fluid. Consequently, the processes that lead to the

initiation and propagation of radicals in hydraulic fracturing fluids are anticipated to influence the formation of these halogenated products. We expected the primary radical initiation pathway to be thermal activation of persulfate[183–185] and that this pathway would also determine the measured persulfate loss rate (Eq. 7).[186] In addition, we considered that persulfate loss can also occur through additional pathways that contribute to either radical initiation (e.g., base catalysis, Eq. 3.8-3.9)[187] or radical propagation (e.g., Eq. 3.10)[188–190] that influence the type and concentrations of radicals in solution. We investigated the occurrence of these additional initiation and propagation reactions pathways alongside thermal activation of persulfate under conditions relevant to hydraulic fracturing to clarify how solution constituents affect radical-mediated reactions.

$$S_2O_8^{2-} \xrightarrow{\Delta} 2SO_4^{\bullet-} \tag{3.7}$$

$$S_2O_8^{2-} + 2H_2O \xrightarrow{OH^-} HO_2^- + 2SO_4^{2-} + 3H^+ \tag{3.8}$$

$$S_2O_8^{2-} + HO_2^- \longrightarrow SO_4^{\bullet-} + SO_4^{2-} + H^+ + O_2^{\bullet-} \tag{3.9}$$

$$S_2O_8^{2-} + SO_4^{\bullet-} \longrightarrow S_2O_8^{\bullet-} + SO_4^{2-} \tag{3.10}$$

We first investigated the effect of temperature on persulfate loss rate at pH 7 (**Figure 3.3a**). We determined that increasing the temperature from 37 to 95°C resulting in the persulfate loss rate increasing 4000-fold from $1.300(\pm0.002)\times10^{-7}$ s^{-1} to $5.10(\pm0.03)\times10^{-4}$ s^{-1}. When fitted to the Arrhenius equation, we determined the activation energy for persulfate thermal activation to be 148±5 kJ/mol at pH 7 (**Figure 3.3a**), which is slightly higher than the previously reported value (119-129 kJ/mol).[191] We also investigated how the increased radical production at higher temperature affects $SO_4^{\bullet-}$ concentrations by measuring the pseudo-first order rate constant for the degradation of benzoate, which is reported to react rapidly with $SO_4^{\bullet-}$ ($k_{benzoate,SO4^{\bullet-}}=1.2\times10^9$ $M^{-1}s^{-1}$).[192] We determined that the pseudo-first order rate of benzoate degradation increased 1000-fold from 37 to 95°C (**Figure S3.6**). The temperature may have had less of an effect on benzoate

degradation than persulfate activation because the rates of reactions leading to $SO_4^{\bullet-}$ loss may have also increased at higher temperatures. Faster rates of $SO_4^{\bullet-}$ loss would partially offset the impact of higher $SO_4^{\bullet-}$ production rates at higher temperature on $SO_4^{\bullet-}$ steady-state concentrations, which determine the rate constant of benzoate degradation.

An alternative radical initiation pathway to persulfate thermal activation is persulfate base activation.[183,187,193] Specifically, Furman et al. proposed that hydroxide ion (OH^-) catalyzes the hydrolysis of a persulfate molecule to produce a hydroperoxyl anion (HO_2^-) (Eq. 8), which then reacts with another persulfate molecule via one-electron transfer to generate a $SO_4^{\bullet-}$ (Eq. 9).[187] We investigated the potential for base activation to contribute to persulfate loss by measuring the persulfate loss rate over a range of temperature (37 to 95°C) and pH values (2–12) (**Figure 3.3a**). Surprisingly, persulfate loss rate did not statistically change across all three pH conditions at each temperature (one-way analysis of variance (ANOVA), $p > 0.05$, **Table S3.7**), contradicting prior reports that OH^- contributes to persulfate activation.[187,193] The reaction of OH^- with persulfate is likely too slow[187] to affect overall persulfate loss rate at the temperatures used in our experiments (**Section 3.5.6**). In addition, the values of activation energy of persulfate loss do not strictly increase at a higher pH (i.e., 123±4, 148±5, and 130±10 kJ/mol at pH 2, 7, and 12, respectively), which contradicts previous literature reporting that the activation energy of persulfate increases from acidic (100–116 kJ/mol)[191] to basic (134–139 kJ/mol)[191] pH conditions. Overall, our results indicated that base activation is negligible as compared to thermal activation at temperatures relevant to hydraulic fracturing.

Although thermal activation appears to be the only important radical initiation reaction in our system, additional propagation mechanisms can also contribute to persulfate loss and may be influenced by solution conditions. Organic compounds have been shown to promote persulfate

decomposition through propagation reactions involving organic radicals.[184,194,195] However, we determined that neither benzoate nor cinnamaldehyde addition (both 0.5 mM) significantly changed the persulfate loss rate at 80°C (**Figure 3.3b**). A possible explanation is that the higher temperature of our experiments led to faster thermal activation of persulfate, such that these organic species at these relatively low concentrations had no measurable additional impact on persulfate loss rate. However, when we included 50 mM isopropanol, the persulfate loss rate constant increased by ~3-fold (**Figure 3.3b**). In this case, isopropanol appears to promote propagation reactions involving organic radicals. These organic radicals may also contribute to cinnamaldehyde loss absent the concurrent formation of halogenated products in the presence of 50 mM isopropanol (**Figure 3.1**).

Halides are also expected to influence propagation reactions by converting $SO_4^{\bullet-}$ to halogen radicals (Eq. 1-2).[175,176] We hypothesized that halogen radicals react more slowly with persulfate than $SO_4^{\bullet-}$ (Eq. 10, k~10^5 $M^{-1}s^{-1}$),[188–190] such that persulfate loss would decrease upon addition of halides to the solution due to scavenging of $SO_4^{\bullet-}$ to form halogen radicals. We determined that at 80°C, the addition of 1.4 M Cl^- and 6 mM Br^- to solution decreased the persulfate loss rate by 30±6% relative to an ionic strength control (1.4 M ClO_4^-) (**Figure 3.3b**). Consequently, the conversion of $SO_4^{\bullet-}$ to halogen radicals in the presence of halides appears both to alter the mechanisms of organic compound transformation by promoting halogenation and to reduce radical propagation mechanisms leading to loss of persulfate under conditions relevant to hydraulic fracturing.

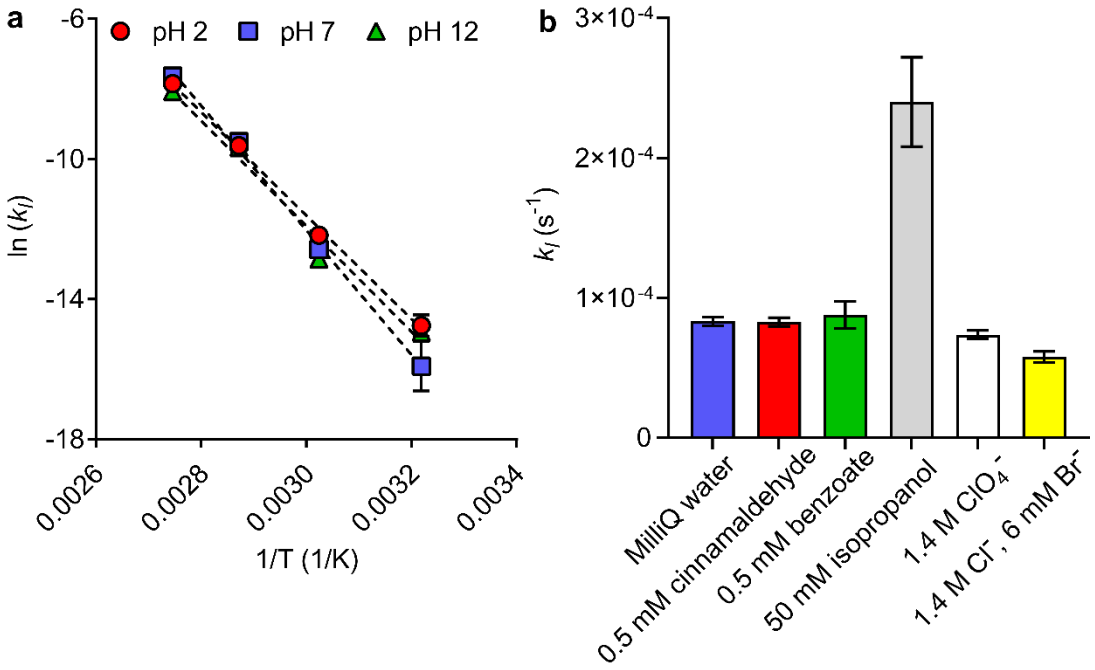

Figure 3.3. Persulfate loss rate constant (k_I, s^{-1}) (**a**) under varying physicochemical conditions (i.e., temperature, pH) relevant to hydraulic fracturing and (**b**) in the presence of solution constituents (i.e., organic compounds, halides; all at 80°C, pH 7). All solutions initially contained 1 mM initial persulfate and 10 mM phosphate buffer (at pH 2, 7, or 12). The experimental durations were 96, 23, 5, and 2 h for 37, 60, 80, 95°C, respectively (**a**), and 2.5 h (**b**).

3.4.4 Effect of radical speciation on degradation kinetics of organic compounds

In addition to enabling halogenation and suppressing persulfate loss, the conversion of $SO_4^{\bullet-}$ to halogen radicals is also expected to alter the kinetics of organic transformation. Except for $Cl^{\bullet}$, halogen radicals typically have lower bimolecular rate constants with organic compounds,[8] frequently resulting in slower degradation rates in halogen radical-dominated systems than systems in which $^{\bullet}OH$ or $SO_4^{\bullet-}$ dominate.[163,164,167] However, the lower reactivity of halogen radicals also can result in decreased scavenging rate constants (e.g., with persulfate, other organic compounds, natural organic matter) – leading to higher steady-state radical concentrations and faster

degradation of certain molecules.[35,164,165] Previously, the conversion of $^{\bullet}OH$ and $SO_4^{\bullet-}$ to halogen radicals in UV/oxidant water treatment has been shown to result in the selective degradation of certain organic constituents over others in organic chemical mixtures.[164] In hydraulic fracturing fluid, the selectivity of halogen radicals may also result in the degradation of certain additives (e.g., cinnamaldehyde) over the degradation of polymer gel (i.e. guar).

We investigated the potential for conversion of $SO_4^{\bullet-}$ to halogen radicals to result in selective chemical degradation under physicochemical conditions relevant to hydraulic fracturing. We began by investigating the degradation rates of benzoate and *para*-hydroxybenzoate mixed in solution. We selected these compounds due to their known rate constants with $SO_4^{\bullet-}$[192] and some halogen radicals (i.e., $Cl_2^{\bullet-}$,[41] $Br_2^{\bullet-}$[196]) that occur at high concentrations in saline water.[8] We first measured the degradation rates of both compounds in solutions adjusted to high ionic strength (1.4 M) using ClO_4^- (**Figure 3.4a**). In these solutions, $SO_4^{\bullet-}$, which reacts with both organic species with comparable rate constants ($k_{benzoate,SO4^{\bullet-}}=1.2\times10^9\ M^{-1}s^{-1}$, $k_{para\text{-}hydroxybenzoate,SO4^{\bullet-}}=2.5\times10^9\ M^{-1}s^{-1}$),[192] is expected to be the dominant radical. Accordingly, benzoate and *para*-hydroxybenzoate were degraded at similar rates in the absence of halides due to the $SO_4^{\bullet-}$ serving as the dominant oxidant (**Figure 3.4a**).

The inclusion of 1.4 M Cl^- is expected to rapidly convert $SO_4^{\bullet-}$ to $Cl^{\bullet}$ (Eq. 1),[47] which then reacts with Cl^- again to produce $Cl_2^{\bullet-}$ ($k_{Cl^-,Cl^{\bullet}}=6.5\times10^9\ M^{-1}s^{-1}$).[180] Whereas $SO_4^{\bullet-}$ reacts with both benzoate and *para*-hydroxybenzoate at similar rate constants, $Cl_2^{\bullet-}$ reacts with benzoate ($k_{benzoate,Cl2^{\bullet-}}=2\times10^6\ M^{-1}s^{-1}$)[41] much more slowly than with *para*-hydroxybenzoate ($k_{para\text{-}hydroxybenzoate,Cl2^{\bullet-}}=2.8\times10^8\ M^{-1}s^{-1}$).[41] The inclusion of 1.4 M Cl^- resulted in the benzoate degradation rate constant decreasing by a factor of ~5 relative to the ionic strength control (**Figure 3.4a**), likely reflecting the conversion of $SO_4^{\bullet-}$ to $Cl_2^{\bullet-}$, which reacts slowly with benzoate. The reduced reaction

rate of radicals with benzoate in the presence of halides may lead to higher steady-state radical concentrations. Coupled with the comparable high rate constant of $Cl_2^{\bullet-}$ with *para*-hydroxybenzoate, we suspect that these elevated radical concentrations likely contributed to the increased rate of *para*-hydroxybenzoate degradation, which increased by a factor of ~2 relative to the ionic strength control (**Figure 3.4a**). Conversion of $SO_4^{\bullet-}$ to $Cl_2^{\bullet-}$ appears to result in the selective degradation of *para*-hydroxybenzoate over benzoate.

The addition of Br^- (6 mM) further increased the degradation rate of *para*-hydroxybenzoate, while simultaneously decreasing the degradation rate of benzoate (**Figure 3.4a**). We expect that the addition of bromide resulted in the formation of Br-containing halogen radicals (i.e., $Br^{\bullet}$,[176] $Br_2^{\bullet-}$,[179] $BrCl^{\bullet-}$)[8] that are more selective than their Cl-containing counterparts. While the rate constants for the reaction of *para*-hydroxybenzoate with Br-containing radicals (e.g., $k_{para\text{-}hydroxybenzoate,Br2^{\bullet-}}=2.3\times10^8\ M^{-1}s^{-1}$)[196] are comparable to the rate constants for its reaction with Cl-containing radicals,[41] we expect that the rate constants for the reaction of benzoate with Br-containing radicals, though not reported, are likely lower than the rate constants for its reaction with Cl-containing radicals. Consequently, we observed that halides occurring in hydraulic fracturing fluids appear to strongly favor the conversion of $SO_4^{\bullet-}$ to more selective halogen radicals under conditions relevant to hydraulic fracturing.

Next, we investigated the potential for conversion of $SO_4^{\bullet-}$ to halogen radicals to result in the selective degradation of certain hydraulic fracturing additives (e.g., cinnamaldehyde). We suspected that cinnamaldehyde, like *para*-hydroxybenzoate, would be selectively degraded by halogen radicals over benzoate when applied in the same solution since cinnamaldehyde appears to react via a radical mediated-pathway to generate halogenated products. Furthermore, we expected that its olefinic group may serve as a moiety that can react rapidly with halogen radicals.[8]

Surprisingly, the inclusion of 1.4 M Cl^- decreased the degradation rate constant of both cinnamaldehyde (by 41±4%) and benzoate (by 60±20%) relative to the ionic strength control (**Figure 3.4b**). Subsequent addition of 6 mM Br^- further decreased the degradation rate constant of cinnamaldehyde (by 74±3% relative to ionic strength control) but had no further impact on benzoate (**Figure 3.4b**). Our results are consistent with a previous study reporting that the degradation of 5 mM cinnamaldehyde was decreased by the addition of halides, though under different experimental conditions.[158]

The unexpected result that conversion of sulfate did not increase cinnamaldehyde degradation in the presence of benzoate challenged our expectation that halogen radicals would selectively react with cinnamaldehyde under conditions relevant to hydraulic fracturing. Specifically, we expected that halogen radicals generated in saline hydraulic fracturing fluids would preferentially react with cinnamaldehyde over other organic molecules, in particular guar. We selected guar, a widely used gelling agent used in hydraulic fracturing fluids,[149] because it is the primary target for $SO_4^{\bullet-}$ generated by persulfate activation in hydraulic fracturing.[53] In comparison to $SO_4^{\bullet-}$, we expected halogen radicals would be relatively slow to react with guar due to its aliphatic alcohol structure (i.e., k=10^2-10^5 $M^{-1}s^{-1}$).[41,197] The resultant decreased scavenging of halogen radicals by guar was expected to increase radical steady-state concentration and thereby increase the cinnamaldehyde degradation rate. However, the inclusion of 1 M Cl^- decreased the degradation rate of cinnamaldehyde in the presence of guar by 60±10% as compared to the ionic strength control (**Figure 3.4c**). Although these results are consistent with the decreased degradation rate of cinnamaldehyde in competition with benzoate, they contradict prior reports that conversion of non-selective radical to halogen radicals increase the degradation of certain

compounds by reducing radical loss to reaction with solution constituents (e.g., natural organic matter).[35,37]

Although the specific reason that halides reduce the degradation rate constant of cinnamaldehyde in competition with benzoate or guar remains unknown, the possible explanations may have important implications for studies on radical reaction kinetics and selectivity. Firstly, non-radical oxidants (e.g., persulfate) may contribute to a portion of the measured cinnamaldehyde degradation that is slowed upon the addition of halides. Oxidation by persulfate would be consistent with the observation that cinnamaldehyde degradation continues in the presence of the radical scavenger isopropanol (**Figure 3.1a**). However, we also observed that cinnamaldehyde (0.5 mM) did not increase the persulfate loss rate (**Figure 3.3b**), suggesting that the bimolecular rate constant between cinnamaldehyde and persulfate must be below 10^{-6} $M^{-1}s^{-1}$ (**Section 3.5.7**). Applying the initial persulfate concentration (1 mM), we find that reaction with persulfate must account for <0.002% of cinnamaldehyde degradation (**Figure 3.1a**) and is therefore insignificant.

An alternative explanation could be that cinnamaldehyde and benzoate (or guar) are not the primary radical scavengers in the solution. The expected increased differential in the rate constants for the degradation of a pair of organic compounds upon addition of halides (as observed for benzoate/*para*-hydroxybenzoate) requires that the organic compounds are the dominant sink for radicals in solution, such that the slower degradation of one compound upon $SO_4^{\bullet-}$ conversion to halogen radicals results in higher steady-state radical concentrations and faster degradation of the other compound. If cinnamaldehyde and its competitor are not exclusively the primary radical sinks, conversion of $SO_4^{\bullet-}$ to halogen radicals may reduce both compound's degradation rates while accelerating reactions with other unmeasured constituents (e.g. reaction products, inorganic species including buffers and persulfate). It is unlikely that reaction products became the primary

radicals sink during the experiment duration because the degradation of the compounds followed first order kinetics, indicating that the formation of reaction products over the experimental duration do not reduce radical concentrations and thereby alter cinnamaldehyde and benzoate degradation kinetics (**Section 3.5.8**). However, due to limitations in known bimolecular rate constants[8] between halogen radicals and other solution constituents, the effect of other unknown scavengers in the solution that are more competitive toward halogen radicals than cinnamaldehyde cannot be excluded.

Lastly, cinnamaldehyde might be particularly susceptible to reactions with other radical species (e.g., organic radicals) that significantly increase its overall degradation rate in solution. Reducing the abundance of radicals formed from the reactions involving $SO_4^{\bullet-}$ may result in decreased cinnamaldehyde degradation rates. Reactions with organic radicals produced upon the reaction of isopropanol with $SO_4^{\bullet-}$ may also contribute to the continued cinnamaldehyde degradation in the presence of isopropanol (**Figure 3.1a**). These possible explanations suggest that radical selectivity experiments used herein and in literature may develop more complexity when expanded to include molecules of additional structural classes due to the potential for these unintended effects.

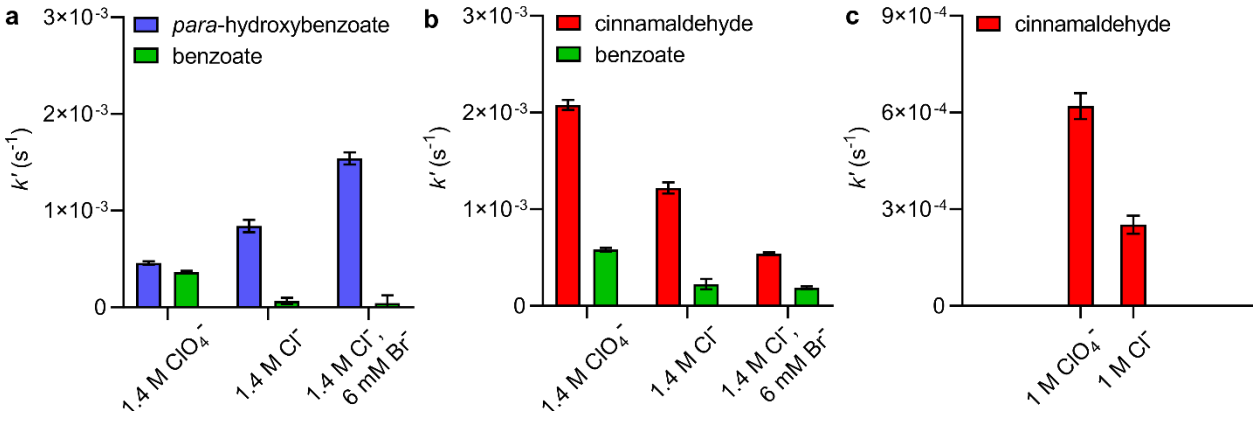

Figure 3.4. Pseudo-first order degradation rate constants (*k'*) for organic compound pairs: (**a**) *para*-hydroxybenzoate and benzoate and (**b**) cinnamaldehyde and benzoate together in solution in the presence of perchlorate (ClO_4^-) or halides (Cl^- and Br^-). Solutions initially contained 1 mM persulfate and each organic compound (50 μM) indicated at pH 7 buffered with 10 mM phosphate buffer. The rate constant for cinnamaldehyde (15 μM) was measured in the presence of 500 mg/L guar and perchlorate (ClO_4^-) or chloride (Cl^-) (**c**). The degradation rate of guar was not measured in the experiments. The solutions initially contained 1 mM persulfate at pH 6.5 buffered with 1 mM phosphate buffer. All experiments were conducted at 80°C for 10 min.

3.5.5 Environmental implications

Our work demonstrates that, even in the presence of high organic content that may scavenge radicals, halogenation of specific organic compounds to produce halogenated compounds still occurs via a pathway mediated by halogen radicals. Consequently, our results demonstrate the first experimental evidence that halogen radicals are the key intermediates in the halogenation of the chemical additives in hydraulic fracturing fluid. These findings are necessary for future improvements in hydraulic fracturing design to reduce the hazard posed by halogenated chemicals in hydraulic fracturing wastewater.

Based on our result that halogen radicals are the key intermediates in the halogenation of organic additives, we proposed a mechanism involving halogen radicals as key intermediates for the halogenation of chemical additives in hydraulic fracturing fluids. In the proposed mechanism (**Scheme 3.1**), persulfate generates $SO_4^{\bullet-}$ primarily through thermal activation (step 1).[183–185] Next, in the presence of halides at present in hydraulic fracturing, $SO_4^{\bullet-}$ are scavenged by halides to produce halogen radicals (step 2).[175,176] The formed halogen radicals then react with chemical

additives (e.g., cinnamaldehyde) to form halogenated products (step 3). However, a key question in our mechanism remains regarding whether halogen radicals directly add to chemical additives (step 3a)[41,42] or form non-radical halogen oxidants (i.e. hypohalous acid, step 3b) via recombination reactions[43–45,48,49] to react with chemical additives (e.g., cinnamaldehyde) for halogenation.[50–52] The recombination processes are expected to be sensitive to radical concentrations due to its second-order dependence on radical concentrations. Future research might exploit this dependency to explore the relative role of direct halogenation by radicals relative to the radical recombination process.

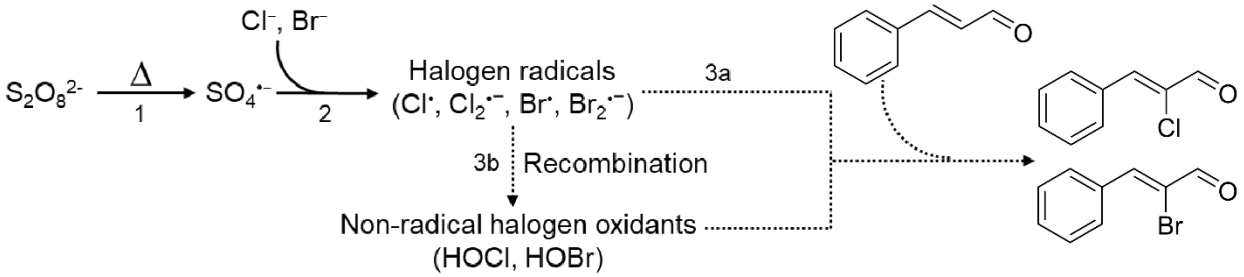

Scheme 1. Proposed mechanism for the halogenation of chemical additives in hydraulic fracturing fluids. **1**) generation of sulfate radicals ($SO_4^{\bullet-}$); **2**) radical speciation from $SO_4^{\bullet-}$ to halogen radicals; **3**) reaction of organic additive (i.e., cinnamaldehyde) through **3a**) radical reaction pathway or **3b**) non-radical halogen oxidants formed from recombination of halogen radicals.

The mechanism proposed herein indicates that knowledge of halogen radical formation and reactivity in advanced oxidative treatments[163–167] and sunlight photochemistry[34–40] in saline water applies to the halogenation of chemical additives in hydraulic fracturing fluids. A remaining barrier to applying knowledge on halogen radicals more directly to this emerging field is that reaction rate constants used in these studies, as well as those cited herein, are largely determined at lower temperatures than those relevant to hydraulic fracturing. In addition, future research should also

explore the temperature-dependence of product yields from reactions associated with halogen radicals and chemical additives in hydraulic fracturing fluids.

Furthermore, because the yields of halogenated cinnamaldehyde found in this study (i.e., <1%) are even lower than previously reported,[158] our results support the prior observation that halogenation may only consist of a small fraction of chemical additive degradation in hydraulic fracturing fluids. Although the conversion of $SO_4^{\bullet-}$ to halogen radicals increased the difference in the rate constants of *para*-hydroxybenzoate and benzoate, it did not increase the observed degradation rate of cinnamaldehyde in competition with either benzoate or guar. Our results suggest that the radical selectivity needs to be more carefully considered when expanded to include molecules of various structural classes. Also, the competition kinetics used to determine the second-order rate constants of radicals should be controlled to ensure that the reaction with halogen radicals or other target radicals (e.g., carbonate) are actually the dominant reaction. This effort will allow further application of halogen radical research to more complex reaction networks in hydraulic fracturing fluids, as well as other high salinity water systems.

3.5 Supporting information

3.5.1 Experimental procedure for cinnamaldehyde halogenation and quantification of α-chloro- and α-bromocinnamaldehyde

In a typical experiment to investigate the halogenation of cinnamaldehyde, solutions (25 mL) containing 1.4 M Cl^-, 6 mM Br^- and 10 mM phosphate buffer were prepared in 40 mL amber vials. The initial concentration of cinnamaldehyde was 0.5 mM (0.0066% by mass), which is about 50-fold higher than the reported concentration in hydraulic fracturing fluid (0.00012% by mass).[162] To evaluate the effect of cinnamaldehyde regarding its concentration, we also conducted an

additional experiment using 50 μM initial cinnamaldehyde. Modifications to other conditions (i.e., increasing Br^- concentration to 60 mM, addition of 50 mM isopropanol) are indicated for specific experiments.

After the temperature of the solutions stabilized at 80°C in the water bath, a small volume (0.25 mL) of 0.1 M persulfate stock solution was added into each vial to achieve an initial concentration of 1 mM persulfate. Over a 2 h duration, aliquots (each 0.5 mL) were collected every 15 min and stored in 2 mL amber vials with 50 μL 0.1 M ascorbic acid, which was in excess of persulfate to quench the reactions. Collected aliquots were then analyzed by high pressure liquid chromatography (HPLC). Concentrations of cinnamaldehyde and halogenated products (α-chlorocinnamaldehyde and α-bromocinnamaldehyde) were used to calculate the product yield (the ratio of the molar concentration of halogenation product detected to the molar concentration loss of cinnamaldehyde during the experiment.

The quantification of cinnamaldehyde, α-chlorocinnamaldehyde and α-bromocinnamaldehyde was conducted on an Agilent 1260 Infinity II High Pressure Liquid Chromatography – UV (HPLC-UV) equipped with an Agilent Eclipse Plus C18 column (3.0 mm × 150 mm, 3.5 μm). An isocratic mobile phase with 60% MilliQ water and 40% acetonitrile/water (99/1, v/v) with 0.5 mL/min flow rate and 10 μL injection volume were used. These compounds were eluted at 8.1, 12.0 and 13.0 min for cinnamaldehyde, α-chlorocinnamaldehyde and α-bromocinnamaldehyde, respectively. UV absorbance at 30 nm was used to quantify their concentrations. The values of the limit of detection (LOD) of cinnamaldehyde, α-chlorocinnamaldehyde, and α-bromocinnamaldehyde measured by this HPLC program are 0.13, 0.08, and 0.07 μM, respectively.

3.5.2 Experimental procedure for citrate halogenation and quantification of trihalomethane

To investigate the halogenation of citrate under physicochemical conditions relevant to hydraulic fracturing, we measured the formation of four trihalomethanes (trichloromethane, dichlorobromomethane, dibromochloromethane, and tribromomethane) from citrate. Note that although citrate has been shown to have a median concentration of 0.15 mM (0.003% by mass),[170] to successfully measure the produced trihalomethanes and investigate the halogenation mechanism, we reduced the concentration of initial citrate to 0.05 mM. In a typical experiment, solutions (20 mL) containing 0.05 mM citrate, 200 mg/L guar, 5 mM potassium persulfate, 1.4 M Cl^-, 60 mM Br^- and 10 mM phosphate buffer were prepared in 40 mL amber vials. All experimental solutions were conducted in a water bath that was preheated to 80°C. After a 2 h period, all experimental solutions were cooled down to room temperature by immersing into ice for 5 min. Then, 2 mL of 0.1 M ascorbic acid, in excess of persulfate, was added to stop the reaction.

Trihalomethanes were detected on gas chromatography – mass spectrometry (GC-MS). After quenching the reaction, samples (22 mL) were spiked with 30 µg/L internal standard 1,2-dibromopropane, extracted vigorously by hand for 2 min with 3 mL of tert-butyl methyl ether (MtBE), and wait for separation for 10 min. The MtBE extracts were further dried by ~2 g anhydrous sodium sulfate and then analyzed using GC-MS (Agilent 7820-5977 MSD) with an HP-5ms fused silica capillary column (30 m × 0.25 mm × 0.25 µm). MtBE extracts of 5 µL were injected in splitless mode (inlet temperature 90°C). The oven temperature was held at 28°C for 11 min, 40°C/min to 139°C, 60°C/min to 274°C and was held for 1 min. The quantification ions,

retention time and lowest standard concentrations of the four trihalomethanes are reported in **Table S3.6**.

To further investigate the halogenation of citrate in hydraulic fracturing fluid, we conducted experiments in more complex solutions incorporating major chemical constituents used in hydraulic fracturing fluid (**Table S3.2**) and measured the formation of trihalomethanes on GC-MS. We selected these compounds and their concentrations based on their reported concentrations (**Table S3.2**).

3.5.3 HPLC quantification of para-hydroxybenzoate, benzoate, and cinnamaldehyde

The quantification of organic compounds used in paired probe systems (i.e., *para*-hydroxybenzoate and benzoate, cinnamaldehyde and benzoate) was conducted on an Agilent 1260 Infinity II High Pressure Liquid Chromatography – UV (HPLC-UV) equipped with an Agilent Eclipse Plus C18 column (3.0 mm × 150 mm, 3.5 μm). For samples from all probe systems, the aqueous phase was 10 mM phosphoric acid (pH 2) in Mill-Q water and the organic phase was acetonitrile/water (99/1, v/v). The flow rate was 0.5 mL/min flow rate and the injection volume was 10 μL. For each pair of probes, gradient elution has been established for the elution of organic compounds:

1) For the *para*-hydroxybenzoate/benzoate pair, gradient elution was carried out using 87% aqueous phase for 7 min, adjusted to 80% at 8 min and held until 19 min, then adjusted to 87% at 20 min. The retention time was 5.6 min for *para*-hydroxybenzoate and 16.4 min for benzoate. The UV absorbance wavelength was 255 nm initially and switched to 227 nm at 8 min.

2) For the cinnamaldehyde/benzoate pair, gradient elution was carried out using 80% aqueous phase for 4 min, adjusted to 60% at 4.2 min and held until 13 min, then adjusted to 80% at 13.2 min. The retention time was 12.0 min for cinnamaldehyde and 8.4 min for BA. The UV absorbance wavelength was 295 nm initially and switched to 227 nm at 8 min.

These compounds have limit of detection values as 0.39, 0.13, and 0.75 µM for *para*-hydroxybenzoate, cinnamaldehyde, and benzoate, respectively.

3.5.4 Experimental procedures for cinnamaldehyde degradation in the presence of guar

To investigate the kinetics of cinnamaldehyde in hydraulic fracturing fluids, solutions (25 mL) containing cinnamaldehyde, guar, and phosphate buffer were prepared. The concentrations of cinnamaldehyde (15 µM)[162] and guar (500 mg/L)[159,162,198] was originally chosen to be similar to the reported concentration in hydraulic fracturing fluid. We also adjusted the concentration of phosphate buffer from 10 mM to 1 mM and pH from 7.0 to 6.5 to minimize the scavenging of radicals by phosphate species to prevent interference with the degradation of cinnamaldehyde at such low concentration.

Due to the presence of guar, we conducted liquid-liquid extraction of cinnamaldehyde before analysis on HPLC. After quenching the aliquot (in water solution), 0.5 mL of dichloromethane was added to each HPLC vial (with a total volume of 1.05 mL). The HPLC vials containing the aqueous and organic phases were vigorously shaken for 5 min followed by 20 min of settling. Then, the organic phase was transferred to a clean HPLC vial that was ready for measurement on HPLC with a method to detect cinnamaldehyde as described in **Section 3.5.3**. The recovery of this liquid-liquid extraction method was 91.9±2.2% and 94.5±1.4% for

experiments in the presence of ClO_4^- and Cl^-, respectively. The cinnamaldehyde concentration in the experimental sample was calculated by its concentration in dichloromethane, which was obtained by comparing the peak area measured on HPLC with a standard curve.

3.5.5 Experimental procedures to determine the production of HOCl and HOBr

To investigate the possible production of HOCl and HOBr from persulfate directly oxidizing Cl^- or Br^-, we added halides (i.e., 1.4 M Cl^- or 60 mM Br^-) in solutions (25 mL) at pH 7 controlled by 10 mM phosphate buffer. After the temperature of the solutions stabilized at 80°C in a water bath, a small volume (0.25 mL) of 0.1 M persulfate stock solution was added into each vial to achieve an initial concentration of 1 mM persulfate. After 2 h, 2 mL of each solution was collected and added with 1 drop of 10 M sodium hydroxide (NaOH) to increase the pH to above 11. Then, the absorbance of hypochlorite (OCl^-) and hypobromite (OBr^-) were measured on a Varian Cary 50 Bio UV-Vis Spectrophotometer at 292 nm[199] and 329 nm,[200] respectively.

The concentration of HOCl was calculated from the UV absorbance of OCl^- by a standard curve directly prepared by diluting a sodium hypochlorite stock solution, with a LOD of 23 μM. HOBr standard solutions were prepared by adding sodium bromide in large excess (i.e., 60 mM) to a known concentration of HOCl (i.e., 12.5-150 μM) at pH around 5. The lowest standard concentration of HOBr 13 μM.

3.5.6 Contribution of base (OH^-) to persulfate loss rate

Furman et al. reported that persulfate decomposed at a rate of 3.3×10^{-3} mM/min (3 M NaOH and 0.5 mM persulfate) at 20°C.[187] From this rate and the known concentrations of NaOH and persulfate, we calculated the bimolecular rate constant for the reaction between persulfate and OH^- to be 3.7×10^{-8} $M^{-1}s^{-1}$. We assume that this rate constant remains unchanged at temperatures up to 95°C.

At pH 12, where we have the highest concentration of OH^- (i.e., 10^{-2} M), we calculated that the pseudo-first order rate constant contributed by OH^- is 3.7×10^{-10} s^{-1}. Therefore, the contribution of OH^- to persulfate loss is 3 and 6 orders of magnitude lower than the measured persulfate loss rate at 37°C (i.e., $1.300(\pm0.002)\times10^{-7}$ s^{-1}) and 95°C (i.e., $5.10(\pm0.03)\times10^{-4}$ s^{-1}) across pH 2-12. Consequently, persulfate degradation in the investigated temperature range is likely to be dominated by the thermal activation of persulfate so that the effect of base activation is insignificant.

3.5.7 Possibility of cinnamaldehyde degradation by persulfate

We analyzed whether cinnamaldehyde was directly oxidized by the non-radical oxidant persulfate ($S_2O_8^{2-}$). Since cinnamaldehyde did not significantly increase the loss rate of persulfate, the bimolecular rate constant between cinnamaldehyde and persulfate was approximated to be lower than 10^{-6} $M^{-1}s^{-1}$, calculated with the LOD (0.03 mM) of persulfate the time frame of the experiment (2.5 h), and the assumption that cinnamaldehyde concentration is constantly at 0.5 mM. Applying 1 mM persulfate, we found that this bimolecular rate constant accounts for a pseudo-first order rate of cinnamaldehyde degradation of below 10^{-9} s^{-1}, which is less than 0.002% as compared to the measured degradation rate of cinnamaldehyde, $5.2\pm0.4\times10^{-5}$ s^{-1} (obtained from

the lower-left panel in **Figure 3.1a** by assuming the first order degradation). Therefore, persulfate oxidizing cinnamaldehyde is not significant in the observed degradation rate of cinnamaldehyde.

3.5.8 Effect of reaction products on the degradation kinetics of cinnamaldehyde and benzoate

Since the conversion of sulfate radicals to halogen radicals decreased the degradation rate of cinnamaldehyde, we hypothesized that other unmeasured constituents in the solution may be more competitive toward halogen radicals than cinnamaldehyde. Possible unmeasured constituents are the reaction products of cinnamaldehyde or benzoate. Consequently, we expected that accumulated products would continuously slow down the degradation rate of cinnamaldehyde and benzoate in the solution. We carried out a residual analysis for the concentrations of cinnamaldehyde and benzoate as they were being degraded over 10 min (**Figure 3.3b**). The residuals are obtained by subtracting modeled values (calculated by *k'* values in **Figure 3.3b**) from measured values. We found that in all experiments with salts, both compounds exhibit slowly decreased degradation rates over the experimental period (**Figure S3.7**). However, these errors between experimental measurements and predicted values (±0.02 μM) are much lower than the concentrations of cinnamaldehyde (>12 μM) and benzoate (>33 μM) at each time point, indicating that the reaction product(s) have no significant influence on the degradation kinetics of cinnamaldehyde and benzoate. Therefore, we concluded that reaction products are not likely more competitive toward halogen radicals than cinnamaldehyde and benzoate.

3.5.9 Supplementary tables

Table S3.2. Chemicals used in this chapter.

Vendor	Chemicals
Acros Organics	benzoic acid (>99.5%)
	potassium persulfate (99+%)
	sodium chloride (99.5%)
	sodium bromide (99.5%)
	α-chlorocinnamaldehyde (97+%)
Fisher Scientific	monobasic sodium phosphate (>99%)
	dibasic sodium phosphate (>99%)
	sodium hydroxide (98.7%)
	sodium hypochlorite (5.65-6%)
	anhydrous sodium sulfate (>99.0%)
	citric acid monohydrate (>99%)
	sodium tetraborate decahydrate (>99%)
Sigma-Aldrich	ascorbic acid (ACS grade)
	trans-cinnamaldehyde (99%)
	para-hydroxybenzoic acid (97%)
	sulfuric acid (95%-98%)
	guar
	dichloromethane (>99.8%)
	EPA501/601 trihalomethane calibration mix
	orange terpenes natural
	petroleum distillate (>99.9%)
	propylene glycol (>99.5%)
	tert-butyl methyl ether (>99.9%)
	sodium carbonate (>99%)
Alfa Aesar	α-bromocinnamaldehyde (99%)
TCI America	1,2-dibromopropane (98+%)

Table S3.2. Selected organic compounds in hydraulic fracturing fluid.

Component	Concentration	Function	Reference
guar	200 mg/L	gelling agent	[162,198]
petroleum distillate	212 mg/L	gelling agent	[162,198]
citrus terpenes	47.2 mg/L	surfactant	[162,198]
propylene glycol	283.4 mg/L	other chemicals	[162,198]
citrate	9.6 mg/L	complexing agent	[162,198]
borate	400 mg/L	cross-linker	[159,162,198]
sodium carbonate	200 mg/L	buffer relevant to flowback water	[162,198]

Table S3.3. Fraction of sulfate radical ($SO_4^{\bullet-}$) scavenged by different solution components in the presence of 1.4 M Cl^- and 6 mM Br^-.

Compound[a]	Concentration (M)	k ($M^{-1}s^{-1}$)	Reference	k×c (s^{-1})	Fraction[b]
$H_2PO_4^-$	6.1×10^{-3}	7.0×10^4	[6]	4.3×10^2	0.0
HPO_4^{2-}	3.9×10^{-3}	1.2×10^6	[6]	4.6×10^3	0.0
$S_2O_8^{2-}$	10^{-3}	$6.3 \times 10^{5,c}$	[188–190]	6.3×10^2	0.0
Cl^-	1.4	4.7×10^8	[175]	6.6×10^8	0.97
Br^-	6.0×10^{-3}	3.5×10^9	[176]	2.1×10^7	0.03

Solution is buffered with 10 mM phosphate buffer (pH 7). The fraction of cinnamaldehyde is neglected because it is less than 0.1 even with the second-order rate constant for the reaction of cinnamaldehyde and sulfate radical is close to the diffusion limit (10^{10} $M^{-1}s^{-1}$).

Calculated based on normalizing the total of k×c values to 1.

An average value of three referenced rate constants.

Table S3.4. Fraction of sulfate radical ($SO_4^{\bullet-}$) scavenged by different solution components in the presence of 1.4 M Cl^- and 60 mM Br^-.

Compound[a]	Concentration (M)	k ($M^{-1}s^{-1}$)	Reference	k×c (s^{-1})	Fraction[b]
$H_2PO_4^-$	6.1×10^{-3}	7.0×10^4	6	4.3×10^2	0.0
HPO_4^{2-}	3.9×10^{-3}	1.2×10^6	6	4.6×10^3	0.0
$S_2O_8^{2-}$	10^{-3}	$6.3 \times 10^{5,c}$	188–190	6.3×10^2	0.0
Cl^-	1.4	4.7×10^8	175	6.6×10^8	0.76
Br^-	6.0×10^{-2}	3.5×10^9	176	2.1×10^8	0.24

a. Solution is buffered with 10 mM phosphate buffer (pH 7). The fraction of cinnamaldehyde is neglected because it is less than 0.1 even with the second-order rate constant for the reaction of cinnamaldehyde and sulfate radical is close to the diffusion limit (10^{10} $M^{-1}s^{-1}$).

b. Calculated based on normalizing the total of k×c values to 1.

c. An average value of three referenced rate constants.

Table S3.5. Fraction of sulfate radical ($SO_4^{\bullet-}$) scavenged by different solution components in the presence of 1.4 M Cl^-, 60 mM Br^- and 50 mM isopropanol.

Compound[a]	Concentration (M)	k ($M^{-1}s^{-1}$)	Reference	k×c (s^{-1})	Fraction[b]
$H_2PO_4^-$	6.1×10^{-3}	7.0×10^4	6	4.3×10^2	0.0
HPO_4^{2-}	3.9×10^{-3}	1.2×10^6	6	4.6×10^3	0.0
$S_2O_8^{2-}$	10^{-3}	$6.3 \times 10^{5,c}$	188–190	6.3×10^2	0.0
Cl^-	1.4	4.7×10^8	175	6.6×10^8	0.76
Br^-	6.0×10^{-2}	3.5×10^9	176	2.1×10^7	0.24
isopropanol	5.0×10^{-2}	8.0×10^7	6	2.5×10^6	0.0

a. Solution is buffered with 10 mM phosphate buffer (pH 7). The fraction of cinnamaldehyde is neglected because it is less than 0.1 even with the second-order rate constant for the reaction of cinnamaldehyde and sulfate radical is close to the diffusion limit (10^{10} $M^{-1}s^{-1}$).

b. Calculated based on normalizing the total of k×c values to 1.

c. An average value of three referenced rate constants.

Table S3.6. Quantification ions, retention times and the lowest standard concentration for trihalomethanes

trihalomethane	quantification ions	retention times (min)	lowest standard concentration (μM)[a]
trichloromethane	83, 85, 87	3.96	8.4×10^{-5}
dichlorobromomethane	83, 85, 129	4.90	6.1×10^{-5}
dibromochloromethane	127, 129, 131	7.62	4.8×10^{-5}
tribromomethane	171, 173, 175	12.11	4.0×10^{-5}
1,2-dibromopropane	41, 121, 123	11.18	NA

a. These values are converted from 10 ng/L, the lowest standard concentrations of all trihalomethanes

Table S3.7. One-way analysis of variance (ANOVA) to assess the significance of the differences in persulfate loss rates at pH 2, 7, and 12 at each temperature.

Temperature (°C)	*p* value[a]	Significant difference among means
37	0.13	No
60	0.18	No
80	0.19	No
95	0.09	No

a. Each *p* value was obtained by analyzing three groups of the measured persulfate loss rates in each replicate experiment at pH 2, 7, and 12 at each temperature. When *p* value is greater than 0.05, there is no significant difference among the means of persulfate loss rates at all pH values at a temperature.

3.5.10 Supplementary figures

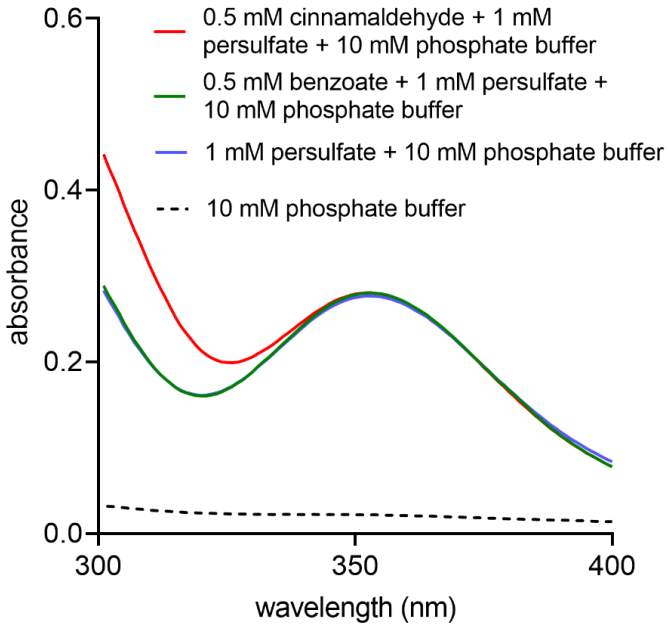

Figure S3.1. UV absorption spectra of persulfate quantified using the potassium iodide method (absorbance at 352 nm) as described in the text. Solutions contained phosphate buffer (pH 7), persulfate and organic compounds as indicated. Data presented for the experiments are the average values from two replicate experiments at each wavelength detected from 300-400 nm.

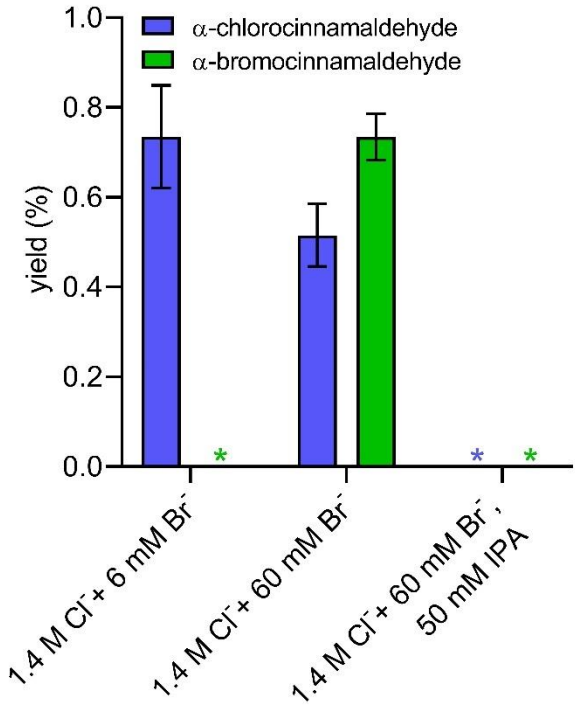

Figure S3.2. Product yields of α-chlorocinnamaldehyde and α-bromocinnamaldehyde from the degradation of cinnamaldehyde after incubation for 2 h at 80°C. Solutions initially contained 1 mM persulfate and 0.5 mM cinnamaldehyde at pH 7 buffered with 10 mM phosphate buffer. Halide and isopropanol (IPA) concentrations are as indicated. Green and blue asterisk signs (*) represent below the limit of detection of α-bromocinnamaldehyde (0.07 μM) and α-chlorocinnamaldehyde (0.08 μM).

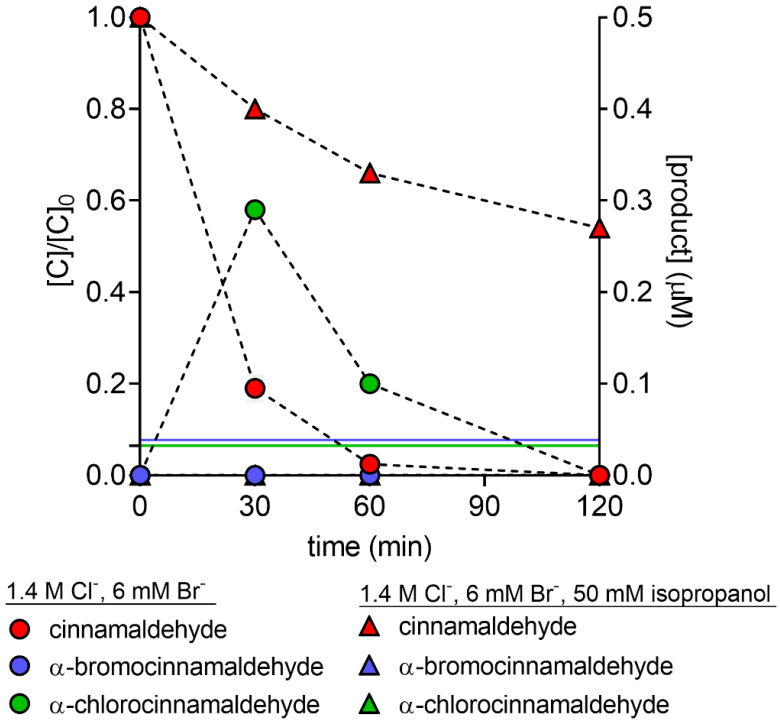

Figure S3.3. Degradation of 0.05 mM cinnamaldehyde and formation of α-chlorocinnamaldehyde and α-bromocinnamaldehyde. Experiments were conducted at 80 °C for 2 h in solutions initially containing 1 mM persulfate and 0.05 mM cinnamaldehyde at pH 7 buffered with 10 mM phosphate buffer. Halides and isopropanol concentrations are as indicated. Green and blue lines represent the limit of detection of α-bromocinnamaldehyde (0.07 μM) and α-chlorocinnamaldehyde (0.08 μM). Error bars represent the range of two replicate experiments.

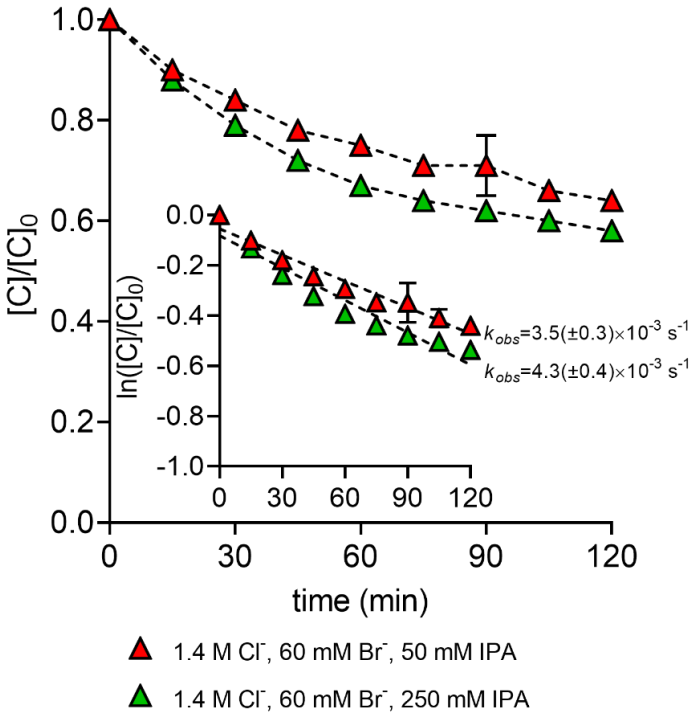

Figure S3.4. Cinnamaldehyde degradation in the presence of isopropanol (IPA). Experiments were conducted at 80°C in solutions initially containing 1 mM persulfate and 0.5 mM cinnamaldehyde at pH 7 buffered with 10 mM phosphate buffer. Halide and isopropanol concentrations are as indicated. Error bars represent the range of two replicate experiments. Note that both experiments were conducted at a later date than experiment presented in **Figure 3.1a**.

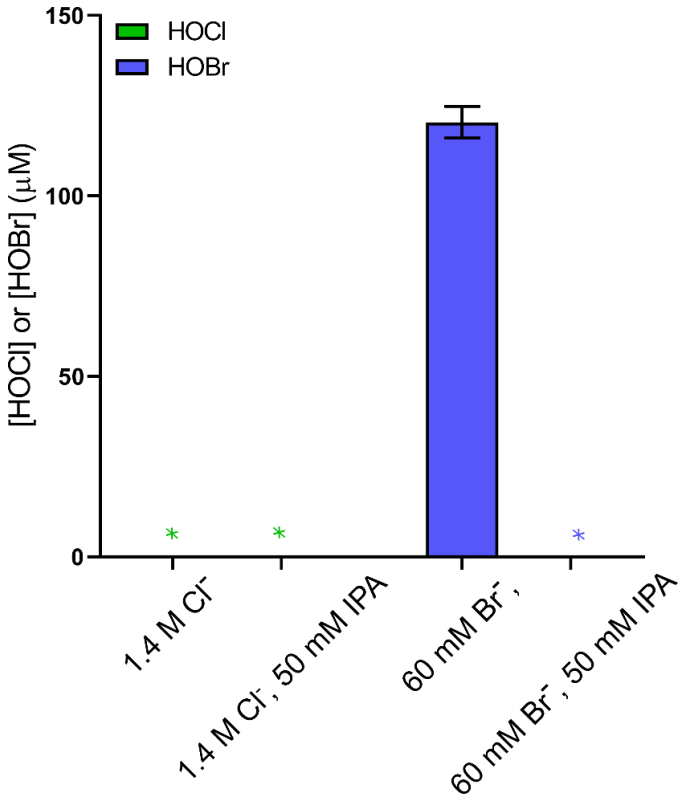

Figure S3.5. HOCl and HOBr formation from persulfate for 2 h at 80°C. Solutions initially contained 1 mM persulfate, halide and isopropanol concentrations as indicated at pH 7 buffered with 10 mM phosphate buffer. Green and blue asterisk signs (*) represent below the limit of detection of HOCl (23 µM) and the lowest standard concentration of HOBr (13 µM).

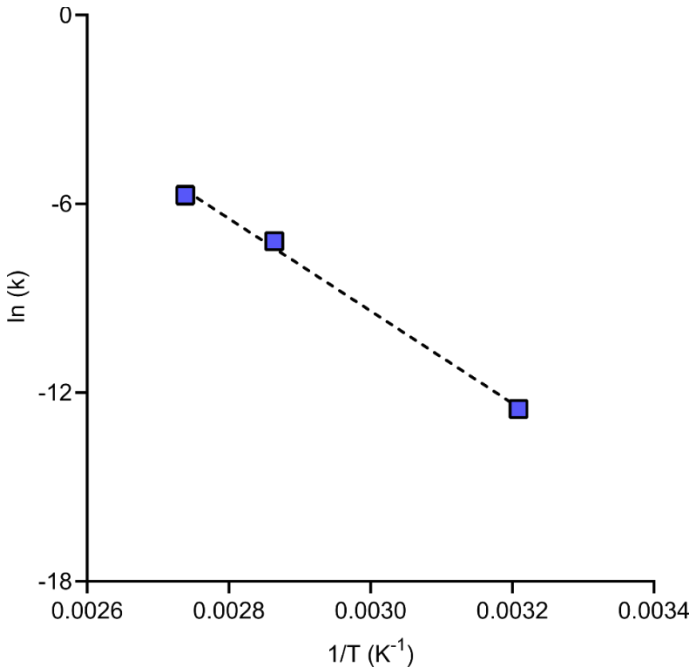

Figure S3.6. Effect of temperature on the pseudo-first order degradation rate (s^{-1}) of benzoate. All solutions initially contained 1 mM initial $S_2O_8^{2-}$ and 50 µM benzoate at pH 7 (10 mM phosphate buffer). Error bars represent the range of two replicate experiments. Solutions also contained 50 µM nitrobenzene as a hydroxyl radical-selective scavenger.

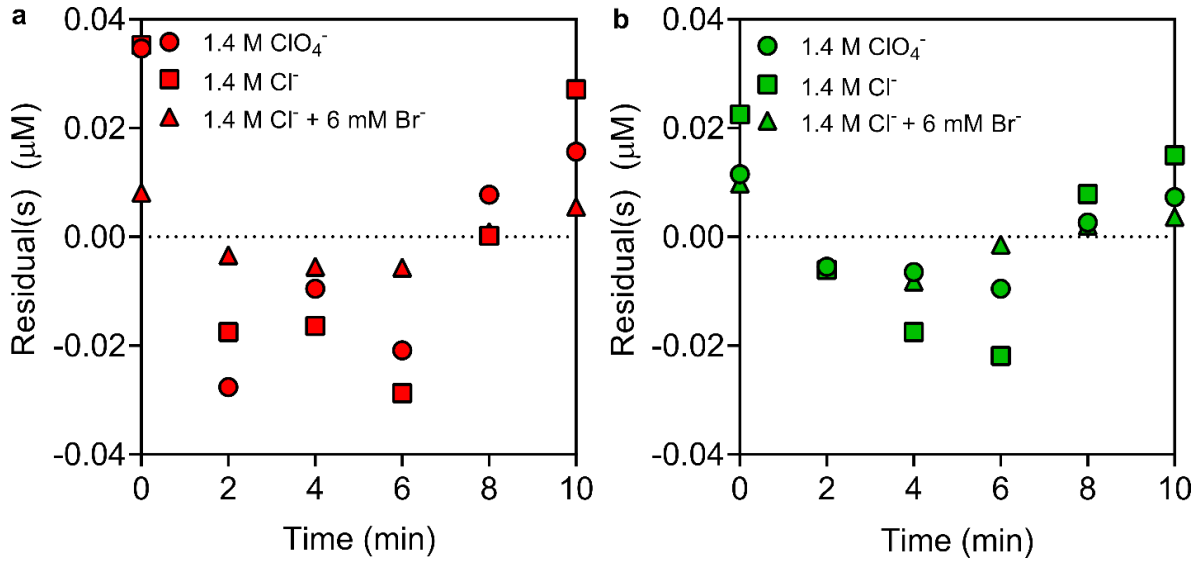

Figure S3.7. Residual analysis for the degradation rates of cinnamaldehyde and benzoate in competition. Residuals represent the difference between modeled (predicted by the k' values obtained in **Figure 4.3b**) and measured concentrations of (a) cinnamaldehyde and (b) benzoate. All experiments were conducted at 80°C for 10 min in solutions with 1 mM initial persulfate, 10 mM phosphate buffer (pH 7), 50 μM each organic compound, and salts as indicated.

Chapter 4: Effects of halides on organic compound degradation during plasma treatment

4.1 Abstract

Plasma has been proposed as an alternative strategy to treat organic contaminants in brines. Chemical degradation in these systems is expected to be partially driven by halogen oxidants, which have been detected in halide-containing solutions exposed to plasma. In this study, we characterized specific mechanisms involving the formation and reactions of halogen oxidants during plasma treatment. We first demonstrated that addition of halides accelerated the degradation of a probe compound known to react quickly with halogen oxidants (i.e., *para*-hydroxybenzoate), but did not affect the degradation of a less reactive probe compound (i.e., benzoate). This effect was attributed to the degradation of *para*-hydroxybenzoate by hypohalous acids, which were produced via a mechanism involving halogen radicals as intermediates. We applied this mechanistic insight to investigate the impact of constituents in brines on reactions driven by halogen oxidants during plasma treatment. Bromide, which is expected alongside chloride in brines, was required to enable halogen oxidant formation, consistent with the generation of halogen radicals from the oxidation of halides by hydroxyl radicals. Other constituents typically present in brines (i.e., carbonates, organic matter) slowed the degradation of organic compounds, consistent with their ability to scavenge species involved during plasma treatment.

4.2 Introduction

Plasma technology has been recently proposed as a promising tool for water treatment due to its simplicity, cost, and effectiveness toward destroying toxic organic compounds.[56,63,201–205] Unlike ultraviolet/oxidant advanced oxidation processes (UV/oxidant AOPs), plasma operates without requiring chemical consumables (e.g., hydrogen peroxide, H_2O_2; hypochlorous acid, HOCl).[205] In addition, the energy requirement for plasma treatment of some organic contaminants has been found to be competitive against other treatment options including UV/oxidant AOPs, electrochemical treatment, and sonolysis.[56,63] Plasma-based water treatment generates an array of oxidative species (e.g., hydroxyl radical, $^{\bullet}OH$; oxygen atom, O; ozone, O_3; hydrogen peroxide, H_2O_2),[55,206–208] among which $^{\bullet}OH$ – known to react with a wide spectrum of organic contaminants[209] – is frequently determined to drive the degradation of several organic contaminants (e.g., pesticides,[58,210,211] pharmaceuticals,[212,213] algal toxins[60,214,215]). In addition to oxidative species, plasma also generates reductive species (e.g., hydrated electron, e_{aq}^-),[216–219] which can degrade highly oxidized organic contaminants including per- and polyfluoroalkyl substances[63,220–222] and halogenated disinfection byproducts.[223–225]

Among possible applications, plasma has particular advantages when applied to degrade organic compounds in brines. Contaminated brines encompass a wide array of waste streams from diverse sources (ion exchange,[226,227] reverse osmosis,[228–230] pharmaceutical production,[231] hydraulic fracturing,[232,233] landfill,[234] textile manufacturing[235]), but all share high concentrations of salts and other constituents that present multiple specific opportunities for plasma treatment. Firstly, relative to conventional AOPs, plasma appears to be less susceptible to inhibition by constituents in complex wastewaters that scavenge reactive species.[230,236] For example, organic compound degradation by plasma was less sensitive to the inclusion of co-occurring constituents

in complex mixtures (i.e., reverse osmosis brine,[230] urine[236]) compared to •OH-based AOPs. Secondly, because reactive species are concentrated at or above the plasma-water interface,[55] salting-out effects in brines can improve the degradation efficiency of some contaminants (i.e., surfactants).[237] For example, the degradation of perfluorooctanoic acid (PFOA), which is known to occur at or above the plasma-water interface,[238] was accelerated upon the addition of salts,[237] consistent with salts causing PFOA to more favorably partition to the water surface.[239–241] Thirdly, increased conductivity at elevated salt concentrations affects plasma properties such as plasma volume and the contact area between plasma and water.[242] These changes can increase the production of reactive species (e.g., •OH),[243] though notably the opposite trend has been observed in other reactors.[236,242] Depending on the impact of conductivity on reactive species production in the specific reactor, the addition of salts has been reported to either accelerate[244,245] or decelerate[237,246,247] the degradation of organic compounds during plasma treatment.

Beyond their contributions as salts to the aforementioned effects, halides present in brines may specifically enable new pathways due to their potential to form halogen oxidants during plasma treatment. For example, in the same plasma reactor, the addition of chloride (Cl^-) to solutions decreased the degradation of one organic compound, which was attributed to elevated conductivity,[237] but increased the degradation of another, which was attributed to the formation of HOCl.[237] Other studies have also invoked halogen oxidants, including HOCl and halogen radicals (i.e., $Cl^•$, $Cl_2^{•-}$), to explain compound degradation during plasma treatment of solutions containing Cl^-.[247–249] In addition, HOCl has been measured to occur in Cl^--containing solutions treated by plasma.[250–252] The specific mechanisms proposed to be responsible for halogen oxidant formation depend on the plasma reactor setup. For example, the inclusion of oxygen (i.e., at 0.1-1%) in the feed gas of some plasma systems enabled the generation of HOCl via the reaction between O and

Cl^- (eq 4.1).[250–252] In other plasma systems, an alternative mechanism involving the reaction between $^{\bullet}OH$ and Cl^- to form $Cl^{\bullet}$ and $Cl_2^{\bullet-}$ has been proposed in multiple studies (eq 4.2; excluding the involvement of bromide, Br^-),[237,247–249] which may either react with organic compounds themselves[247,249] or recombine to form HOCl that drives compound degradation.[237,247,248]

$$O + Cl^- + H^+ \longrightarrow HOCl \tag{4.1}$$

$$Cl^- + {}^{\bullet}OH \longleftrightarrow ClOH^{\bullet-} \xrightarrow{+H^+(+Cl^-,Br^-)} Cl^{\bullet}(\text{or } Cl_2^{\bullet-}, ClBr^{\bullet-}) + H_2O \tag{4.2}$$

These studies characterizing halogen oxidants in plasma-treated water have only investigated the impact of Cl^-,[237,247–252] which cannot account for the unique roles of other chemical species occurring in brines. In particular, brines, like natural waters,[253] also contain some Br^- typically present at 0.1-1 mol percent of Cl^-.[167,233,254] The inclusion of Br^- in real brines is particularly relevant to mechanisms involving halogen radicals.[8] Whereas HOCl formation from O can proceed in Cl^--only systems,[250–252] the presence of Br^- (even a trace contaminant in Cl^- reagent)[164,165] is known to dominate the oxidation of halides by $^{\bullet}OH$ to halogen radicals.[8] Specifically, Cl^- itself is ineffective in scavenging $^{\bullet}OH$ to produce halogen radicals due to the fast reverse reaction of the intermediate $ClOH^{\bullet-}$ to regenerate the initial reactants (eq 4.2),[8,177] whereas $BrOH^{\bullet-}$ generated in the presence of Br^- predominantly reacts further to produce halogen radicals (eq 4.3).[8,178] Therefore, the previously proposed mechanism involving halogen radical formation in Cl^--only systems treated by plasma[237,247–249] has been typically considered negligible in other contexts (e.g., conventional AOPs).[8] Beyond the effect of Br^-, other brine constituents (i.e., carbonates, organic matter) may also impact the formation and reactions of halogen oxidants during plasma treatment depending on the specific reactive species involved.[164,165,167,255]

$$Br^- + {}^{\bullet}OH \longleftrightarrow BrOH^{\bullet-} \xrightarrow{+H^+(+Cl^-,Br^-)} Br^{\bullet}(\text{or } ClBr^{\bullet-}, Br_2^{\bullet-}) + H_2O \tag{4.3}$$

In this study, we aimed to extend the state of knowledge regarding the role of the halogen oxidants during plasma treatment of halide-containing waters to incorporate consideration of Br^- and other constituents (i.e., carbonates, organic matter) occurring in brines alongside Cl^-. We specifically focused on the formation of halogen oxidants mediated by halogen radicals (eq 4.2-4.3) rather than O (eq 4.1) because we anticipated the inclusion of Br^- would play a key role in this mechanism. To this end, we measured the degradation of probe compounds to provide insight into the formation of halogen oxidants in solutions of different chemistries, as well as to evaluate whether halogen radicals reacted with these compounds directly or recombined to form hypohalous acids that drove the reaction instead. We complemented our experiments with characterization of reactive species in plasma over solutions with and without halides. We applied our mechanistic insight to evaluate organic compound degradation in the presence of brine constituents, including known competitors for radicals (i.e., carbonates, organic matter).[164,165,167] Overall, our work enables the formation mechanism and reactions of halogen oxidants to be accurately understood in the presence of key additional constituents beyond Cl^- during plasma treatment of contaminated brines.

4.3 Materials and Methods

4.3.1 Chemicals and reagents

All chemicals used in this work are listed in Supporting Information, **Table S4.1**. All experimental solutions were prepared in Milli-Q water. Stock solutions of HOCl and hypobromous acid (HOBr) were prepared from sodium hypochlorite (5-6%) directly or by reacting with a stoichiometric amount of Br^- and standardized spectrophotometrically at 292 nm[199] or 329 nm,[256] respectively.

4.3.2 Plasma setup

To generate plasma, a high-voltage power supply (Information Unlimited) was used to provide a voltage of 3 kV with a discharge frequency of 20 kHz. The experimental system consisted of a round-bottom glass flask with a volume of 100 mL (Chemglass) (**Figure S4.1**). A sharpened stainless steel rod (0.8 cm diameter) was placed in the headspace in the flask as the high voltage electrode and an aluminum ring (3.8 cm outer diameter, 2.0 cm inner diameter) was fitted outside the bottom of the flask as the ground electrode. The electrodes were spaced 4.3 cm apart with the high voltage electrode being positioned 1.0 cm above the solution during experiments. Salts found to be deposited on the electrode after plasma treatment of halide-containing solutions were analyzed for composition using a scanning electron microscope (Thermo Fisher Scientific).

To control headspace pressure and gas composition, the flask was connected to a gas port equipped with a vacuum pump and an argon inlet. We used 99.999% argon (Linde Gas & Equipment Inc.) as the feed gas in our system. The absence of oxygen in the feed gas is consistent with feed gas compositions previously shown to lead to negligible hypohalous acid formation mediated by O (eq 4.1),[252] consistent with our goal to investigate pathways mediated by halogen radicals (eq 4.2-4.3). While O-mediated hypohalous acid formation is negligible without oxygen in the feed gas (i.e., <2 ppm_v, **Table S4.1**), some O may be generated due to the presence of lower amounts of oxygen from other sources (e.g., ambient air, residual air, oxygen impurity in feed gas).[257]

To minimize water loss during plasma treatment, the flask was partially immersed in an ice bath (4 °C) and connected to a vapor condenser. Using this setup, the loss of water during plasma treatment was confirmed to be negligible (**Figure S4.2**). Exposure to plasma was found to promote internal mixing (**Figure S4.3**), such that mechanical mixing (e.g., a stir bar) was not

required. We omitted components required for stirring to avoid additional complexities in the reactor design.

4.3.3 Treatment of Solutions by Plasma

To investigate the mechanism of how halides contributed to organic compound degradation, two probe compounds (i.e., benzoate and *para*-hydroxybenzoate) were used during plasma treatment. Solutions (50 mL) were prepared with 10 mM phosphate buffer (pH 7), 50 μM of each probe compound, and halides at indicated concentrations. In experiments containing both Br^- and Cl^-, Br^- was added at 1 mol percent of Cl^-, corresponding to molar ratios reported in brines (i.e., 0.1-1 mol percent, **Table S4.2**).[167,227,231,233,234,254,258–283] When isolating the effect of Cl^- alone, different experiments were performed with both lower purity (i.e., ⩾99.0%, <0.007 mol percent Br^-) and higher purity (99.999%) Cl^- reagents as indicated in corresponding figures. When Br^- was added, the lower purity Cl^- was used because the trace Br^- in the Cl^- reagent is negligible relative to the added Br^-. Perchlorate (ClO_4^-) was used as a control for ionic strength. Because conductivity affects reactive species production during plasma exposure,[236,242,243] we confirmed that halide- and ClO_4^--containing solutions at the same ionic strength had comparable solution conductivity (**Figure S4.4**). Isopropanol (50 mM) was added in specific experiments as a scavenger for radicals.

Prior to all experiments, the system was held at a low pressure (i.e., 25 Torr) for 5 min to degas solutions. Then, the headspace of the flask was purged three times before filling with argon at 100 Torr. This subatmospheric pressure was selected to achieve greater radical density during plasma treatment.[284] We confirmed that the degradation of probe compounds at 100 Torr was faster than at atmospheric pressure (i.e., 760 Torr) in both halide- and ClO_4^--containing solutions and that the effect of halides was consistent at both pressures (**Figure S4.5**). After exposure to plasma

at indicated times, aliquots (each 0.5 mL) were collected by a syringe through a septum. Then, each aliquot was transferred to a 2 mL amber vial, quenched by 5 µL 0.1 M ascorbic acid, and analyzed for probe compound concentrations. Concentrations of hypohalous acids were measured by sampling 2 mL aliquots either at the end of the experiment (if a single concentration was determined) or at multiple time points in experiments separate from probe compound measurements. All sampling removed <24% of overall solution volume over the experiment duration.

Additional experiments were performed by further modifying the solution composition. In addition to the probe compounds used above, four organic contaminants (i.e., salicylate, acetaminophen, sulfamethoxazole, anthranilate) were selected based on their different reactivities toward halogen oxidants (**Table S4.3**).[7,41,196,285–289] Like Cl^- and Br^-, additional constituents (i.e., sulfate, SO_4^{2-}; nitrate, NO_3^-; carbonates; organic matter) were added at brine-relevant concentrations (**Table S4.2**).[167,227,231,233,234,254,258–283] Some of these constituents have known reactivities with the reactive species of interest (**Table S4.4**).[167,209,255,290–298] All salts used in this study contained sodium as the cation. While calcium and magnesium were present in some brines (**Table S4.2**),[167,227,231,233,234,254,258–283] these cations were excluded from the present study to avoid precipitation of solids with some anions (i.e., SO_4^{2-}, carbonates).[299–301] When included, carbonates were introduced to the solution using a syringe after the headspace was filled with argon to prevent loss of carbonates as carbon dioxide during degassing. The ionic strength of all solutions was adjusted to a constant value (2.0 M) using ClO_4^-.

4.3.4 Analysis of Dissolved Species

The summed concentrations of hypohalous acids (i.e., HOCl, HOBr) were measured by the N,N-diethyl-phenylenediamine (DPD) colorimetric method[302] using a UV−vis spectrophotometer

(Varian Cary) or Nanodrop (Thermo Fisher Scientific). The total concentrations of hypohalous acids were calculated by standard curves for HOCl or HOBr, which were found to be identical (**Figure S4.6**). The concentrations of organic compounds were quantified on an Agilent 1260 Infinity II High Pressure Liquid Chromatography – UV as described in **Section 4.5.1**. The retention times, UV wavelengths, and values of the limit of detection (LOD) of organic compounds were reported in **Table S5**.

4.3.5. Analysis of Species in Plasma by Optical Emission Spectroscopy (OES)

To investigate reactive species present in plasma over solutions of different chemistries, analysis using two different OES spectrometers was carried out using a glass vessel with optical windows (quartz) as a custom feature made in Department of Chemistry at Washington University in St. Louis (modified from the aforementioned reactor design as shown in **Figure S4.1**). Firstly, a low-resolution OES spectrometer (Ocean Optics HR4000 CG-UV-NIR) was used to obtain broadband OES spectra (i.e., 200-1100 nm) to identify species with strong emission intensities in plasma. Secondly, a high-resolution OES spectrometer (Princeton Instrument SpectraPro HRS-750) was used over narrow ranges of wavelengths to observe species with weak emission intensities. The identification of species by each OES spectrometer was achieved by comparing wavelengths to those reported previously (**Table S4.6**).[303–306] While OES provides information about the presence of observable species, it does not directly provide information about species concentrations in plasma.

4.3.6 Statistical analysis

All experiments were conducted in duplicate. Errors in concentrations represent the range of measurements from duplicate experiments, while errors in degradation rate constants and rates

represent the standard errors of the slopes obtained from linear regression. The significance of differences was evaluated using GraphPad Prism with a confidence level set to be $\leqslant 0.05$.

4.4 Results and Discussion

4.4.1 Effects of halides on probe compound degradation

We first aimed to verify that halogen oxidants were generated during plasma treatment of solutions containing mixed halides (i.e., 1 M Cl^- along with 10 mM Br^-). In addition to the chlorine-relevant species (i.e., $Cl^•$, $Cl_2^{•-}$, HOCl) invoked in prior studies,[237,247–249] Br^- is also expected to enable the formation of bromine-relevant radicals (i.e., $Br^•$, $Br_2^{•-}$), mixed halogen radicals (i.e., $ClBr^{•-}$), and HOBr.[8] To this end, we compared the degradation rates of two probe compounds, benzoate and *para*-hydroxybenzoate, selected due to their reported bimolecular rate constants with both chlorine and bromine species (**Table S4.3**).[7,41,196,285–287] In the absence of halides, both probe compounds are expected to degrade at similar rates due to their similar rate constants for reactions with common species generated by plasma (e.g., $^•OH$, e_{aq}^-, **Table S4.3**).[307–309] In contrast, if halogen oxidants are formed in the presence of halides, *para*-hydroxybenzoate is expected to degrade more quickly than benzoate, corresponding to its substantially higher bimolecular rate constants with both halogen radicals[41,196,286] and hypohalous acids.[7,285]

In the absence of halides, benzoate and *para*-hydroxybenzoate degraded at similar rates in a solution with 1 M ClO_4^- added to increase ionic strength (**Figure 4.1a**). Consistent with the reported kinetics of other organic compounds treated by plasma,[58,63,211,222,236,238] the degradation of both compounds followed pseudo-first-order kinetics, resulting in rate constants of 0.0121 ± 0.0007 min^{-1} and 0.0108 ± 0.0006 min^{-1} for the degradation of benzoate and *para*-hydroxybenzoate, respectively (**Figure 4.1a**). To determine the effect of ionic strength in our

reactor, we measured probe compound degradation in solutions without ClO_4^-, finding that each rate constant increased by 40-50% (i.e., to 0.017±0.001 min^{-1} for benzoate and 0.016±0.001 min^{-1} for *para*-hydroxybenzoate (**Figure S4.7**). This result suggests that ionic strength in our reactor slightly suppresses probe compound degradation, but that reactive species with comparable reactivities towards both compounds (i.e., •OH, **Table S4.3**)[307,308] dominate the reaction regardless of ionic strength.

Consistent with our hypothesis, the addition of halides (i.e., 1 M Cl^-, 10 mM Br^-) marginally affected benzoate degradation (**Figure 4.1b**), but accelerated *para*-hydroxybenzoate degradation (**Figure 4.1c**). However, before proceeding with quantitative analysis of these effects, we were first required to address our observation that the kinetics of *para*-hydroxybenzoate degradation in the presence of halides appeared to deviate from pseudo-first-order (**Figure 4.1c**). Additional residual analysis supported our observation that, unlike the probe compound degradation in the presence of ClO_4^-, *para*-hydroxybenzoate degradation in the presence of halides more closely followed zero-order kinetics (**Figure S4.8**). Because benzoate was degraded by <20% over the same time frame in the presence of halides, analysis of the reaction order was not attempted. To facilitate comparisons among probe compound degradation in different chemistries that alter reaction order, we opted to report observed zero-order degradation rates of each compound during the first 30 min of exposure to plasma (**Figure 4.1b,c**). Using this approach, we determined that the degradation rate of benzoate was not significantly impacted by replacing ClO_4^- with halides, while the degradation rate of *para*-hydroxybenzoate was selectively increased 3-fold.

In addition to affecting our quantitative analysis, the degradation of *para*-hydroxybenzoate by observed zero-order kinetics also enabled us to evaluate the potential for each class of halogen oxidants (i.e., halogen radicals or hypohalous acids) to contribute directly (i.e., as opposed to

acting as intermediates) to the accelerated rate in the presence of halides. If halogen radicals directly reacted with *para*-hydroxybenzoate, we expected that the reaction would follow pseudo-first-order kinetics, consistent with organic compound degradation in UV/oxidant AOP treatment of halide-containing waters.[164,165,310] Therefore, we instead hypothesized that hypohalous acids, which form from the recombination of radical species,[8] react with *para*-hydroxybenzoate. Our hypothesis was based on the observation that the overall concentration of hypohalous acids – both in the absence and presence of probe compounds – increased as the exposure of the solution to plasma increased (**Figure 4.1d**), which might allow the reaction rate to be maintained even as *para*-hydroxybenzoate concentration diminished.

To determine if the increasing amount of hypohalous acids was quantitatively consistent with the observed zero-order kinetics of *para*-hydroxybenzoate, we analyzed the instantaneous rate of *para*-hydroxybenzoate loss at each time point using the equation:

$$-\mathrm{d[C]/dt} = k_{\mathrm{C,HOCl}}\,[\mathrm{HOCl}][\mathrm{C}] + k_{\mathrm{C,HOBr}}\,[\mathrm{HOBr}][\mathrm{C}] \quad (4)$$

where [C] represents the measured concentration of *para*-hydroxybenzoate (**Figure 4.1c** in the presence of halides); t represents the duration of exposure to plasma; $k_{\mathrm{C,HOCl}}$ and $k_{\mathrm{C,HOBr}}$ represent the apparent bimolecular rate constant between *para*-hydroxybenzoate and each hypohalous acid (either found in or estimated from literature, **Section S4.5.2**, **Table S4.3**);[285,287] and [HOCl] and [HOBr] represent the concentrations of HOCl and HOBr. Reactions involving the conjugate bases of HOCl and HOBr were assumed to be negligible due to both their lower concentrations at the experimental pH and their slower reactivities toward substituted aromatics.[287,311]

To further simplify this equation, we defined the term $\mathrm{f_{HOCl}}$ as the fraction of hypohalous acid present as HOCl (i.e., $\mathrm{f_{HOCl}} = [\mathrm{HOCl}]/[\mathrm{HOX}]_{\mathrm{tot}}$, where $[\mathrm{HOX}]_{\mathrm{tot}}$ is the total concentration of

hypohalous acids). Then, [HOCl] and [HOBr] in eq 4 were substituted with $f_{HOCl}[HOX]_{tot}$ and $(1 - f_{HOCl})[HOX]_{tot}$, respectively, to generate:

$$-d[C]/dt = [k_{C,HOCl} f_{HOCl} + k_{C,HOBr}(1 - f_{HOCl})][HOX]_{tot}[C] \quad (5)$$

Consequently, if f_{HOCl} is approximately constant during the experiment (consistent with the constant pH and near-constant concentrations of Cl^- and Br^-),[287] *para*-hydroxybenzoate is expected to degrade upon reactions with hypohalous acids following observed zero-order kinetics (i.e., d[C]/dt is constant), if the multiplication product of the concentrations of *para*-hydroxybenzoate and total hypohalous acids (i.e., $[HOX]_{tot}[C]$) is near-constant. When we calculated this term using experimental concentrations of *para*-hydroxybenzoate (**Figure 4.1c**, condition: with halides) and hypohalous acids (**Figure 4.1d**, condition: with probe compounds), we found that the value of $[HOX]_{tot}[C]$ did not vary during the experimental period (i.e., slope of 0±2 μM^2/min, **Figure S4.9**), consistent with the observed zero-order kinetics of *para*-hydroxybenzoate degradation.

In addition to confirming that measured hypohalous acid concentrations were consistent with the observed reaction order, we also evaluated if the amount of hypohalous acids measured in our system could feasibly account for the observed rate of *para*-hydroxybenzoate degradation using bimolecular rate constants available or estimated from literature.[285,287] Assuming all hypohalous acid was present as HOCl (i.e., $f_{HOCl} = 1$), the calculated *para*-hydroxybenzoate degradation rate (i.e., 0.22±0.09 μM/min, **Figure S4.10**) is lower than but within the same order of magnitude as the measured rate (i.e., 1.36±0.07 μM/min, **Figure 4.1c**). Conversely, if HOBr is assumed to be exclusively present (i.e., $f_{HOCl} = 0$), the calculated rate (i.e., 900±400 μM/min, **Figure S4.10**) is >2 orders of magnitude higher than the measured rate. Because HOBr has been modeled to occur at higher concentrations than HOCl in seawater containing 0.0015 mol-Br^-/mol-

Cl^-,[312] HOBr is expected to also dominate in our system, which has both higher halide concentrations and Br^-/Cl^- ratio. Consequently, our measured $[HOX]_{tot}$, if present primarily as HOBr, overpredicts the observed degradation rate of *para*-hydroxybenzoate, possibly due to an overestimation of the bimolecular rate constant between *para*-hydroxybenzoate and HOBr (**Table S4.3**). Recently, reactions with organic compounds involving previously overlooked species (e.g., Br_2O, Br_2) have been found to contribute to rate constants for reactions attributed to HOBr being overestimated by similar orders of magnitude.[124,313] While re-evaluation of this bimolecular rate constant is beyond the scope of this work, our analysis with currently available values suggests that hypohalous acids are present at sufficient concentrations, if not in excess, to account for the observed rate of *para*-hydroxybenzoate degradation.

While our results are consistent with hypohalous acids acting as the primary species directly reacting with *para*-hydroxybenzoate to accelerate its degradation in the presence of halides, we still hypothesized that radicals (i.e., $^{\bullet}OH$, halogen radicals) act as intermediates that go on to form hypohalous acids via recombination reactions.[8] To test this hypothesis, we repeated our experiments in solutions including 50 mM isopropanol, a known scavenger of both $^{\bullet}OH$ (i.e., $k_{\text{isopropanol},^{\bullet}OH} = 1.9 \times 10^9\ M^{-1}s^{-1}$)[209] and halogen radicals (i.e., $k_{\text{isopropanol},Cl_2^{\bullet-}} = 1.2 \times 10^5\ M^{-1}s^{-1}$,[41] $k_{\text{isopropanol},Br^{\bullet}} = 6.6 \times 10^6\ M^{-1}s^{-1}$).[179] In addition, isopropanol is not expected to quench hypohalous acids directly due to slow reported rate constants (e.g., $k_{\text{isopropanol,HOBr}} < 3.9 \times 10^{-4}\ M^{-1}s^{-1}$),[182] which we confirmed by demonstrating that isopropanol did not impact *para*-hydroxybenzoate degradation by hypohalous acids added directly as HOCl to halide-containing solutions (**Figure S4.11**). The addition of isopropanol to halide-containing solutions decreased the degradation rate of *para*-hydroxybenzoate to 0.20±0.02 μM/min, which was 6-fold lower than the rate measured in halide-containing solutions without isopropanol (**Figure 4.1c**).

Consistent with our proposed pathway of hypohalous acid formation from radical recombination, we determined that the addition of isopropanol reduced the concentration of hypohalous acids after plasma treatment to below their LOD (**Figure S4.12**).

The above evidence supports our expectation that our plasma system generates hypohalous acids through a radical-mediated pathway (i.e., recombination of halogen radicals formed from halide oxidation by •OH) in solutions containing Cl^- and Br^- together. This pathway has been invoked previously to explain results obtained during plasma treatment of solutions containing Cl^- as the sole halide,[237,247–249] which contradicts prior work that suggests Cl^- oxidation by •OH is negligible.[8] This discrepancy was possibly due to a trace amount of Br^- impurity occurring in the Cl^- reagent, which has previously been implicated in halogen radical formation.[164,165] We found that the inclusion of 1 M Cl^- added as a low purity reagent (i.e., ⩾99.0% with <0.007 mol percent Br^-) increased the degradation rate of *para*-hydroxybenzoate by 22±9% relative to the ionic strength control (p=0.02, **Figures 4.1e**). In contrast, the inclusion of 1 M Cl^- added as a high purity reagent (i.e., 99.999%) did not increase the rate relative to the control (**Figure 4.1e**). Similarly, hypohalous acid concentrations after treatment for 30 min were measurable in solutions prepared with low purity Cl^- (i.e., 4.2±0.8 µM), but below the LOD (i.e., 0.8 µM) in solutions prepared with either ClO_4^- or high purity Cl^- (**Figure 4.1e**). These results suggest that plasma treatment of solutions containing Cl^- as the sole halide is unlikely to generate hypohalous acids via a radical-mediated pathway, as well as indicate that a trace amount of Br^- impurity, which varies in magnitude among Cl^- reagents, may contribute to some effects previously attributed to Cl^- alone during plasma treatment.

While the effect of 1 mM Cl^- as the sole halide was negligible in our system, the inclusion of 10 mM Br^- (along with 1 M ClO_4^- to control the ionic strength) affected both compound

degradation and hypohalous acid formation to similar extents with or without 1 M Cl^- present (**Figure 4.1e**). The degradation rate of *para*-hydroxybenzoate in the Br^--only solution was 81±7% of the rate when Br^- and Cl^- were present together, and the concentration of hypohalous acid was indistinguishable between the two solutions after 30 min of exposure to plasma. In $^{\bullet}OH$-initiated pathways, lower concentrations of Br^- alone (i.e., 0.001-0.1 mM) have been previously reported to negligibly affect downstream reactions,[310,314,315] whereas higher concentrations of Br^- alone (i.e., 1 mM) accelerated organic compound degradation.[315] Consistent with these findings, the elevated Br^- concentration used in our study (10 mM, corresponding to 1 mol percent Cl^-) appears to be sufficient to account for the halide-dependent reactions in our plasma system regardless of the presence of Cl^-.

Though the amount of Br^- relative to Cl^- is relatively consistent in brines (i.e., 0.1-1 mol percent Br^-, **Table S4.2**), the absolute concentrations of halides vary substantially (e.g., 0.007-2 M Cl^-, **Table S4.2**).[167,227,231,233,234,254,258–283] Therefore, we expanded our experiments to evaluate the effect of halides at different concentrations, but at a constant ratio of Br^- to Cl^- (i.e., 0.1-2 M Cl^- with 1 mol percent of Br^-). The inclusion of halides at concentrations higher than 0.5 M Cl^- and 5 mM Br^- increased the degradation rate of *para*-hydroxybenzoate by 2- to 4-fold relative to ClO_4^- at the same ionic strength (**Figure 4.1f**). We also observed hypohalous acid formation across all tested halide concentrations (**Figure S4.13**). Both the acceleration of *para*-hydroxybenzoate degradation and hypohalous acid formation increased to lesser degrees upon increasing addition of halides at high concentrations, possibly due to other limitations (e.g., $^{\bullet}OH$ generation by plasma).

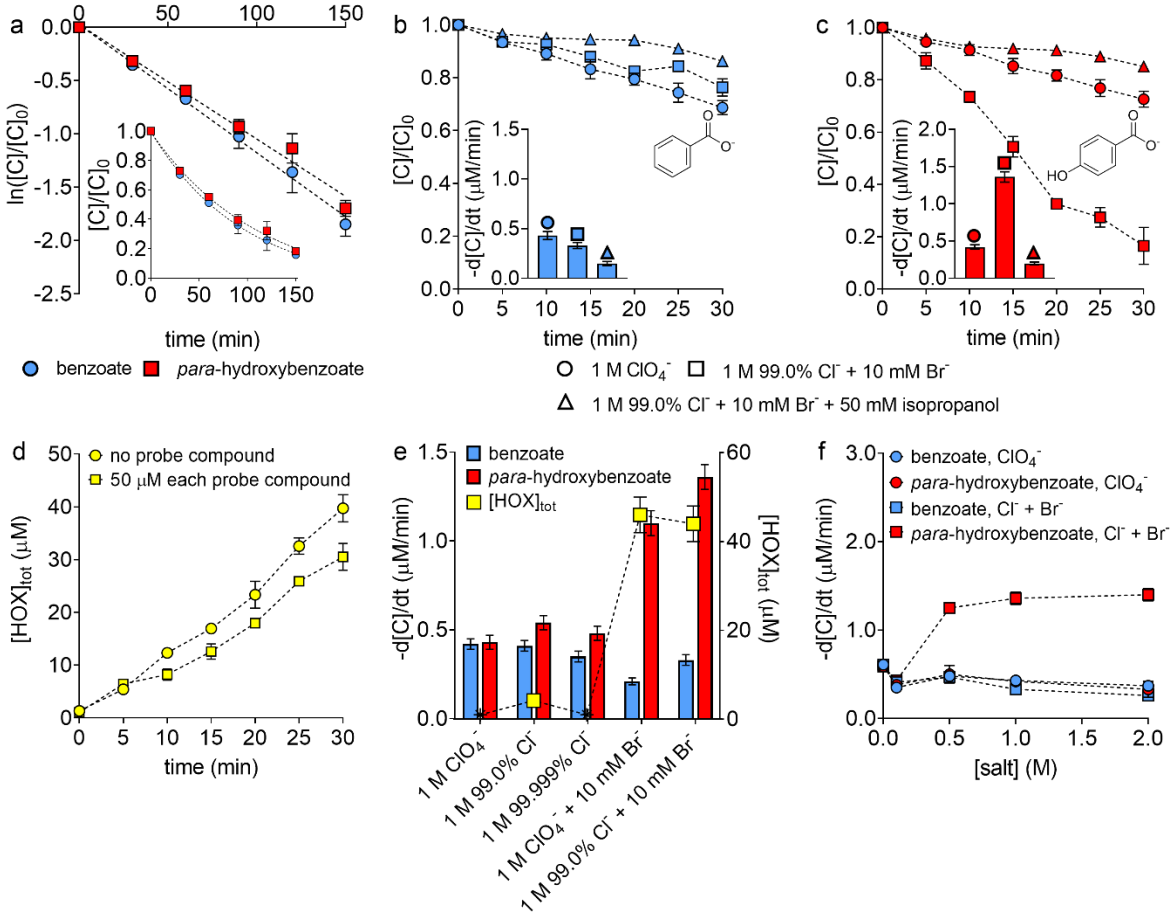

Figure 4.1. Degradation of probe compounds (i.e., benzoate, *para*-hydroxybenzoate) and formation of hypohalous acids during plasma treatment of solutions with varying chemical constituents (all containing 10 mM phosphate buffer, pH 7). (**a**) Degradation of benzoate and *para*-hydroxybenzoate (each initially present at 50 µM) in the presence of 1 M ClO_4^-. (**b-c**) Degradation of (**b**) benzoate and (**c**) *para*-hydroxybenzoate in the presence of salts and/or isopropanol. (**d**) Formation of hypohalous acids in the presence of 1 M Cl^- and 10 mM Br^-. (**e**) Degradation rates of probe compounds and hypohalous acid concentrations in solutions with different halide combinations after plasma treatment for 30 min. Asterisks (*) represent measurements below the LOD ($[HOX]_{tot}$ = 0.8 µM). For corresponding conditions, results in (**e**) are from the same experiments used to obtain results presented in (**b-c**), while results presented in (**d**) were collected

independently to reduce the volume of solution removed during the experiments. The measured concentrations of hypohalous acids at 30 min under the same condition (with probe compounds and halides) in (**d**) and (**e**) had no significant difference (p=0.10). (**f**) Degradation rates of probe compounds over 30 min in the presence of ClO_4^- or halides (i.e., Cl^-, purity: 99.0%, with 1 mol percent added Br^-); results collected with 1 M salt are reproduced from (**b-c**). Errors on concentrations represent the range of measurements from duplicate experiments, while errors on degradation rates represent the standard errors of the slopes obtained from linear regression.

4.4.2 Effects of halides on reactive species in plasma

We next investigated reactive species in plasma using low- (**Figure S4.14**) or high-resolution OES (**Figures 4.2,S4.15**). Consistent with our proposed mechanism of halogen oxidants from halide oxidation by •OH (eq 2-3), we detected the presence of •OH in plasma by both the low-resolution and high-resolution OES above all solutions regardless of the presence of halides or ionic strength (**Figures S14,15, Table S4.6**). Although our feed gas did not include oxygen in amounts required to generate hypohalous acids from O (eq 1),[252] O was also detected by high-resolution OES (**Figure 4.2k, Table S4.6**), though not by low-resolution OES (**Figure S4.14**). The presence of O in plasma has been previously observed even when oxygen was not added in the feed gas.[257]

The collected OES spectra also afforded us the opportunity to determine if halogen species (i.e., Cl•, Br•, as well as molecular halogens, i.e., Cl_2, Br_2) could be detected in the plasma phase during treatment of halide-containing solutions. In addition to their possible generation at the interface of the plasma and liquid in our reactor,[55] we also noticed evidence that halide-containing aerosols – which may allow heterogeneous oxidation of halides by •OH at their interface[316–318] –

were generated in our system during plasma treatment. Specifically, we noted salt deposition on the electrode after plasma treatment, which we determined to be primarily composed of sodium chloride (**Figures S4.16,4.17**) likely transferred to the electrode by aerosols generated during plasma exposure.[55] Using low-resolution OES, we also observed a large sodium (Na) peak above solutions containing either halides (i.e., 1 M Cl^-, 10 mM Br^-) or 1 M ClO_4^-, suggesting that salts in solutions may generate plasma species (**Figure S4.14**). However, no halogen species were detected in the plasma regardless of the presence of halides (**Figure 4.2**, **Table S4.6**), suggesting either that these species were present below their LOD (which could not be quantified for OES) or that halogen oxidants were primarily confined to the liquid phase of the reactor.

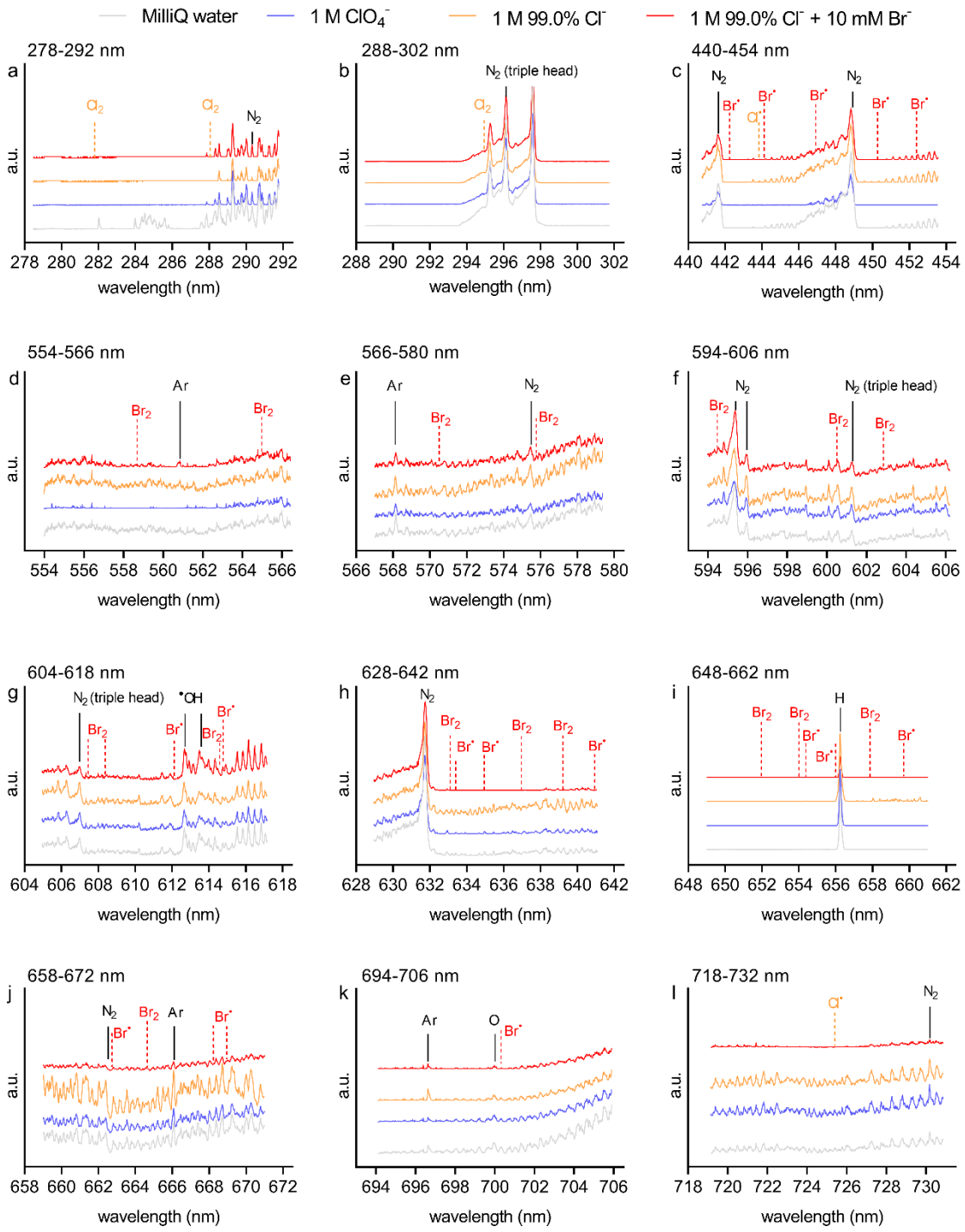

Figure 4.2. High-resolution OES spectra at selected wavelengths from 278 to 732 nm in plasma over either MilliQ water or solutions containing salts. Solutions containing salts also contained 10 mM phosphate buffer (pH 7) and 50 µM each benzoate and *para*-hydroxybenzoate. The black

solid lines indicate wavelengths where oxygen, nitrogen, and argon species were identified. The orange and red dashed lines indicate wavelengths where halogen radicals and molecular halogens were previously reported (**Table S4.6**)[303,304] but not identified in this study.

4.4.3 Effects of brine constituents on organic contaminant degradation

We expanded our experiments to include four organic contaminants selected due to their reported bimolecular rate constants toward hypohalous acids, which span orders of magnitude (**Table S4.3**).[7,285,287,289] In the ionic strength control, all contaminants degraded at rates comparable to the probe compounds (**Figure 4.3a**), in agreement with their similar bimolecular rate constants toward species generated by plasma in the absence of halides (e.g., $^{\bullet}OH$, e^{-}_{aq}, **Table S4.3**).[307–309,319–322] The addition of halides selectively accelerated the degradation of two contaminants (i.e., sulfamethoxazole, anthranilate) to extents similar to or greater than *para*-hydroxybenzoate (**Figure 4.3a**); like *para*-hydroxybenzoate, the accelerated degradation of these contaminants (e.g., anthranilate) also followed zero-order kinetics (**Figure S4.18**). The acceleration of degradation rates of the compounds upon halide addition correlated with their reactivity towards hypohalous acids, which occurred at measurable concentrations (i.e., 35±5 μM after 30 min of exposure to plasma, **Figure S4.19**). Specifically, the bimolecular rate constants for the reactions of five of the six compounds with HOCl (available for all compounds, **Table S4.3**,[7,285] which typically trend with rate constants with HOBr)[287] correlate with greater degradation rates (**Figure 4.3a**). The bimolecular rate constants involving HOBr, which have only been reported for three of these compounds (**Table S4.3**),[287,289] may explain the one exception: acetaminophen, which did not undergo faster degradation upon halide addition despite reacting with HOCl with a rate constant comparable to *para*-hydroxybenzoate,[7,285] reacts more slowly with HOBr (**Table S4.3**).[287,289]

We next evaluated the impact of additional constituents reported to occur in brines (**Table S4.2**)[167,227,231,233,234,254,258–283] on the degradation of these compounds in the presence of halides, beginning with two species – SO_4^{2-} and NO_3^- – not expected to affect our proposed pathway. Neither SO_4^{2-} nor NO_3^- scavenges $^{\bullet}OH$ (**Table S4.4**);[292,293] though NO_3^- reacts with e_{aq}^- (**Table S4.4**),[296] e_{aq}^- is not invoked in the radical-mediated generation of hypohalous acids. Consistent with our expectation, both degradation rates of organic compounds (**Figure 3a**) and hypohalous acid concentrations (**Figure S4.19**) were comparable in the presence of these anions at their median concentrations reported in brines (i.e., 0.25 M SO_4^{2-}, 0.08 M NO_3^-, **Table S4.2**).[167,227,231,233,234,254,258–283]

Among the four contaminants, we selected one exhibiting accelerated degradation in the presence of halides and one not (sulfamethoxazole and acetaminophen, respectively) for additional experiments involving brine constituents expected to impact our pathway, beginning with carbonates. Carbonates (i.e., bicarbonate, HCO_3^-; carbonate, CO_3^{2-}) react with both $^{\bullet}OH$ and halogen radicals to produce carbonate radicals ($CO_3^{\bullet-}$, **Table S4.4**).[209,290,291,294] $CO_3^{\bullet-}$ reacts rapidly with both contaminants (i.e., $k_{\text{acetaminophen},CO_3^{\bullet-}} = 1.9 \times 10^9\ \text{M}^{-1}\text{s}^{-1}$, $k_{\text{sulfamethoxazole},CO_3^{\bullet-}} = 4.4 \times 10^8\ \text{M}^{-1}\text{s}^{-1}$).[323] However, the scavenging of halogen radicals by carbonates[164] is expected to reduce the formation of hypohalous acids, which thereby suppresses resultant contaminant degradation. In the presence of halides without carbonates, the degradation rates of both acetaminophen and sulfamethoxazole were 2-fold higher when isolated as a pair of compounds (**Figure 4.3b**) than when present with the four other compounds (**Figure 4.3a**); this increase is attributable to the reduced competition for reactive species that also lead to 1.5-fold higher hypohalous acid concentration (i.e., 51±2 after 30 min, **Figure S4.20**). While the addition of carbonates did not alter the degradation rate of acetaminophen, the degradation rate of

sulfamethoxazole was reduced by 6-fold when carbonates were added at 0.16 M (**Figure 4.3b**). The addition of carbonates also reduced the formation of hypohalous acids; their measured concentration decreased to 1.5±0.5 μM after solution exposure to plasma for 30 min in the presence of 0.16 M carbonates (**Figure S4.20**).

Organic matter is another brine constituent expected to inhibit our proposed pathway due to its known reactions with both radicals (e.g., $^{\bullet}OH$, **Table S4.4**)[167,295] and hypohalous acids (**Table S4.4**).[255] The addition of organic matter (i.e., Aldrich humic acid, AHA; Suwannee River natural organic matter, SRNOM) to halide-containing solutions did not impact the degradation of acetaminophen, but decreased the degradation rate of sulfamethoxazole (**Figure 4.3c**). Relative to UV/oxidant AOPs, a higher concentration of organic matter was required to suppress contaminant degradation to a comparable extent during plasma treatment. For example, while the addition of organic matter at 100 mg-C/L only decreased the degradation rate of sulfamethoxazole by 19-40% during plasma treatment (**Figure 4.3c**), the addition of organic matter at a lower concentration (i.e., 36 mg-C/L) to saline waters decreased pharmaceutical degradation by 60-90% during treatment by UV/oxidant AOPs.[167]

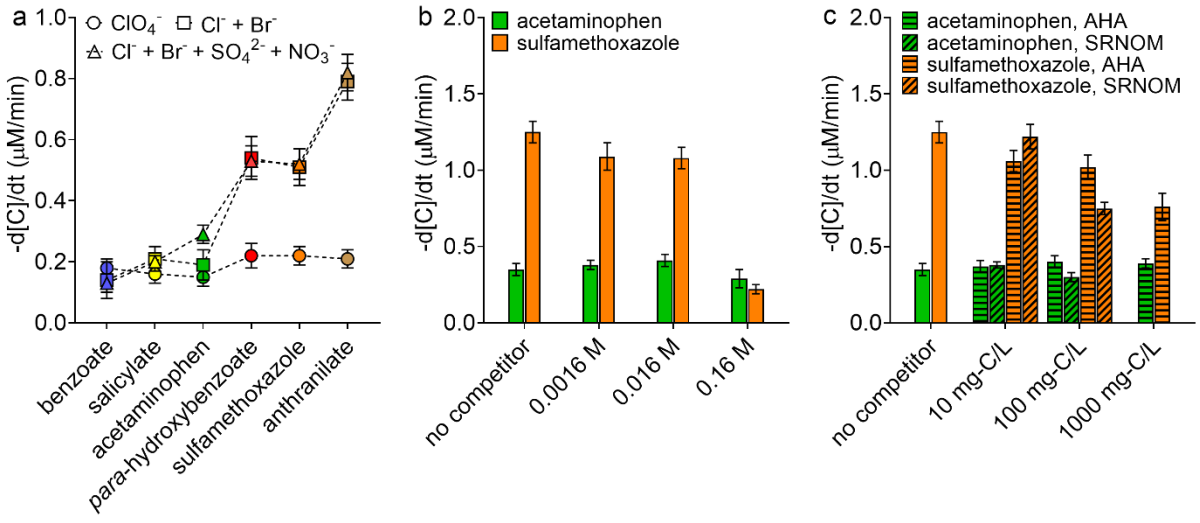

Figure 4.3. Degradation rates of selected compounds during plasma treatment of solutions with additional brine constituents. All solutions contained 10 mM phosphate buffer (pH 7) and had ionic strength adjusted to 2.0 M by ClO_4^-. (**a**) Degradation rates of benzoate, salicylate, acetaminophen, *para*-hydroxybenzoate, sulfamethoxazole, and anthranilate (each initially present at 50 μM) in the presence of salts. The concentrations of Cl^-, Br^-, SO_4^{2-}, and NO_3^-, when present, were 1 M, 10 mM, 0.25 M, and 0.08 M, respectively. (**b**-**c**) Degradation rates of acetaminophen and sulfamethoxazole (each initially present at 50 μM) in the presence of (**b**) carbonates or (**c**) organic matter (i.e., Aldrich humic acid, AHA; Suwannee River natural organic matter, SRNOM). All solutions in (**b**-**c**) initially contained Cl^-, Br^-, SO_4^{2-}, and NO_3^- at concentrations used in (**a**). The data in (**b**) and (**c**) for the degradation rates of acetaminophen and sulfamethoxazole in the absence of competitors were obtained from the same experiments. Errors on degradation rates represent the standard errors of the slopes obtained from linear regression.

4.4.4 Environmental implications

In this work, we demonstrated that Br^-, despite only occurring in low amounts relative to Cl^- in brines, plays a crucial role during plasma treatment of halide-containing solutions. Our finding is consistent with prior work demonstrating that the generation of halogen radicals via halide oxidation by $^{\bullet}OH$ requires Br^- to be present along with Cl^- (eq 3).[8] The dependency of halogen radical formation on the presence of Br^- may be harnessed in future applications to distinguish hypohalous acid formation via halogen radicals from their formation mediated by O, which was reported to require only Cl^- (eq 1),[250–252] in plasma reactors wherein both pathways are feasible. In these applications, the potential for trace Br^- occurring in Cl^- reagents to enable halogen radical formation must be considered, as previously demonstrated for UV/oxidant AOPs.[164,165] Furthermore, the unique role of Br^- must be accounted for when translating prior studies on plasma treatment in Cl^--only solutions[237,247–249] to more complex chemistries occurring in brines, as well as other halide-containing solutions (i.e., blood serum)[324] exposed to plasma.[325]

Whereas the degradation of organic compounds in halide-containing solutions during UV/oxidant AOP treatment is typically attributable to their reactions with halogen radicals,[164,165,310] our results suggest that organic compounds in our system are primarily degraded due to reactions with hypohalous acids, which are generated by the recombination of halogen radicals.[8] A possible cause for this difference is that the generation of radical species during plasma treatment primarily occurs at the plasma-water interface,[55] potentially leading to localized regions of high radical concentrations that accelerates the recombination reactions. Beyond determining the kinetics of compound degradation, the formation of hypohalous acids during plasma treatment is relevant if applications of plasma for disinfection[326–328] are expanded to systems wherein halides are present. In addition, the formation of hypohalous acids potentially leads to the generation of

halogenated byproducts,[15,329] though these byproducts may also undergo dehalogenation by reductive species[223–225] generated by plasma.

By elucidating the distinct roles of both radicals and hypohalous acids in organic contaminant degradation during plasma treatment of halide-containing waters, our work also informs more accurate consideration of the impact of other brine constituents on these reactions. Only constituents with known reactions with radicals and/or hypohalous acids (i.e., carbonates, organic matter, as opposed to SO_4^{2-} and NO_3^-) suppressed contaminant degradation. The ability of carbonates to prevent hypohalous acid formation by scavenging halogen radicals[164] appeared to dominate over the potential for $CO_3^{\bullet-}$ to itself contribute to contaminant degradation,[323,330] resulting in slower degradation rates. Hypohalous acids formed during plasma treatment may also be less susceptible to scavenging by organic matter than radicals (**Table S4**),[167,255,295] contributing to smaller reductions in contaminant degradation than reported in UV/oxidant AOPs.[167]

Our results also impact approaches that enable plasma systems to be compared to other technologies for brine treatment. A typical basis for comparison is energy consumption, which has been quantified as the electrical energy required per order of magnitude compound degradation (E_{EO}) using pseudo-first-order rate constants.[331] In the presence of ClO_4^-, we calculated the E_{EO} of probe compounds based on their pseudo-first-order degradation rate constants (**Figure 1a**). Using the total power output (i.e., 15 W) and the solution volume (i.e., 0.05 L), the E_{EO} for probe compounds ranged from 950-1,070 kWh/m^3 per order, which was within the same order of magnitude as previously reported E_{EO} for pharmaceutical degradation during plasma treatment.[236] However, our results demonstrate that this approach is unsuitable as a basis to compare plasma technologies for brine treatment due to the impact of halides on reaction order. Instead, energy

cost calculations for brine treatment by plasma must account for complexities arising from the non-steady-state concentrations of hypohalous acids generated during plasma exposure.

4.5 Supporting information

4.5.1 Quantification of organic compounds.

The concentrations of two probe compounds (i.e., benzoate, *para*-hydroxybenzoate) were quantified on an Agilent 1260 Infinity II High Pressure Liquid Chromatography – UV (HPLC-UV) equipped with an Agilent Eclipse Plus C18 column (3.0 mm × 150 mm, 3.5 μm). The flow rate was 0.5 mL/min and the injection volume was 10 μL. An isocratic mobile phase was used with 80% aqueous phase (10 mM phosphoric acid, pH 2) and 20% organic phase (acetonitrile/water, 99/1 v/v). In other experiments, the concentrations of two probe compounds together with other four contaminants (i.e., salicylate, acetaminophen, sulfamethoxazole, anthranilate) were quantified using the same HPLC-UV setup except for the mobile phase, which was isocratic with 85% formic acid/water (0.1/99.9 v/v) and 15% acetonitrile/water (99/1 v/v). The retention times, UV wavelengths, and values of the limit of detection (LOD) of organic compounds were reported in **Table S4.5**.

4.5.2 Calculation of the apparent bimolecular rate constant between *para*-hydroxybenzoate and hypochlorous acid at pH 7.

The bimolecular rate constants of substituted phenols toward hypochlorous acid (i.e., HOCl) rely on the reactivity of their phenoxide ions (i.e., ArO^-), which are 5-orders of magnitude greater than the reactivity of substituted phenols (i.e., ArOH) toward hypochlorous acid.[7] Using the Hammett-type model described previously,[7] a prior study obtained the bimolecular rate constant for the reaction between the phenoxide ion of *para*-hydroxybenzoate and hypochlorous

acid (i.e., $k = 3.5 \times 10^3\ \mathrm{M^{-1}s^{-1}}$).[285] Then, accounting for the fractions of hypochlorous acid (α_{HOCl}, $\mathrm{pK_a}$ 7.5[7]) and the phenoxide ion of *para*-hydroxybenzoate ($\alpha_{\mathrm{ArO^-}}$, $\mathrm{pK_a}$ 9.3[285]), the previous study calculated an apparent bimolecular rate constant $k_{app}(\mathrm{HOCl}) = k\alpha_{\mathrm{HOCl}}\alpha_{\mathrm{ArO^-}} = 27\ \mathrm{M^{-1}s^{-1}}$ at pH 7.5.[285] Using the same method, we calculated the apparent bimolecular rate constant between *para*-hydroxybenzoate and hypochlorous acid at pH 7 to be $k_{app}(\mathrm{HOCl}) = k\alpha_{\mathrm{HOCl}}\alpha_{\mathrm{ArO^-}} = 13\ \mathrm{M^{-1}s^{-1}}$.

4.5.3 Supplementary tables

Table S4.1 Chemicals used in this chapter.

Vendor	Chemical	Use
Millipore-Sigma	ascorbic acid (ACS grade) (>99.5%)	quencher
	sulfuric acid (95%-98%)	pH adjustment
	sodium chloride (99.999%)	brine constituent
	sodium perchlorate (99+%)	ionic strength control
	sodium nitrate (99.0%)	brine constituent
	sodium sulfate (99.0%)	brine constituent
	sodium bicarbonate (≥99.7%)	brine constituent
	Aldrich Humic Acid	brine constituent
	para-hydroxybenzoic acid (≥99%)	analyte
	anthranilic acid (≥99.0%)	analyte
	acetaminophen (≥99.0%)	analyte
	acetonitrile (HPLC grade)	eluent
	sulfuric acid (98%)	pH adjustment

Fisher	sodium chloride (≥99.0%, <0.007 mol percent bromide)	brine constituent
	monobasic sodium phosphate (100%)	buffer
	dibasic sodium phosphate (100%)	buffer
	sodium hydroxide (98.7%)	pH adjustment
	sodium hypochlorite (5-6%)	oxidant
	isopropanol (LC-MS grade)	scavenger
	0.1% formic acid (LC-MS grade)	eluent preparation
TCI America	sulfamethoxazole (>98.0%)	analyte
	salicylic acid (>99.5%)	analyte
Alfa Aesar	N,N-diethyl-p-phenylenediamine sulfate, 97%	residual oxidant analysis
Acros Organics	sodium bromide (99.5%)	brine constituent
	benzoic acid (99.5%)	analyte
International Humic Substances Society	Suwannee River natural organic matter	brine constituent
Linde Gas & Equipment Inc.	argon (99.999%, <2 ppm_v oxygen, <3 ppm_v water, <0.5 ppm_v total hydrocarbon)	feed gas of the plasma system
McCormick	Food-grade green food color	dye experiments

Table S4.2. Characteristics of brines in literature, including ions (i.e., calcium, Ca^{2+}; magnesium, Mg^{2+}; sodium, Na^{+}; chloride, Cl^{-}; sulfate, SO_4^{2-}; nitrate, NO_3^{-}; carbonates, HCO_3^{-}, CO_3^{2-}), pH, and total organic carbon (TOC).

reference	treatment goal[a]	source brine	Ca^{2+} (g/L)	Mg^{2+} (g/L)	Na^{+} (g/L)	Cl^{-} (g/L)	SO_4^{2-} (g/L)	NO_3^{-} (g/L)	carbonates[b] (g/L)	pH	TOC (mg-C/L)
Anion exchange (IX)											
An et al. 2005[280]	As removal	simulated IX in laboratory	-	-	-	24	0.6	-	0.3	-	-
An et al. 2011[281]	As removal	simulated IX in laboratory	-	-	24	36	0.6	-	0.3	-	-
Arias-Paic and Korak 2020[282]	Cr removal	drinking water treatment plant	-	-	23	15	35	0.7	2.9	9.2	-
Bergquist et al. 2016[283]	NO_3^- removal	drinking water treatment plant	0.011	0.003	45	70	1.8	6.5	1.2	-	-
Clifford and Liu 1993[258]	NO_3^- removal	simulated IX in laboratory	-	-	-	8.4-11.2	1.7-2.1	2.7-3.7	5.8-9.1	8.0-9.2	-
Haddad et al. 2019[259]	Recover NaCl and DOC	drinking water treatment plant	-	-	35.4	54.6	1	-	-	-	1000
Haddad et al. 2021[260]	Recover NaCl and DOC	drinking water treatment plant	-	-	32	-	1	-	-	-	1000
Hiremath et al.2006[261]	ClO_4^- removal	drinking water treatment plant	0.022	0.003	-	-	1.8	1.6	-	5-10	-
			-	0.004	21	32	2.8	2	11	-	-

Homan et al. 2018[262]	Cr removal	drinking water treatment plant	-	-	44	49	27.9	0.7	1.2	-	-
			-	-	29	37	11.3	1.5	1.9	-	-
			-	-	41	46	18.0	3.1	2.6	-	-
			-	-	41	45	18.3	4.7	3.9	-	-
			-	-	23	5	0.2	0.7	54.1	-	-
Hutchison and Zilles 2018[263]	NO_3^- removal	drinking water treatment plant	0.512	0.367	46	75	2.4	9.4	-	7.0	
Korak et al. 2018[264]	Cr removal	drinking water treatment plant	-	-	41	50	16.3	2.3	2.9	8.3	-
			-	-	39	39	13.4	4.7	4.0	8.7	-
			-	-	37	50	9.1	1.8	2.0	8.9	-
Leong et al. 2015[265]	DOC removal	drinking water treatment plant	0.26	0.047	34.6	50.2	5.1	-	-	7.3	5418
Liu et al. 2013[266]	ClO_4^- removal	drinking water treatment plant	-	-	-	32	4.7	2.4	4.3	7.4	-
McAdam and Judd 2008[267]	NO_3^- removal	drinking water treatment plant	0.039	-	19	12	2.6	2.1	0.1	6.8	-
			0.171	-	42	51	4.4	8.8	0.43	7.4	-
Pakzadeh and Batista 2011[268]	As removal	drinking water treatment plant	-	-	16-27	24-73	4.8-48	-	-	-	-
Plummer et al. 2018[269]	Cr removal	drinking water treatment plant	-	-	-	49	18	-	-	-	-

Schaefer et al. 2020[270]	PFAS removal	synthetic brine	-	-	0.8-19.6	1.2-30	-	-	-	-	-
Singh et al. 2020[227]	PFAS removal	simulated IX in laboratory	-	-	7.8	12	-	-	-	-	-
Vaudevire et al. 2019[271]	COD removal	simulated IX in laboratory	0.025	-	15	13	7.5	0.3	7.1	-	540
Yang et al. 2013[272]	NO_3^- removal	drinking water treatment plant	0.027	0.021	17	25	6	1.7	-	7.8	24
	Reverse Osmosis (RO)										
Hajbi et al. 2010[273]	desalination	drinking water	2	0.8	5.1	14.2	-	-	-	7.2	-
Ji et al. 2010[274]	desalination	simulated RO process of synthetic brackish water	0.625	2.02	15	28.8	3.1	-	0.2	-	2.1
Justo et al. 2013[254]	NA	wastewater treatment plant	0.477	0.145	1.065	1.540	0.569	0.084	-	8.3	27.6
Lior and Kim 2018[275]	desalination	RO plant discharge	0.17-1.2	0.31-2.9	1.9-25	2.9-44	-	-	0.12-0.66	6.4-7.8	-
Ma et al. 2020[279]	NO_3^- removal	simulated RO of synthetic brackish water	0.525	0.39	1.8	3.1	0.4	0.07	2	-	-

Opong et al. 2022[276]	gold mining	cleaning waste	0.9	1.5	2.5	0.26	12	-	-	7.4-7.7	-
Walker et al. 2014[277]	desalination	brackish groundwater RO	1.03	0.515	0.88	3	0.9	0.08	1.0	-	-
	desalination	brackish groundwater RO	0.612	0.326	3.9	4.4	4.0	-	1.4	-	-
Yang et al. 2016[167]	wastewater recycling	wastewater RO	-	-	-	1.160	1.766	0.009	-	8.3	68.2
			-	-	-	2.015	1.437	0.341	-	8.4	50.6
Other											
Eeso 2022[278]	NA	landfill leachate	-	-	-	<30	-	-	-	-	<5000
Jose and Philip 2021[231]	NA	pharmaceutical waste brine	0.760	-	27	41	0.67	-	-	3.3	9300
Sun et al. 2013[233]	NA	hydraulic fracturing flowback	-	-	-	23	-	-	-	6.93	26.7
		hydraulic fracturing produced water	-	-	-	110	-	-	-	4.74	16.9
Singh et al. 2021[234]	NA	landfill leachate	-	-	-	-	-	-	-	-	2000

summary	Ca^{2+} (g/L)	Mg^{2+} (g/L)	Na^{+} (g/L)	Cl^{-} (g/L)	SO_4^{2-} (g/L)	NO_3^{-} (g/L)	carbonates[b] (g/L)	pH	TOC (mg-C/L)
	0.01-2	0.003-2.9	1-45	0.26-73	0.6-48	0.1-10	0.1-54	3.3-10	0-9300
	Ca^{2+} (M)	Mg^{2+} (M)	Na^{+} (M)	Cl^{-} (M)	SO_4^{2-} (M)	NO_3^{-} (M)	carbonates (M)	pH	TOC (mg-C/L)
	0.0025-0.05	0.0013-0.121	0.04-2	0.007-2	0.01-0.5	0.0016-0.16	0.0016-0.9	3.3-10	0-9300
selected in this study[c]	0[d]	0[d]	1.58-1.74	1.0	0.25	0.08	0.0016-0.16	7	10-1000

a. Arsenic (As), chromium (Cr), nitrate (NO_3^-), perchlorate (ClO_4^-), sodium chloride (NaCl), dissolved organic carbon (DOC), per- and polyfluoroalkyl substances (PFAS), chemical oxidation demand (COD).
b. The concentration of carbonates was shown as (g HCO_3^-)/L.
c. Bromide (Br^-) concentrations were reported in a small number of studies (i.e., 0.12 mM in Justo et al. 2013,[254] 0.03-0.04 mM in Yang et al. 2016,[167] 3-20 mM in Sun et al. 2013[233]). Using the Cl^- concentrations from the same studies, the Br^- concentrations corresponded to mol percent of 0.1-1 relative to Cl^-.
d. While Ca^{2+} and Mg^{2+} are present in some brines, the inclusion of these cations leads to the precipitation of solids with some anions (i.e., SO_4^{2-}, carbonates).[299–301] Given our focus on examining the impact of carbonates as competitors for radicals on organic compound degradation, we excluded Ca^{2+} and Mg^{2+} in our solutions containing brine constituents.

Table S4.3. Selected organic compounds and their bimolecular rate constants toward hydroxyl radical ($^{\bullet}OH$), hydrated electron (e_{aq}^{-}), halogen radicals ($Cl_2^{\bullet-}$, $Br^{\bullet}$, $Br_2^{\bullet-}$), HOCl, and hypobromous acid (HOBr).

compound	bimolecular rate constant ($M^{-1}s^{-1}$)						
	$k(^{\bullet}OH)$[a]	$k(e_{aq}^{-})$[b]	$k(Cl_2^{\bullet-})$[c]	$k(Br^{\bullet})$[d]	$k(Br_2^{\bullet-})$[e]	k(HOCl)[f]	k(HOBr)[g]
benzoate	6×10^9	3.6×10^9	2×10^6	$6.1(\pm0.1)\times10^8$	1×10^5	negligible	NA[h]
salicylate	1.2×10^{10}	1×10^{10}	$2.1(\pm0.2)\times10^8$	$5.9(\pm0.8)\times10^9$	$1.6(\pm0.2)\times10^7$	0.1 (pH 7.2)	NA[h]
acetaminophen	9.8×10^9	2.5×10^8	$4.3(\pm0.4)\times10^8$	$1.3(\pm0.3)\times10^{10}$	$4.7(\pm0.5)\times10^7$	13	570 (pH 8)
para-hydroxybenzoate	6.0×10^9	2×10^9	2.8×10^8	NA[h]	2.3×10^8	27 (pH 7.5)	5.2×10^4
sulfamethoxazole	5.5×10^9	8.5×10^9	$4.7(\pm0.4)\times10^8$	$1.44(\pm0.03)\times10^{10}$	$1.68(\pm0.09)\times10^8$	1.8×10^3	$1.6(\pm0.3)\times10^3$ (pH 8)
anthranilate	1.1×10^{10}	1.9×10^9	1.1×10^9	NA[h]	NA[h]	$>3\times10^4$	NA[h]

a. References: Ashton et al. 1995,[307] Amphlett et al. 1968,[319] Bisby and Tabassum 1988,[320] Anderson et al. 1987,[308] Mezyk et al. 2007,[321] Prutz and Land 1974.[322]
b. References: Anbar et al. 1967,[309] Amphlett et al. 1968,[319] Bisby and Tabassum 1988,[320] Anderson et al. 1987,[308] Mezyk et al. 2007,[321] Prutz and Land 1974.[322]
c. References: Hasegawa and Neta 1978;[41] Lei et al. 2019.[288] Instead of the rate constant for anthranilate (2-aminobenzoate), which was unavailable from literature, we substituted the rate constant for its isomer 4-aminobenzoate.[41] Substituents at the *ortho*- and *para*- positions have been previously shown to result in similar reactivity of phenols toward halogen oxidants.[7]
d. References: Lei et al. 2021.[286]
e. Reference: Lei et al. 2021;[286] Kemsley et al. 1974.[196]
f. k(HOCl) represents the apparent bimolecular rate constant between HOCl (pK_a 7.5)[7] and organic contaminants at pH 7 unless otherwise noted. Except for *para*-hydroxybenzoate, all apparent bimolecular rate constants were from Deborde and Von Gunten 2008.[7] The k(HOCl) for *para*-hydroxybenzoate at pH 7.5 was obtained from Jiang et al. 2020.[285] Additional calculation based on this value was applied to estimate k(HOCl) for *para*-hydroxybenzoate at pH 7 (**Text S2**), which was used in eq 5.
g. k(HOBr) represents the apparent bimolecular rate constant between HOBr (pK_a 8.7)[287] at pH 7 unless otherwise noted. References: Heeb et al. 2014;[287] Barazesh et al. 2016.[289]
h. NA: not available from literature.

Table S4.4. Known reactions of brine constituents with reactive species of interest.

reaction	rate constant ($M^{-1}s^{-1}$)	reference
$^{\bullet}OH + SO_4^{2-} \longrightarrow$ product	negligible	Jiang et al. 1992[292]
$^{\bullet}OH + NO_3^{-} \longrightarrow$ product	negligible	Katsumura et al. 1991[293]
$^{\bullet}OH + HCO_3^{-} \longrightarrow CO_3^{\bullet-} + H_2O$	8.5×10^6	Buxton et al. 1986[294]
$^{\bullet}OH + CO_3^{2-} \longrightarrow CO_3^{\bullet-} + OH^{-}$	3.9×10^8	Buxton et al. 1988[209]
$^{\bullet}OH$ + organic matter $\longrightarrow$ products	$1.60\pm(0.24)\times10^{8,a}$	Westerhoff et al. 2007[295]

$^{\bullet}OH$ + organic matter ⟶ products	2.23×10^{8}[b]	Westerhoff et al. 2007[295]
$^{\bullet}OH$ + organic matter ⟶ products	4.0×10^{8}[c]	Yang et al. 2016[167]
e_{aq}^{-} + NO_3^- ⟶ NO_2^-	9.2×10^{9}	Chen et al. 1994[296]
e_{aq}^{-} + SO_4^{2-} ⟶ products	$<1\times10^{6}$	Thomas et al. 1964[297]
e_{aq}^{-} + CO_3^{2-} ⟶ products	3.9×10^{5}	Nash et al. 1981[298]
$Cl^{\bullet}$ + HCO_3^- ⟶ Cl^- + $CO_3^{\bullet-}$ + H^+	2.2×10^{8}	Mertens and von Sonntag[290]
$Cl^{\bullet}$ + CO_3^{2-} ⟶ Cl^- + $CO_3^{\bullet-}$	5×10^{8}	Mertens and von Sonntag[290]
$Br_2^{\bullet-}$ + CO_3^{2-} ⟶ $2Br^-$ + $CO_3^{\bullet-}$	1.1×10^{5}	Huie et al. 1991[291]
HOCl + organic matter ⟶ products	50-500[d] 0.7-5[e]	Westerhoff et al. 2004[255]
HOBr + organic matter ⟶ products	500-5000[f] 15-167[g]	Westerhoff et al. 2004[255]

a. Suwannee River fulvic acid, unit: $(mol\text{-}C/L)^{-1}s^{-1}$.

b. Average of seven dissolved organic matter isolates fractioned from surface water, unit: $(mol\text{-}C/L)^{-1}s^{-1}$.

c. Effluent organic matter isolated from RO brine, unit: $(mol\text{-}C/L)^{-1}s^{-1}$. The bimolecular rate constant was converted from the reported value 3.3×10^{4} $(mg\text{-}C/L)^{-1}s^{-1}$ in literature,[167] assuming 12 g-C/mol-C.

d. Organic matter isolates from surface water, pH 5-11, unit: $(mol\text{-}C/L)^{-1}s^{-1}$. The rate constant was obtained based on the degradation of organic matter by HOCl for 1-5 min.

e. Organic matter isolates from surface water, pH 5-11, unit: $(mol\text{-}C/L)^{-1}s^{-1}$. The rate constant was obtained based on the degradation of organic matter by HOCl for 60 min.

f. Organic matter isolates from surface water, pH 5-11, unit: $(mol\text{-}C/L)^{-1}s^{-1}$. The rate constant was obtained based on the degradation of organic matter by HOBr for <15 s.

g. Organic matter isolates from surface water, pH 5-11, unit: $(mol\text{-}C/L)^{-1}s^{-1}$. The rate constant was obtained based on the degradation of organic matter by HOBr for 120 s.

Table S4.5. Retention times, UV wavelengths of detection, and values of limit of detection (LOD) of organic compounds measured on HPLC.

compound	retention time (min)	UV wavelength (nm)	LOD (μM)
two probe compound quantification mobile phase: 80% 10 mM phosphoric acid (pH 2), 20% acetonitrile/water (99/1 v/v)			
para-hydroxybenzoate	3.1	255	1[a]
benzoate	12.0	227	1[a]
six organic compound quantification mobile phase: 85% formic acid/water (99.9/0.1 v/v), 15% acetonitrile/water (99/1 v/v)			
acetaminophen	3.1	275	1[a]
para-hydroxybenzoate	4.0	275	1[a]
anthranilate	11.2	227	1[a]
benzoate	24.2	227	1
sulfamethoxazole	26.5	275	1[a]
salicylate	29.5	227	2

a. These values are the concentrations of the lowest standard analyzed, which are higher than the calculated values of LOD based on standard curves.

Table S4.6. Emission wavelengths for species in the analysis of optical mission spectrometry (OES) spectra.

species[a]	wavelength (nm)[b]	OES instrument	result
$^{\bullet}OH$	306.4	low-resolution	identified
	306.4, 309.2, 612.8[c]	high-resolution	identified

O	700.2	low-resolution	not detected
		high-resolution	identified
N_2	315.9, 337.1	low-resolution	identified
	293.6, 297.7, 441.7, 449.0, 575.5, 595.9, 601.4, 607.0, 631.8[d], 662.4	high-resolution	identified
Na	589.0	low-resolution	identified
	-	high-resolution	not attempted
Ar	696.5, 706.7, 738.4, 750.4, 763.5, 772.3, 794.8, 800.6, 801.5, 810.4, 811.5, 840.8, 842.6, 852.1, 912.3	low-resolution	identified
	560.7, 568.2, 696.5	high-resolution	identified
H	656.3	low-resolution	identified
		high-resolution	identified
$Cl^{\bullet}$	837	low-resolution	not detected
	443.8, 725.7	high-resolution	not detected
$Br^{\bullet}$	827	low-resolution	not detected
	442.5, 444.2, 447.3, 449.0, 451.3, 452.6, 612.2, 614.9, 633.6, 635.1, 641.0, 654.5, 656.0, 658.2, 663.2, 668.2, 669.2, 700.5	high-resolution	not detected
Cl_2	281.9, 288.1, 295.7	low-resolution	not detected
		high-resolution	not detected

Br_2	558.6, 564.4, 570.0, 575.8, 594.6, 600.5, 602.8, 607.5, 608.3, 614.5, 633.3, 637.2, 639.3, 652.0, 654.1,657.9, 664.6	low-resolution	not detected
		high-resolution	not detected

a. Hydroxyl radical (•OH), oxygen atom (O), nitrogen (N_2), sodium (Na), argon (Ar), hydrogen (H), halogen radicals (Cl•, Br•), molecular halogens (Cl_2, Br_2).
b. References: Pearse and Gaydon 1941,[303] National Institute of Standards and Technology (NIST) Atomic Spectra Database,[304] Hong et al. 2012,[305] Zhang et al. 2016.[306]
c. Second-order peak for •OH at 306.4 nm.
d. Second-order peak for N_2 at 315.9 nm.

4.5.3 Supplementary figures

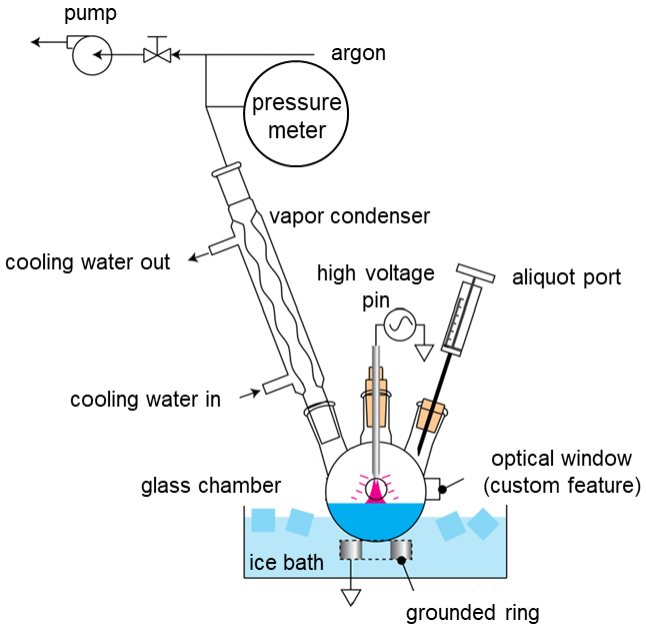

Figure S4.1. Plasma reactor setup. The optical window (quartz) is a custom feature of a vessel modified from the original reactor design, which was made in Department of Chemistry at Washington University in St. Louis. The vessel without modification was used in all experiments except for the OES analysis, where the modified vessel with an optical window was used.

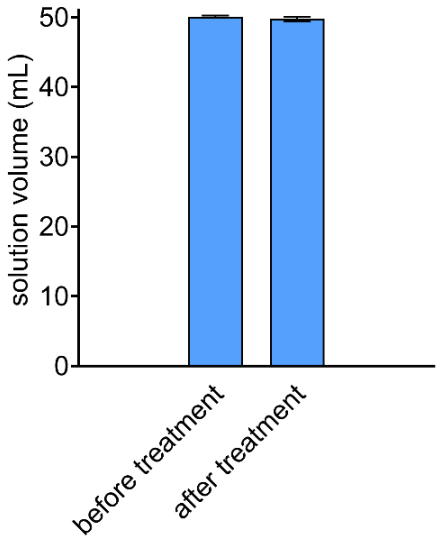

Figure S4.2. Volume of water solutions before and after plasma treatment for 30 min. All solutions were initially 50 mL, containing 1 M Cl^-, 10 mM Br^-, and 10 mM phosphate buffer (pH 7). This experiment was performed separately from chemical analysis to avoid the removal of sample volumes as specified in the method section in the manuscript. Errors represent the range of measurements from duplicate experiments.

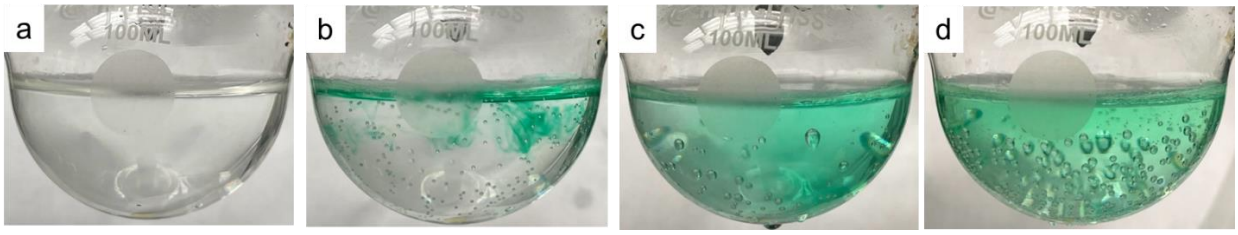

Figure S4.3. Mixing of a dye during plasma treatment. The solution contained 1 M 99.0% Cl^-, 10 mM Br^-, and 10 mM phosphate buffer (pH 7). Images were taken for (a) before adding the dye, (b) the moment added in 10 µL dye, (c) after plasma treatment for 1 min, and (d) after plasma treatment for 2 min. Images in (c-d) were taken after turning off plasma and removing the ice bath. The bubbles in (c-d) were typically observed in our experiments when plasma operates.

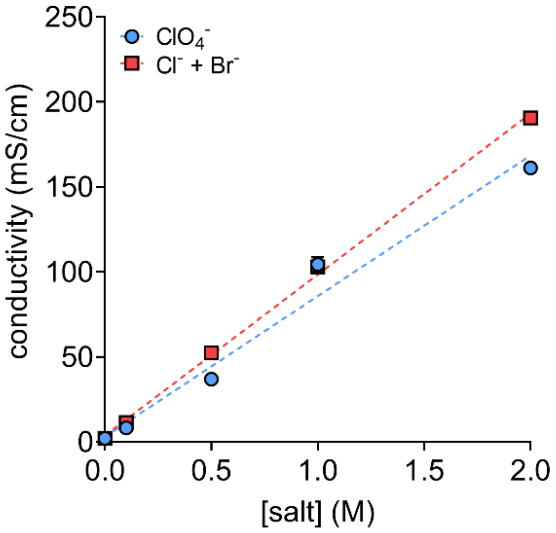

Figure S4.4. Measured conductivity of solutions containing salts. All solutions initially contained 10 mM phosphate buffer (pH 7), 50 µM each benzoate and para-hydroxybenzoate, and ClO_4^- or halides (i.e., Cl^-, purity: 99.0%, with 1 mol percent added Br^-). Errors represent the range of measurements from duplicate experiments.

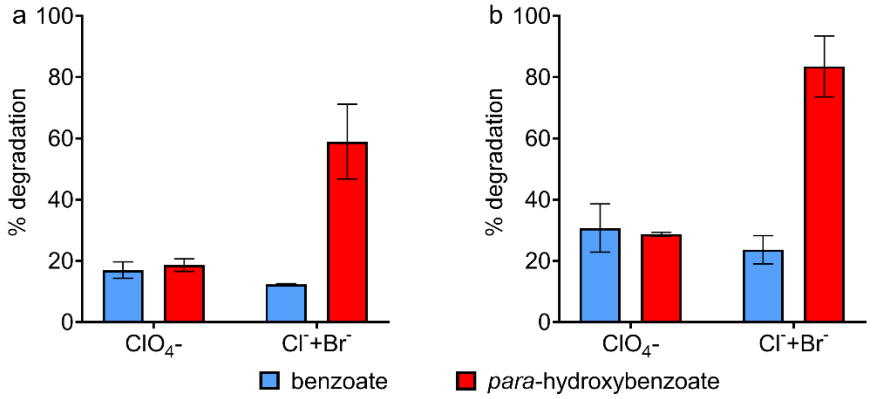

Figure S4.5. Degradation of benzoate and para-hydroxybenzoate at (**a**) 760 Torr and (**b**) 100 Torr after plasma treatment for 30 min. All solutions initially contained 10 mM phosphate buffer (pH 7), 50 µM each benzoate and para-hydroxybenzoate, and 1 M ClO_4^- or 1 M Cl^- together with 10 mM Br^-. Errors represent the range of measurements from duplicate experiments.

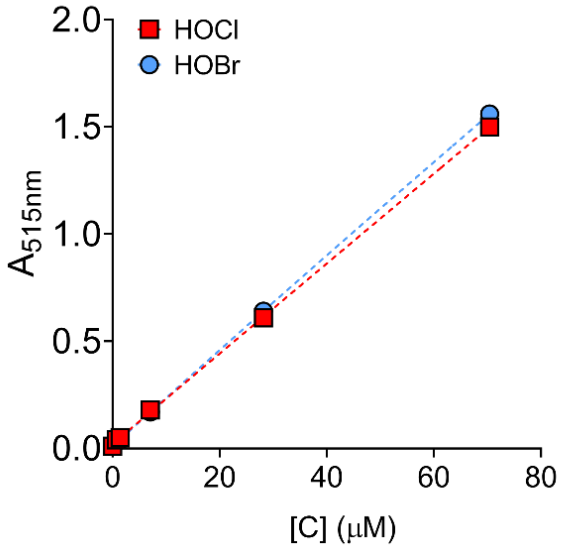

Figure S4.6. Standard curves of HOCl and HOBr measured by the N,N-diethyl-phenylenediamine (DPD) colorimetric method.[302] A_{515nm} represents the absorbance at 515 nm.

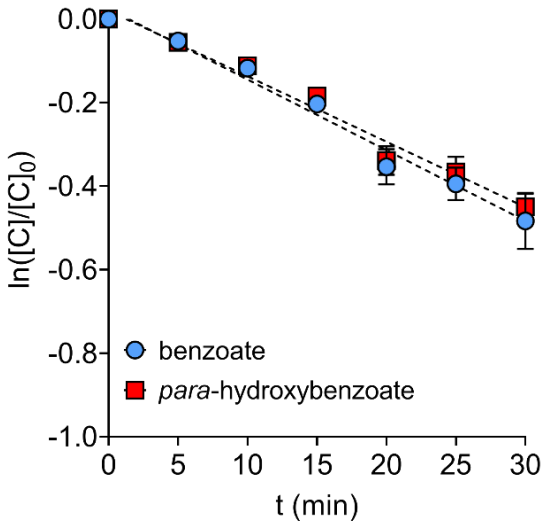

Figure S4.7. Pseudo-first-order degradation of benzoate and para-hydroxybenzoate in MilliQ water. All solutions initially contained 10 mM phosphate buffer (pH 7) and 50 µM each benzoate and para-hydroxybenzoate. Errors represent the range of measurements from duplicate experiments.

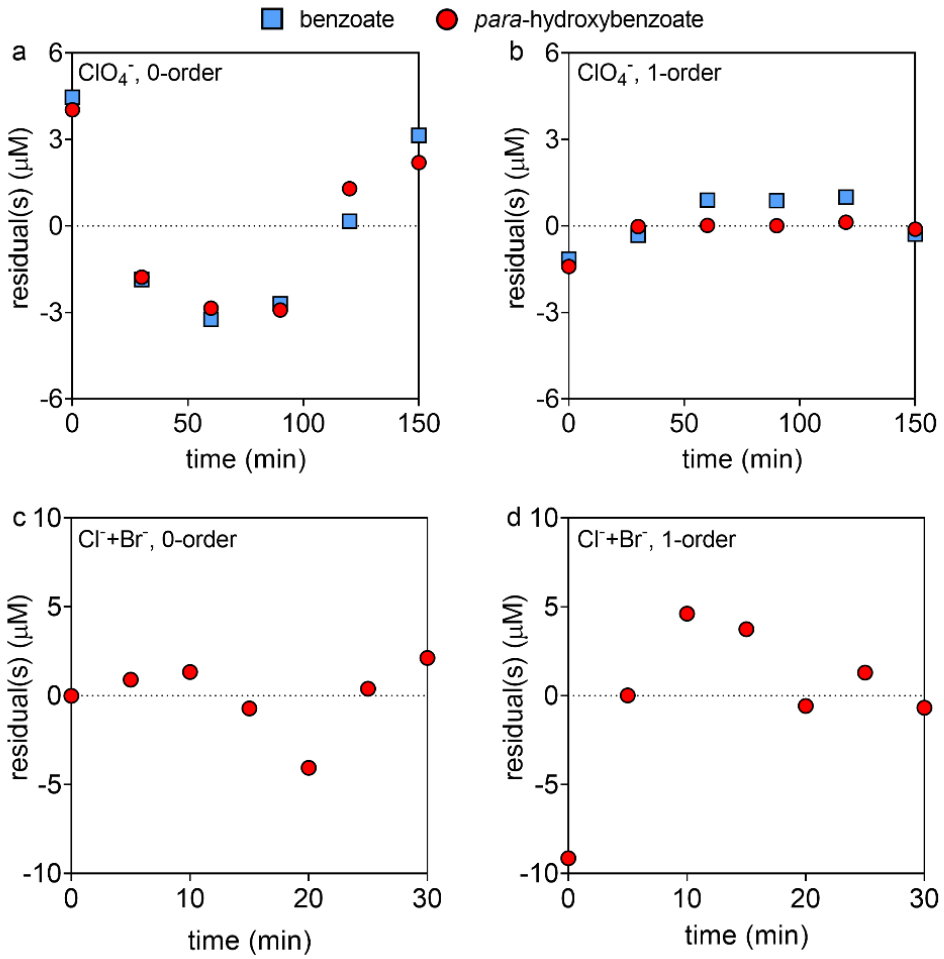

Figure S4.8. Residual for the degradation rates of benzoate and para-hydroxybenzoate during plasma treatment. Residuals were calculated by subtracting the calculated concentrations (predicted by zero-order degradation rate or pseudo-first-order rate constant values obtained from data in **Figure 4.1a,c**) from the measured concentrations of benzoate and para-hydroxybenzoate. All solutions initially contain 10 mM phosphate buffer (pH 7), 50 µM each benzoate and para-hydroxybenzoate, and (**a,b**) 1M ClO_4^- or (**c,d**) 1M Cl^- and 10 mM Br^-. The analysis of benzoate in (**c,d**) was excluded due to <20% degradation during plasma treatment for 30 min in the presence of halides.

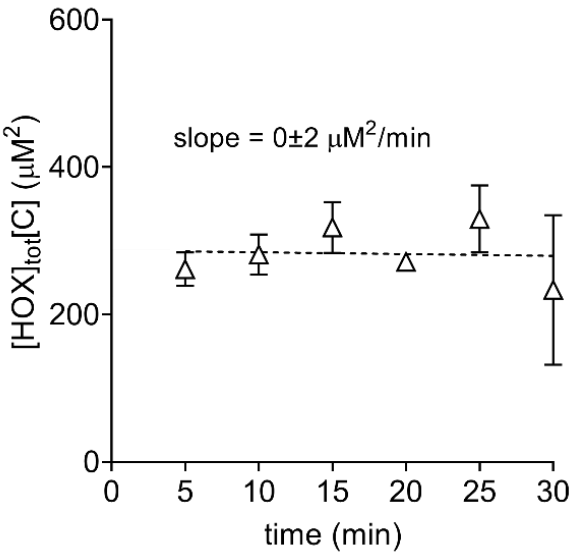

Figure S4.9. The multiplication product of the concentrations of total hypohalous acids and para-hydroxybenzoate (i.e., $[HOX]_{tot}[C]$). $[HOX]_{tot}$ represents the measured total concentration of hypohalous acids (**Figure 4.1d**, condition: with probe compounds) and [C] represents the concentrations of para-hydroxybenzoate (**Figure 4.1c**, condition: with halides). The slope of the fitted line (i.e., 0±2 μM^2/min) was not significantly different from zero (p=0.89). Errors represent the range of measurements from duplicate experiments.

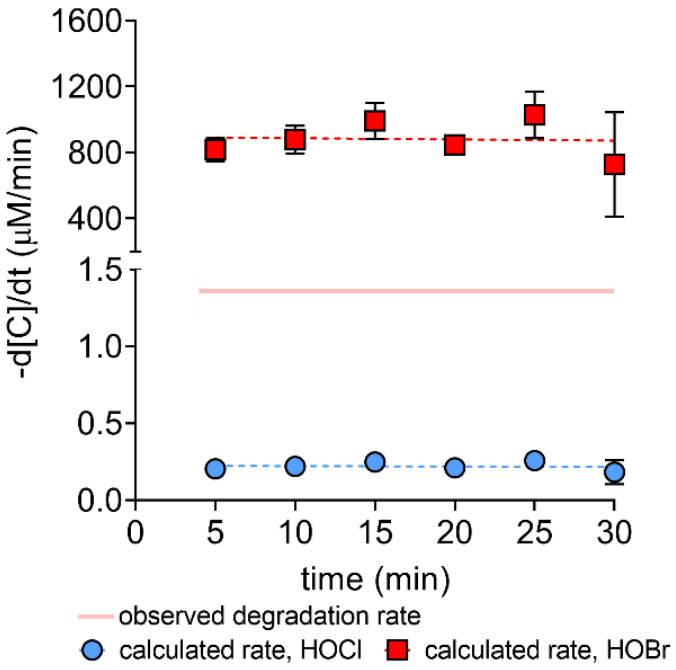

Figure S4.10. The observed and calculated degradation rates of para-hydroxybenzoate. The observed degradation rate was 1.36±0.07 µM/min (**Figure 4.1c**). The calculated degradation rate at each time point was based on $-d[C]/dt = [k_{C,HOCl} f_{HOCl} + k_{C,HOBr}(1 - f_{HOCl})][HOX]_{tot}[C]$ (eq 5 in the manuscript) when assuming the fraction of hypohalous acids present as HOCl (i.e., f_{HOCl}) was 1 or 0. $k_{C,HOCl}$ and $k_{C,HOBr}$ represent the apparent bimolecular rate constant between para-hydroxybenzoate and HOCl (i.e., 13 $M^{-1}s^{-1}$, pH 7, calculated based on a rate constant at a different pH[285] as described in **Text S4.2**) or HOBr (i.e., $k_{C,HOBr} = 5.2 \times 10^4\ M^{-1}s^{-1}$, pH 7);[287] $[HOX]_{tot}$ represents the measured total concentration of hypohalous acids (**Figure 4.1d**, condition: with probe compounds); [C] represents the concentration of para-hydroxybenzoate (**Figure 4.1c**, condition: with halides); Errors represent the range of measurements from duplicate experiments.

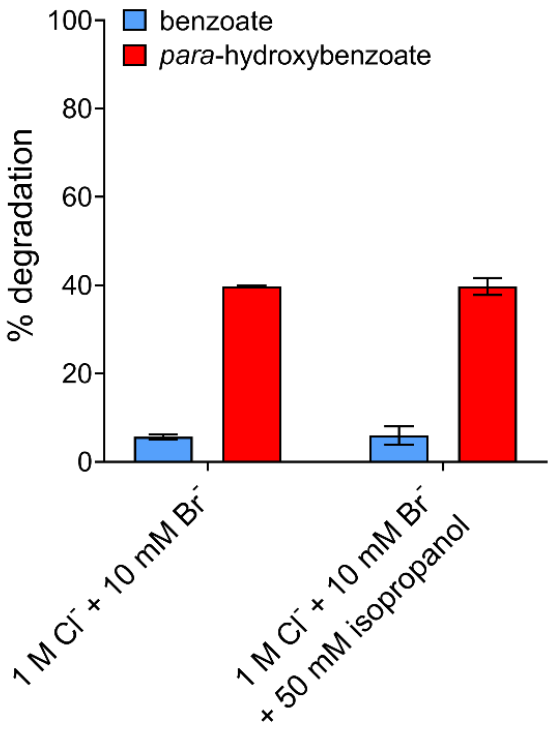

Figure S4.11. Effect of isopropanol on the degradation of benzoate and para-hydroxybenzoate by direct addition of HOCl. The experimental time was 30 min. All solutions initially contained 10 mM phosphate buffer (pH 7), 50 µM each benzoate and para-hydroxybenzoate, 1 M Cl^-, 10 mM Br^-, 50 µM HOCl, and isopropanol at the indicated concentration. Errors represent the range of measurements from duplicate experiments.

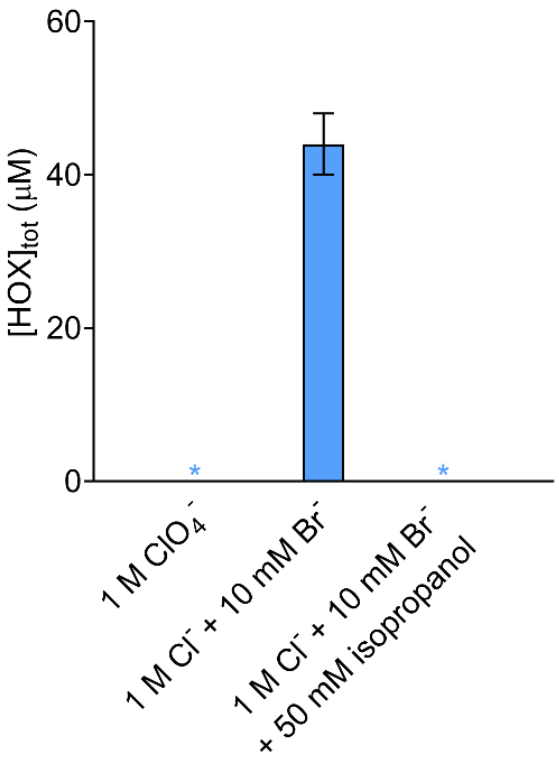

Figure S4.12. Effects of halides and isopropanol on the measured concentration of hypohalous acids ($[HOX]_{tot}$) after the exposure of solutions to plasma for 30 min. All solutions initially contained 10 mM phosphate buffer (pH 7), 50 µM each benzoate and para-hydroxybenzoate, salts, and isopropanol at indicated concentrations. Results in the presence of 1 M ClO_4^- or 1 M Cl^- and 10 mM Br^- are reproduced from **Figure 4.1e**. Asterisks (*) represent below the LOD of hypohalous acids (i.e., $[HOX]_{tot}$ =0.8 µM). Errors represent the range of measurements from duplicate experiments.

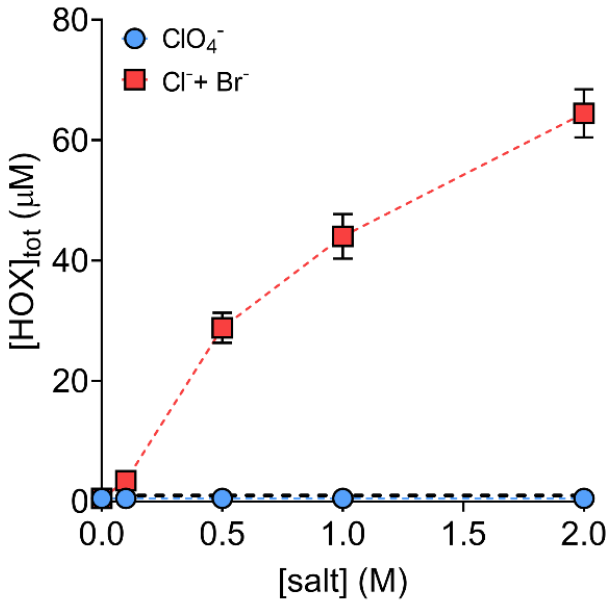

Figure S4.13. Measured concentrations of hypohalous acids ($[HOX]_{tot}$) after the exposure of solutions to plasma for 30 min. All solutions initially containing 10 mM phosphate buffer (pH 7), 50 μM each benzoate and para-hydroxybenzoate, and ClO_4^- or halides (i.e., Cl^-, purity: 99.0%, with 1 mol percent added Br^-); results collected with 1 M salt are reproduced from **Figure 4.1e**. Errors represent the range of measurements from duplicate experiments.

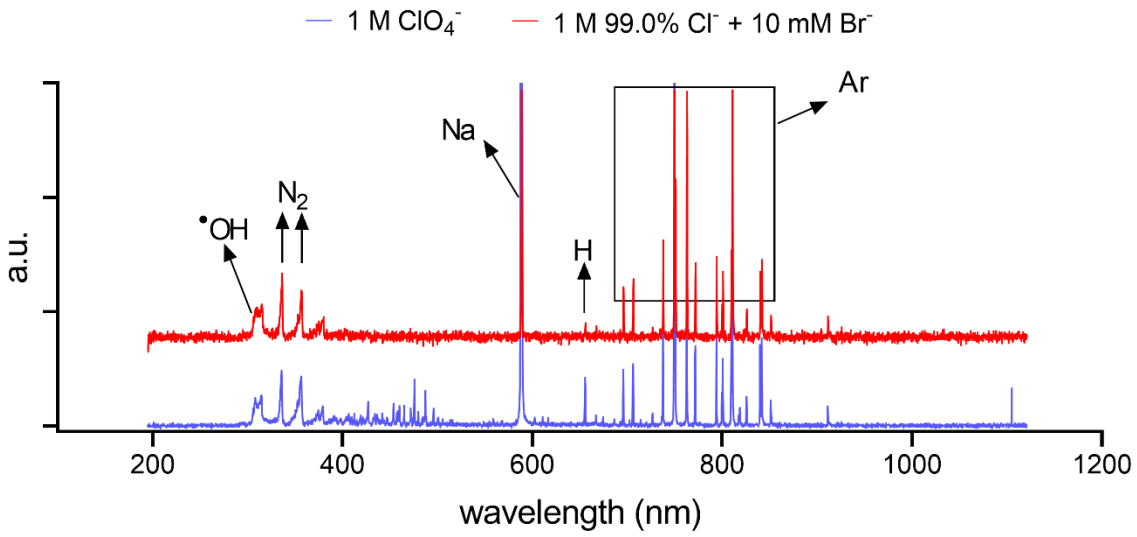

Figure S4.14. Low-resolution OES spectrum (200-1100 nm) of plasma over solutions containing 1 M ClO_4^- or 1 M Cl^- and 10 mM Br^-. All solutions contain 10 mM phosphate buffer (pH 7) and 50 µM each benzoate and *para*-hydroxybenzoate.

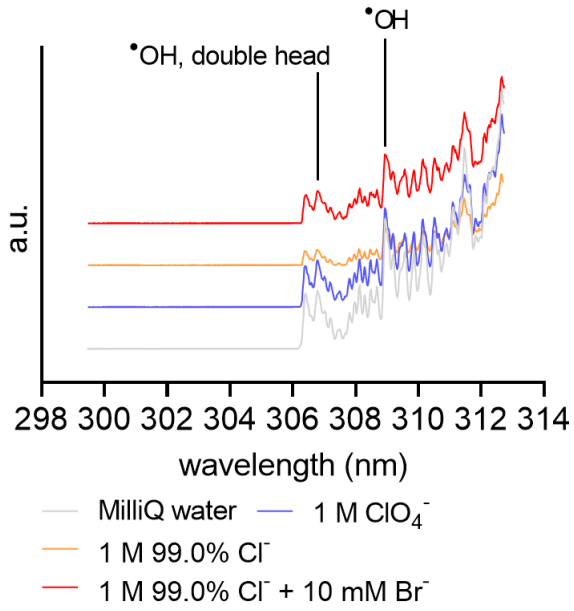

Figure S4.15. High-resolution OES spectra (299-313 nm) of plasma over MilliQ water or solutions containing salts using the high-resolution OES spectrometer. Solutions containing salts also contained 10 mM phosphate buffer (pH 7) and 50 µM each benzoate and para-hydroxybenzoate. •OH was identified at 306.4 and 309.2 nm.[303,305]

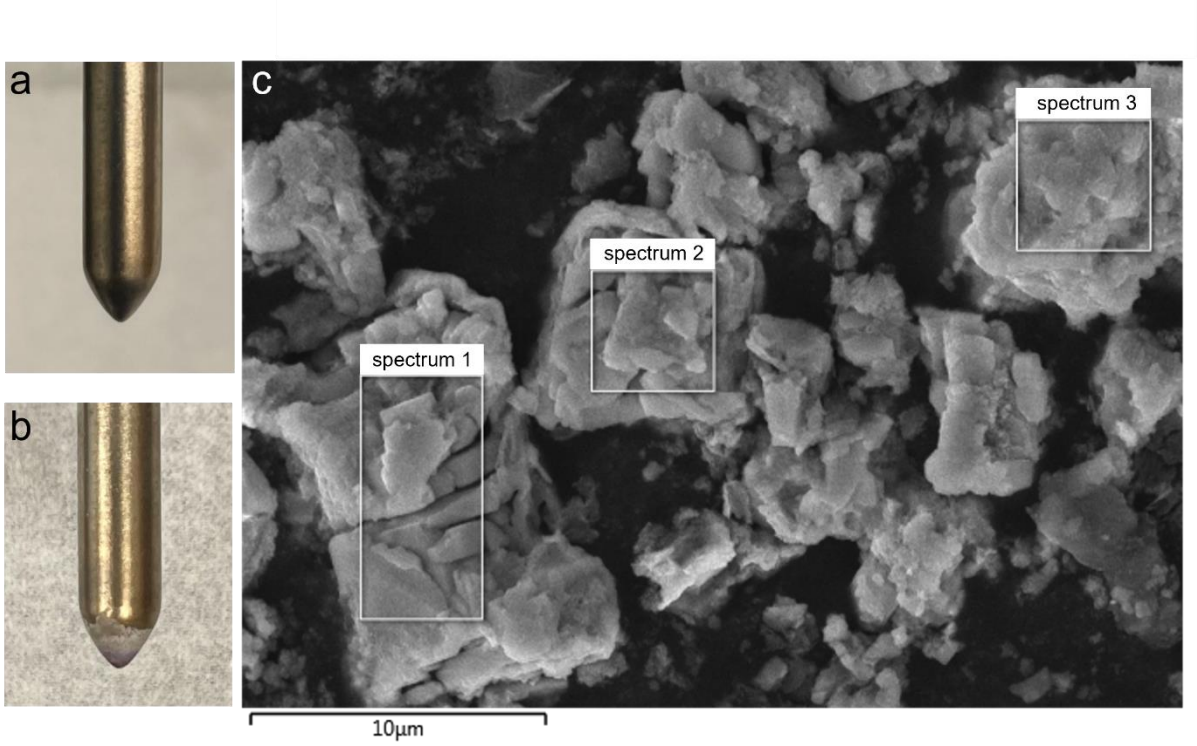

Figure S4.16. Scanning electron microscopy (SEM) analysis of salt deposition on the electrode after plasma treatment. (**a**) Electrode before plasma treatment. (**b**) Electrode after plasma treatment for 1 h. The treated solution initially contained 10 mM phosphate buffer (pH 7), 50 µM each benzoate and para-hydroxybenzoate, 1 M 99.0% Cl^-, and 10 mM Br^-. (**c**) The SEM image of deposited salts, which was obtained by a Thermofisher Quattro S environmental scanning electron microscope under a high vacuum mode (0.001 Pa), with a 10 mm working distance. The electron source was a Schottky field emission gun operated at 10kV. The selected areas overlaid on the image were used to collect energy-dispersive X-ray spectra shown in **Figure S4.17**.

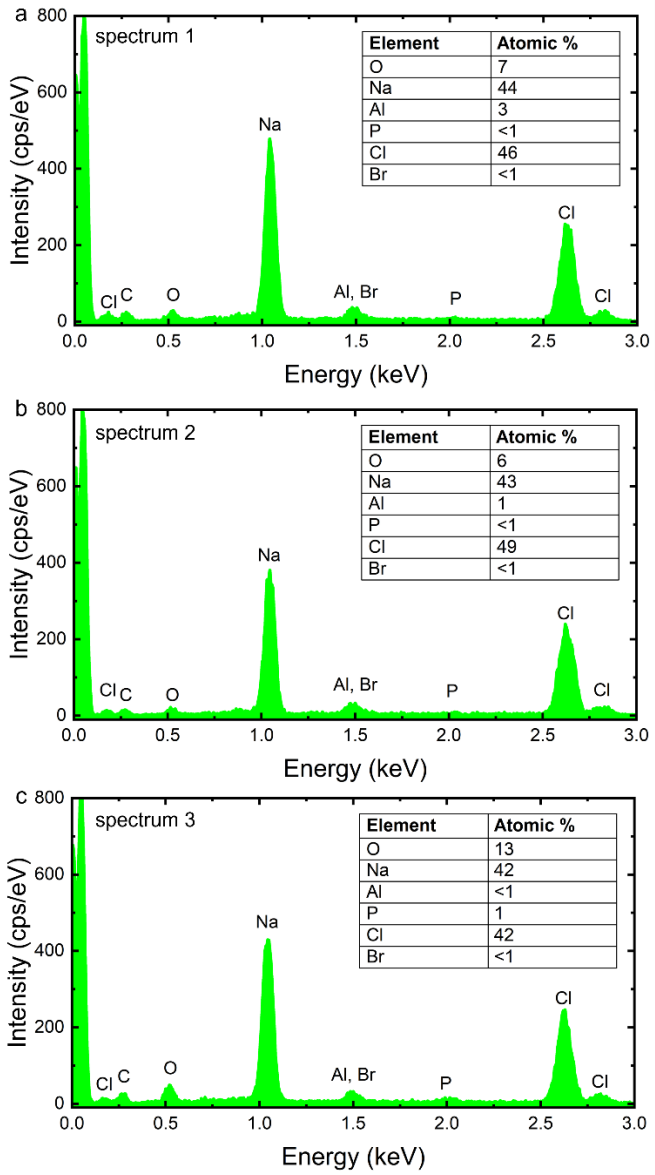

Figure S4.17. Energy-dispersive X-ray spectra for elemental analysis of salt deposit on the electrode after plasma treatment. Three spectra (**a-c**) were collected by rastering the electron beam in the areas marked spectrum 1-3 in **Figure S4.16**, respectively. The elemental analysis was conducted on an Oxford AzTec Energy Dispersive X-ray Spectrometer equipped on a Thermofisher Quattro S Environmental Scanning Electron Microscope.

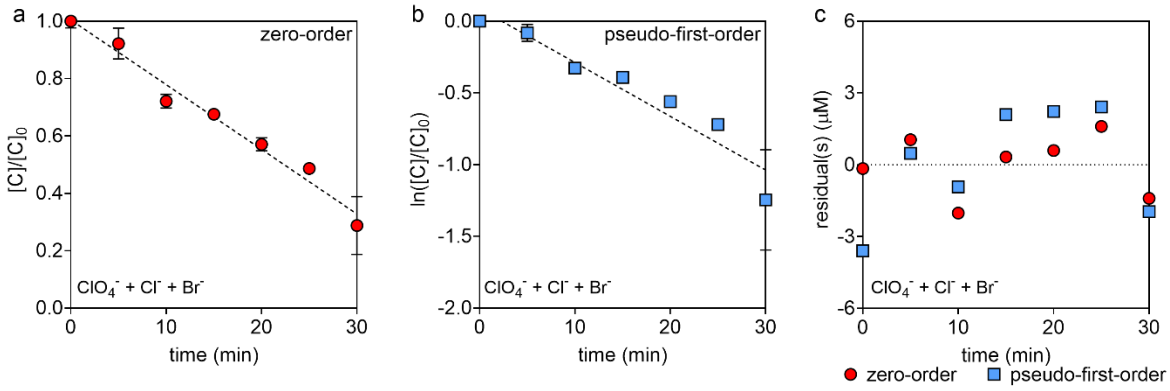

Figure S4.18. Analysis of the degradation kinetics of anthranilate in the presence of halides (**Figure 4.3a**) assuming zero- or pseudo-first-order kinetics. All experiments initially contained 10 mM phosphate buffer (pH 7), 50 µM each of the six organic compounds (i.e., benzoate, acetaminophen, salicylate, para-hydroxybenzoate, sulfamethoxazole, anthranilate) and 0.99 M ClO_4^-, 1 M Cl^-, and 10 mM Br^- (ionic strength 2.0 M). Errors in (**a-b**) represent the range of measurements from duplicate experiments.

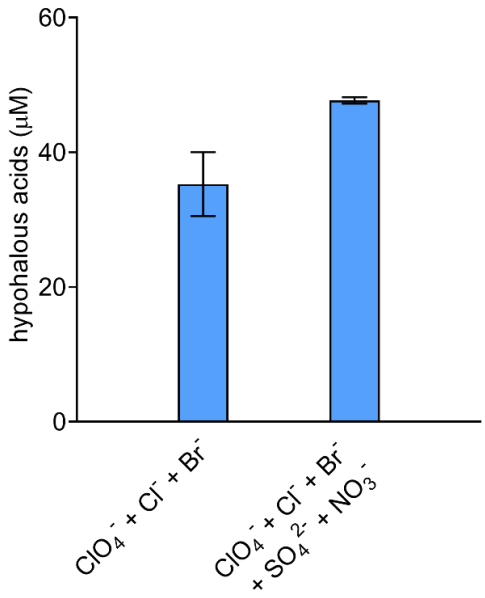

Figure S4.19. Concentrations of hypohalous acids produced after plasma treatment of six organic compounds. Experiments were conducted for 30 min with solutions initially containing 10 mM phosphate buffer (pH 7), 50 μM each benzoate, salicylate, acetaminophen, *para*-hydroxybenzoate, sulfamethoxazole, anthranilate, and indicated salts. The ionic strength of all solutions was adjusted to 2.0 M by ClO_4^-. The concentrations of Cl^-, Br^-, SO_4^{2-}, and NO_3^-, when present, were 1 M, 10 mM, 0.25 M, and 0.08 M, respectively. The concentrations of hypohalous acids measured under these two different conditions have no significant difference ($p=0.07$). Errors represent the range of measurements from duplicate experiments.

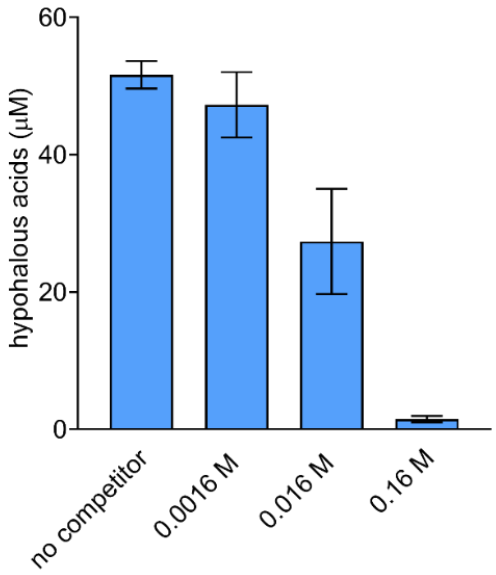

Figure S4.20. Effects of carbonates on the measured concentration of hypohalous acids after plasma treatment of acetaminophen and sulfamethoxazole. Experiments were conducted for 30 min with solutions initially containing 10 mM phosphate buffer (pH 7), 50 μM each acetaminophen and sulfamethoxazole, 1 M 99.0% Cl^-, 10 mM Br^-, 0.25 M SO_4^{2-}, 0.08 M NO_3^-, and carbonates at indicated concentrations. The ionic strength of all solutions was adjusted to 2.0 M by ClO_4^-. Errors represent the range of measurements from duplicate experiments.

Chapter 5: Conclusions and implications

To advance the understanding of the role of halogen oxidants in engineered aquatic systems, this dissertation evaluated the halogenation mechanisms and degradation kinetics of organic compounds in both conventional drinking water treatment (Chapter 2) and emerging radical-based oxidative processes (Chapters 3 and 4). This dissertation overall provides necessary information for future engineering designs to develop effective strategies that degrade organic compounds while reducing the hazard posed by halogenated byproducts. Specific conclusions and implications for each objective are drawn below:

1. In conventional drinking water treatment (Chapter 2), this work specifically demonstrated that while permanganate preoxidation tended to decrease the formation of halogenated byproducts formation from NOM, permanganate preoxidation increased the formation of certain halogenated byproducts during chlorination and chloramination of AOM. Specifically, this work demonstrated how permanganate reacted with specific organic moieties (e.g., organic amines) in AOM to alter the formation potential of certain halogenated byproducts. These findings need to be considered during the treatment of HAB-impacted water.
2. In hydraulic fracturing fluids (Chapter 3), this work provided the first evidence that, despite the presence of high organic content that could scavenge radicals, halogenation of specific organic additives and the subsequent production of halogenated compounds still occur through a mechanism mediated by halogen radicals. In addition, while previous research on AOPs focused on the direct reactions between organic compounds and halogen radicals,[8] the recombination products of halogen radicals (i.e., hypohalous acids) are also important oxidants that lead to the formation of halogenated byproducts in hydraulic fracturing fluids. These findings are necessary to evaluate the adverse impact of using radical-based breakers on target

organic compound degradation and the unintentional formation of toxic halogenated byproducts in future hydraulic fracturing designs.

3. In plasma-based water treatment (Chapter 4), this work demonstrated that halides in brines contributed to the formation of hypohalous acids via a mechanism mediated by halogen radicals, resulting in the selective degradation of organic compounds. While the effect of chloride was negligible, bromide particularly contributed to the selective degradation of organic compounds during plasma treatment. These results indicate that knowledge of halogen radical formation in conventional AOPs is applicable to plasma-based water treatment. In addition, rather than halogen radicals themselves, their recombination products (i.e., hypohalous acids) had a dominant role in organic compound degradation, which distinguishes plasma reactors from conventional AOPs. This work contributed to the precise understanding of the mechanism mediated by halogen radicals during plasma treatment of brines.

References

(1) Broséus, R.; Vincent, S.; Aboulfadl, K.; Daneshvar, A.; Sauvé, S.; Barbeau, B.; Prévost, M. Ozone Oxidation of Pharmaceuticals, Endocrine Disruptors and Pesticides during Drinking Water Treatment. *Water Res.* **2009**, *43* (18), 4707–4717. https://doi.org/10.1016/j.watres.2009.07.031.

(2) Ormad, M. P.; Miguel, N.; Claver, A.; Matesanz, J. M.; Ovelleiro, J. L. Pesticides Removal in the Process of Drinking Water Production. *Chemosphere* **2008**, *71* (1), 97–106. https://doi.org/10.1016/j.chemosphere.2007.10.006.

(3) Saleh, I. A.; Zouari, N.; Al-Ghouti, M. A. Removal of Pesticides from Water and Wastewater: Chemical, Physical and Biological Treatment Approaches. *Environ. Technol. Innov.* **2020**, *19*, 101026. https://doi.org/10.1016/j.eti.2020.101026.

(4) Ternes, T. A.; Meisenheimer, M.; McDowell, D.; Sacher, F.; Brauch, H. J.; Haist-Gulde, B.; Preuss, G.; Wilme, U.; Zulei-Seibert, N. Removal of Pharmaceuticals during Drinking Water Treatment. *Environ. Sci. Technol.* **2002**, *36* (17), 3855–3863. https://doi.org/10.1021/es015757k.

(5) Buxton, G. V.; Greenstock, C. L.; Helman, W. P.; Ross, A. B. Critical Review of Rate Constants for Reactions of Hydrated Electrons, Hydrogen Atoms and Hydroxyl Radicals (•OH/•O^- in Aqueous Solution. *J. Phys. Chem. Ref. Data* **1988**, *17* (2), 513–886. https://doi.org/10.1063/1.555805.

(6) Neta, P.; Huie, R. E.; Ross, A. B. Rate Constants for Reactions of Inorganic Radicals in Aqueous Solution. *J. Phys. Chem. Ref. Data* **1988**, *17* (3), 1027–1284. https://doi.org/10.1063/1.555978.

(7) Deborde, M.; von Gunten, U. Reactions of Chlorine with Inorganic and Organic Compounds during Water Treatment-Kinetics and Mechanisms: A Critical Review. *Water Res.* **2008**, *42* (1–2), 13–51. https://doi.org/10.1016/j.watres.2007.07.025.

(8) Zhang, K.; Parker, K. M.; Science, E. Halogen Radical Oxidants in Natural and Engineered Aquatic Systems. *Environ. Sci. Technol.* **2018**, *52* (17), 9579–9594. https://doi.org/10.1021/acs.est.8b02219.

(9) Richardson, S. D. Disinfection By-Products and Other Emerging Contaminants in Drinking Water. *TrAC - Trends Anal. Chem.* **2003**, *22* (10), 666–684. https://doi.org/10.1016/S0165-9936(03)01003-3.

(10) Krasner, S. W.; Weinberg, H. S.; Richardson, S. D.; Pastor, S. J.; Chinn, R.; Sclimenti, M. J.; Onstad, G. D.; Thruston, A. D. Occurrence of a New Generation of Disinfection Byproducts. *Environ. Sci. Technol.* **2006**, *40* (23), 7175–7185. https://doi.org/10.1021/es060353j.

(11) U.S. EPA. *Alternative Disinfectants and Oxidants Guidance Manual*; 1999.

(12) Lin, Y. wen; Li, D.; Gu, A. Z.; Zeng, S. yu; He, M. Bacterial Regrowth in Water Reclamation and Distribution Systems Revealed by Viable Bacterial Detection Assays. *Chemosphere* **2016**, *144*, 2165–2174. https://doi.org/10.1016/j.chemosphere.2015.10.071.

(13) Jjemba, P. K.; Weinrich, L. A.; Cheng, W.; Giraldo, E.; LeChevallier, M. W. Regrowth of Potential Opportunistic Pathogens and Algae in Reclaimed-Water Distribution Systems. *Appl. Environ. Microbiol.* **2010**, *76* (13), 4169–4178. https://doi.org/10.1128/AEM.03147-09.

(14) Richardson, S. D.; Plewa, M. J.; Wagner, E. D.; Schoeny, R.; DeMarini, D. M. Occurrence, Genotoxicity, and Carcinogenicity of Regulated and Emerging Disinfection by-Products in Drinking Water: A Review and Roadmap for Research. *Mutat. Res. - Rev. Mutat. Res.* **2007**, *636* (1–3), 178–242. https://doi.org/10.1016/j.mrrev.2007.09.001.

(15) Hua, G.; Reckhow, D. A. Comparison of Disinfection Byproduct Formation from Chlorine and Alternative Disinfectants. *Water Res.* **2007**, *41* (8), 1667–1678. https://doi.org/10.1016/j.watres.2007.01.032.

(16) Krasner, S. W.; Westerhoff, P.; Chen, B.; Rittmann, B. E.; Amy, G. Occurrence of Disinfection Byproducts in United States Wastewater Treatment Plant Effluents. *Environ. Sci. Technol.* **2009**, *43* (21), 8320–8325. https://doi.org/10.1021/es901611m.

(17) Kim, D.; Amy, G. L.; Karanfil, T. Disinfection By-Product Formation during Seawater Desalination: A Review. *Water Res.* **2015**, *81*, 343–355. https://doi.org/10.1016/j.watres.2015.05.040.

(18) U.S. EPA. National Primary Drinking Water Regulations https://www.epa.gov/ground-water-and-drinking-water/national-primary-drinking-water-regulations (accessed Oct 12, 2022).

(19) Selbes, M.; Beita-Sandí, W.; Kim, D.; Karanfil, T. The Role of Chloramine Species in NDMA Formation. *Water Res.* **2018**, *140*, 100–109. https://doi.org/10.1016/j.watres.2018.04.033.

(20) Le Roux, J.; Gallard, H.; Croué, J. P. Chloramination of Nitrogenous Contaminants (Pharmaceuticals and Pesticides): NDMA and Halogenated DBPs Formation. *Water Res.* **2011**, *45* (10), 3164–3174. https://doi.org/10.1016/j.watres.2011.03.035.

(21) Schreiber, I. M.; Mitch, W. A. Nitrosamine Formation Pathway Revisited: The Importance of Chloramine Speciation and Dissolved Oxygen. *Environ. Sci. Technol.* **2006**, *40* (19), 6007–6014. https://doi.org/10.1021/es060978h.

(22) Fang, J.; Ma, J.; Yang, X.; Shang, C. Formation of Carbonaceous and Nitrogenous Disinfection By-Products from the Chlorination of Microcystis Aeruginosa. *Water Res.* **2010**, *44* (6), 1934–1940. https://doi.org/10.1016/j.watres.2009.11.046.

(23) Fang, J.; Yang, X.; Ma, J.; Shang, C.; Zhao, Q. Characterization of Algal Organic Matter and Formation of DBPs from Chlor(Am)Ination. *Water Res.* **2010**, *44* (20), 5897–5906. https://doi.org/10.1016/j.watres.2010.07.009.

(24) Coral, L. A.; Zamyadi, A.; Barbeau, B.; Bassetti, F. J.; Lapolli, F. R.; Prévost, M. Oxidation of *Microcystis aeruginosa* and *Anabaena flos-aquae* by Ozone: Impacts on Cell Integrity and Chlorination by-Product Formation. *Water Res.* **2013**, *47* (9), 2983–2994. https://doi.org/10.1016/j.watres.2013.03.012.

(25) Zhou, S.; Shao, Y.; Gao, N.; Li, L.; Deng, J.; Zhu, M.; Zhu, S. Effect of Chlorine Dioxide on Cyanobacterial Cell Integrity, Toxin Degradation and Disinfection by-Product

Formation. *Sci. Total Environ.* **2014**, *482–483* (1), 208–213. https://doi.org/10.1016/j.scitotenv.2014.03.007.

(26) Fan, J.; Ho, L.; Hobson, P.; Brookes, J. Evaluating the Effectiveness of Copper Sulphate, Chlorine, Potassium Permanganate, Hydrogen Peroxide and Ozone on Cyanobacterial Cell Integrity. *Water Res.* **2013**, *47* (14), 5153–5164. https://doi.org/10.1016/j.watres.2013.05.057.

(27) Shah, A. D.; Mitch, W. A. Halonitroalkanes, Halonitriles, Haloamides, and N-Nitrosamines: A Critical Review of Nitrogenous Disinfection Byproduct Formation Pathways. *Environ. Sci. Technol.* **2012**, *46* (1), 119–131. https://doi.org/10.1021/es203312s.

(28) Wojnárovits, L.; Takács, E. Rate Constants of Sulfate Radical Anion Reactions with Organic Molecules: A Review. *Chemosphere* **2019**, *220*, 1014–1032. https://doi.org/10.1016/j.chemosphere.2018.12.156.

(29) Clifton, C. L.; Huie, R. E. Rate Constants for Hydrogen Abstraction Reactions of the Sulfate Radical, SO_4^-. Alcohols. *Int. J. Chem. Kinet.* **1989**, *21* (8), 677–687. https://doi.org/10.1002/kin.550210807.

(30) Huie, R. E.; Clifton, C. L. Rate Constants for Hydrogen Abstraction Reactions of the Sulfate Radical, SO_4^-. Alkanes and Ethers. *Int. J. Chem. Kinet.* **1989**, *21* (8), 611–619. https://doi.org/10.1002/kin.550210802.

(31) Huie, R. E.; Clifton, C. L.; Kafafi, S. A. Rate Constants for Hydrogen Abstraction Reactions of the Sulfate Radical, SO_4^-. Experimental and Theoretical Results for Cyclic Ethers. *J. Phys. Chem.* **1991**, *95* (23), 9336–9340. https://doi.org/10.1021/j100176a055.

(32) Neta, P.; Madhavan, V.; Zemel, H.; Fessenden, R. W. Rate Constants and Mechanism of Reaction of SO_4^-. with Aromatic Compounds. *J. Am. Chem. Soc.* **1977**, *99* (1), 163–164. https://doi.org/10.1021/ja00443a030.

(33) Huang, K. C.; Zhao, Z.; Hoag, G. E.; Dahmani, A.; Block, P. A. Degradation of Volatile Organic Compounds with Thermally Activated Persulfate Oxidation. *Chemosphere* **2005**, *61* (4), 551–560. https://doi.org/10.1016/j.chemosphere.2005.02.032.

(34) Parker, K. M.; Reichwaldt, E. S.; Ghadouani, A.; Mitch, W. A. Halogen Radicals Promote the Photodegradation of Microcystins in Estuarine Systems. *Environ. Sci. Technol.* **2016**, *50* (16), 8505–8513. https://doi.org/10.1021/acs.est.6b01801.

(35) Parker, K. M.; Mitch, W. A. Halogen Radicals Contribute to Photooxidation in Coastal and Estuarine Waters. *Proc. Natl. Acad. Sci. U. S. A.* **2016**, *113* (21), 5868–5873. https://doi.org/10.1073/pnas.1602595113.

(36) Chu, C.; Stamatelatos, D.; McNeill, K. Aquatic Indirect Photochemical Transformations of Natural Peptidic Thiols: Impact of Thiol Properties, Solution pH, Solution Salinity and Metal Ions. *Environ. Sci. Process. Impacts* **2017**, *19* (12), 1518–1527. https://doi.org/10.1039/c7em00324b.

(37) Grebel, J. E.; Pignatello, J. J.; Song, W.; Cooper, W. J.; Mitch, W. A. Impact of Halides on the Photobleaching of Dissolved Organic Matter. *Mar. Chem.* **2009**, *115* (1–2), 134–144. https://doi.org/10.1016/j.marchem.2009.07.009.

(38) Méndez-Díaz, J. D.; Shimabuku, K. K.; Ma, J.; Enumah, Z. O.; Pignatello, J. J.; Mitch, W. A.; Dodd, M. C. Sunlight-Driven Photochemical Halogenation of Dissolved Organic Matter in Seawater: A Natural Abiotic Source of Organobromine and Organoiodine. *Environ. Sci. Technol.* **2014**, *48* (13), 7418–7427. https://doi.org/10.1021/es5016668.

(39) Leri, A. C.; Mayer, L. M.; Thornton, K. R.; Ravel, B. Bromination of Marine Particulate Organic Matter through Oxidative Mechanisms. *Geochim. Cosmochim. Acta* **2014**, *142* (1), 53–63. https://doi.org/10.1016/j.gca.2014.08.012.

(40) Leri, A. C.; Mayer, L. M.; Thornton, K. R.; Northrup, P. A.; Dunigan, M. R.; Ness, K. J.; Gellis, A. B. A Marine Sink for Chlorine in Natural Organic Matter. *Nat. Geosci.* **2015**, *8* (8), 620–624. https://doi.org/10.1038/ngeo2481.

(41) Hasegawa, K.; Neta, P. Rate Constants and Mechanisms of Reaction of Chloride (Cl2-) Radicals. *J. Phys. Chem.* **1978**, *82* (8), 854–857. https://doi.org/10.1021/j100497a003.

(42) Guha, S. N.; Schoneich, C.; Asmus, K.-D. Free Radical Reductive Degradation of Vic-Dibromoalkanes and Reaction of Bromine Atoms with Polyunsaturated Fatty Acids: Possible Involvement of Br. in the 1,2-Dibromoethane-Induced Lipid-Peroxidation. *Arch. Biochem. Biophys.* **1993**, *305* (1), 132–140.

(43) Yu, X. Y.; Barker, J. R. Hydrogen Peroxide Photolysis in Acidic Aqueous Solutions Containing Chloride Ions. I. Chemical Mechanism. *J. Phys. Chem. A* **2003**, *107* (9), 1313–1324. https://doi.org/10.1021/jp0266648.

(44) Wu, D.; Wong, D.; Di Bartolo, B. Evolution of Cl-2 in Aqueous NaCl Solutions. *J. Photochem.* **1980**, *14* (4), 303–310. https://doi.org/10.1016/0047-2670(80)85102-1.

(45) Yu, X. Y.; Bao, Z. C.; Barker, J. R. Free Radical Reactions Involving $Cl^{\bullet}$, $Cl_2^{\bullet-}$, and $SO_4^{\bullet-}$. in the 248 nm Photolysis of Aqueous Solutions Containing $S_2O_8^{2-}$ and Cl^-. *J. Phys. Chem. A* **2004**, *108* (2), 295–308. https://doi.org/10.1021/jp036211i.

(46) Ershov, B. G.; Kelm, M.; Gordeev, A. V.; Janata, E. A Pulse Radiolysis Study of the Oxidation of Br^- by $Cl_2^{\bullet-}$ in Aqueous Solution: Formation and Properties of ClBr·-. *Phys. Chem. Chem. Phys.* **2002**, *4* (10), 1872–1875. https://doi.org/10.1039/b110362h.

(47) Matthew, B. M.; Anastasio, C. A Chemical Probe Technique for the Determination of Reactive Halogen Species in Aqueous Solution: Part 1 - Bromide Solutions. *Atmos. Chem. Phys.* **2006**, *6* (1), 899–940. https://doi.org/10.5194/acp-6-2423-2006.

(48) Wong, D.; Di Bartolo, B. Evolution of the Dihalide Ion Br-2 in Aqueous Solutions. *J. Photochem.* **1975**, *4* (4), 249–268. https://doi.org/10.1016/0047-2670(75)87003-1.

(49) Matheson, M. S.; Mulac, W. A.; Weeks, J. L.; Rabani, J. The Pulse Radiolysis of Deaerated Aqueous Bromide Solutions. *J. Phys. Chem.* **1966**, *70* (7), 2092–2099. https://doi.org/10.1021/j100879a004.

(50) Deborde, M.; von Gunten, U. Reactions of Chlorine with Inorganic and Organic Compounds during Water Treatment-Kinetics and Mechanisms: A Critical Review. *Water Res.* **2008**, *42* (1–2), 13–51. https://doi.org/10.1016/j.watres.2007.07.025.

(51) Heeb, M. B.; Criquet, J.; Zimmermann-Steffens, S. G.; Von Gunten, U. Oxidative Treatment of Bromide-Containing Waters: Formation of Bromine and Its Reactions with Inorganic and Organic Compounds - A Critical Review. *Water Res.* **2014**, *48* (1), 15–42.

https://doi.org/10.1016/j.watres.2013.08.030.

(52) Criquet, J.; Rodriguez, E. M.; Allard, S.; Wellauer, S.; Salhi, E.; Joll, C. A.; von Gunten, U. Reaction of Bromine and Chlorine with Phenolic Compounds and Natural Organic Matter Extracts - Electrophilic Aromatic Substitution and Oxidation. *Water Res.* **2015**, *85*, 476–486. https://doi.org/10.1016/j.watres.2015.08.051.

(53) Al-Muntasheri, G. A.; Li, L.; Liang, F.; Gomaa, A. M. Concepts in Cleanup of Fracturing Fluids Used in Conventional Reservoirs: A Literature Review. *SPE Prod. Oper.* **2018**, *33* (2), 196–213. https://doi.org/10.2118/186112-pa.

(54) Montgomery, C. Fracturing Fluid Components. In *Effective and Sustainable Hydraulic Fracturing*; IntechOpen, 2013; pp 25–45. https://doi.org/http://dx.doi.org/10.5772/57353.

(55) Bruggeman, P. J.; Kushner, M. J.; Locke, B. R.; Gardeniers, J. G. E.; Graham, W. G.; Graves, D. B.; Hofman-Caris, R. C. H. M.; Maric, D.; Reid, J. P.; Ceriani, E.; et al. Plasma-Liquid Interactions: A Review and Roadmap. *Plasma Sources Sci. Technol.* **2016**, *25* (5). https://doi.org/10.1088/0963-0252/25/5/053002.

(56) Sharma, A. K.; Josephson, G. B.; Camaioni, D. M.; Goheen, S. C. Destruction of Pentachlorophenol Using Glow Discharge Plasma Process. *Environ. Sci. Technol.* **2000**, *34* (11), 2267–2272. https://doi.org/10.1021/es981001i.

(57) Johnson, D. C.; Shamamian, V. A.; Callahan, J. H.; Denes, F. S.; Manolache, S. O.; Dandy, D. S. Treatment of Methyl Tert-Butyl Ether Contaminated Water Using a Dense Medium Plasma Reactor: A Mechanistic and Kinetic Investigation. *Environ. Sci. Technol.* **2003**, *37* (20), 4804–4810. https://doi.org/10.1021/es0263487.

(58) Wardenier, N.; Gorbanev, Y.; Van Moer, I.; Nikiforov, A.; Van Hulle, S. W. H.; Surmont, P.; Lynen, F.; Leys, C.; Bogaerts, A.; Vanraes, P. Removal of Alachlor in Water by Non-Thermal Plasma: Reactive Species and Pathways in Batch and Continuous Process. *Water Res.* **2019**, *161*, 549–559. https://doi.org/10.1016/j.watres.2019.06.022.

(59) Magureanu, M.; Mandache, N. B.; Parvulescu, V. I. Degradation of Pharmaceutical Compounds in Water by Non-Thermal Plasma Treatment. *Water Res.* **2015**, *81*, 124–136. https://doi.org/10.1016/j.watres.2015.05.037.

(60) Zhang, H.; Huang, Q.; Ke, Z.; Yang, L.; Wang, X.; Yu, Z. Degradation of Microcystin-LR in Water by Glow Discharge Plasma Oxidation at the Gas-Solution Interface and Its Safety Evaluation. *Water Res.* **2012**, *46* (19), 6554–6562. https://doi.org/10.1016/j.watres.2012.09.041.

(61) Saleem, M.; Biondo, O.; Sretenović, G.; Tomei, G.; Magarotto, M.; Pavarin, D.; Marotta, E.; Paradisi, C. Comparative Performance Assessment of Plasma Reactors for the Treatment of PFOA; Reactor Design, Kinetics, Mineralization and Energy Yield. *Chem. Eng. J.* **2020**, *382* (September 2019), 123031. https://doi.org/10.1016/j.cej.2019.123031.

(62) Jovicic, V.; Khan, M. J.; Zbogar-Rasic, A.; Fedorova, N.; Poser, A.; Swoboda, P.; Delgado, A. Degradation of Low Concentrated Perfluorinated Compounds (PFCs) from Water Samples Using Non-Thermal Atmospheric Plasma (NTAP). *Energies* **2018**, *11* (5). https://doi.org/10.3390/en11051290.

(63) Stratton, G. R.; Dai, F.; Bellona, C. L.; Holsen, T. M.; Dickenson, E. R. V.; Mededovic

Thagard, S. Plasma-Based Water Treatment: Efficient Transformation of Perfluoroalkyl Substances in Prepared Solutions and Contaminated Groundwater. *Environ. Sci. Technol.* **2017**, *51* (3), 1643–1648. https://doi.org/10.1021/acs.est.6b04215.

(64) Lewis, A. J.; Joyce, T.; Hadaya, M.; Ebrahimi, F.; Dragiev, I.; Giardetti, N.; Yang, J.; Fridman, G.; Rabinovich, A.; Fridman, A. A.; et al. Rapid Degradation of PFAS in Aqueous Solutions by Reverse Vortex Flow Gliding Arc Plasma. *Environ. Sci. Water Res. Technol.* **2020**, *6* (4), 1044–1057. https://doi.org/10.1039/c9ew01050e.

(65) Laszakovits, J. R.; Somogyi, A.; Mackay, A. A. Chemical Alterations of Dissolved Organic Matter by Permanganate Oxidation. *Environ. Sci. Technol.* **2020**, *54* (6), 3256–3266. https://doi.org/10.1021/acs.est.9b06675.

(66) Waldemer, R. H.; Tratnyek, P. G. Kinetics of Contaminant Degradation by Permanganate. *Environ. Sci. Technol.* **2006**, *40* (3), 1055–1061. https://doi.org/10.1021/es051330s.

(67) Perez-Benito, J. F. Autocatalytic Reaction Pathway on Manganese Dioxide Colloidal Particles in the Permanganate Oxidation of Glycine. *J. Phys. Chem. C* **2009**, *113* (36), 15982–15991. https://doi.org/10.1021/jp9014178.

(68) He, S.; Ren, N. Permanganate/Bisulfite Pre-Oxidation of Natural Organic Matter Enhances Nitrogenous Disinfection By-Products Formation during Subsequent Chlorination. *Water* **2022**, *14*, 507. https://doi.org/https://doi.org/ 10.3390/w14030507.

(69) Hidayah, E. N.; Yeh, H. H. Effect of Permanganate Preoxidation to Natural Organic Matter and Disinfection By-Products Formation Potential Removal. *J. Phys. Conf. Ser.* **2018**, *953* (1), 012218. https://doi.org/10.1088/1742-6596/953/1/012218.

(70) Hu, J.; Chu, W.; Sui, M.; Xu, B.; Gao, N.; Ding, S. Comparison of Drinking Water Treatment Processes Combinations for the Minimization of Subsequent Disinfection By-Products Formation during Chlorination and Chloramination. *Chem. Eng. J.* **2018**, *335* (July 2017), 352–361. https://doi.org/10.1016/j.cej.2017.10.144.

(71) Rougé, V.; Von Gunten, U.; Lafont De Sentenac, M.; Massi, M.; Wright, P. J.; Croué, J. P.; Allard, S. Comparison of the Impact of Ozone, Chlorine Dioxide, Ferrate and Permanganate Pre-Oxidation on Organic Disinfection Byproduct Formation during Post-Chlorination. *Environ. Sci. Water Res. Technol.* **2020**, *6* (9), 2382–2395. https://doi.org/10.1039/d0ew00411a.

(72) Rougé, V.; von Gunten, U.; Allard, S. Efficiency of Pre-Oxidation of Natural Organic Matter for the Mitigation of Disinfection Byproducts: Electron Donating Capacity and UV Absorbance as Surrogate Parameters. *Water Res.* **2020**, *187*. https://doi.org/10.1016/j.watres.2020.116418.

(73) Hallegraeff, G.; Enevoldsen, H.; Zingone, A. Global Harmful Algal Bloom Status Reporting. *Harmful Algae* **2021**, *102*. https://doi.org/10.1016/j.hal.2021.101992.

(74) Hallegraeff, G. M.; Anderson, D. M.; Belin, C.; Bottein, M.-Y. D.; Bresnan, E.; Chinain, M.; Enevoldsen, H.; Iwataki, M.; Karlson, B.; McKenzie, C. H.; et al. Perceived Global Increase in Algal Blooms Is Attributable to Intensified Monitoring and Emerging Bloom Impacts. *Commun. Earth Environ.* **2021**, *2* (1), 117. https://doi.org/10.1038/s43247-021-00178-8.

(75) Hudnell, H. K. The State of U.S. Freshwater Harmful Algal Blooms Assessments, Policy and Legislation. *Toxicon* **2010**, *55* (5), 1024–1034. https://doi.org/10.1016/j.toxicon.2009.07.021.

(76) Roberts, V. A.; Vigar, M.; Backer, L.; Veytsel, G. E.; Hilborn, E. D.; Hamelin, E. I.; Vanden Esschert, K. L.; Lively, J. Y.; Cope, J. R.; Hlavsa, M. C.; et al. Surveillance for Harmful Algal Bloom Events and Associated Human and Animal Illnesses — One Health Harmful Algal Bloom System, United States, 2016–2018. *MMWR. Morb. Mortal. Wkly. Rep.* **2020**, *69* (50), 1889–1894. https://doi.org/10.15585/mmwr.mm6950a2.

(77) Piezer, K.; Li, L.; Jeon, Y.; Kadudula, A.; Seo, Y. The Application of Potassium Permanganate to Treat Cyanobacteria-Laden Water: A Review. *Process Saf. Environ. Prot.* **2021**, *148*, 400–414. https://doi.org/10.1016/j.psep.2020.09.058.

(78) Xie, P.; Chen, Y.; Ma, J.; Zhang, X.; Zou, J.; Wang, Z. A Mini Review of Preoxidation to Improve Coagulation. *Chemosphere* **2016**, *155*, 550–563. https://doi.org/10.1016/j.chemosphere.2016.04.003.

(79) Naceradska, J.; Pivokonsky, M.; Pivokonska, L.; Baresova, M.; Henderson, R. K.; Zamyadi, A.; Janda, V. The Impact of Pre-Oxidation with Potassium Permanganate on Cyanobacterial Organic Matter Removal by Coagulation. *Water Res.* **2017**, *114*, 42–49. https://doi.org/10.1016/j.watres.2017.02.029.

(80) Chen, J. J.; Yeh, H. H. The Mechanisms of Potassium Permanganate on Algae Removal. *Water Res.* **2005**, *39* (18), 4420–4428. https://doi.org/10.1016/j.watres.2005.08.032.

(81) Qi, J.; Ma, B.; Miao, S.; Liu, R.; Hu, C.; Qu, J. Pre-Oxidation Enhanced Cyanobacteria Removal in Drinking Water Treatment: A Review. *J. Environ. Sci.* **2021**, *110*, 160–168. https://doi.org/10.1016/j.jes.2021.03.040.

(82) Xie, P.; Ma, J.; Fang, J.; Guan, Y.; Yue, S.; Li, X.; Chen, L. Comparison of Permanganate Preoxidation and Preozonation on Algae Containing Water: Cell Integrity, Characteristics, and Chlorinated Disinfection Byproduct Formation. *Environ. Sci. Technol.* **2013**, *47* (24), 14051–14061. https://doi.org/10.1021/es4027024.

(83) Greenstein, K. E.; Zamyadi, A.; Glover, C. M.; Adams, C.; Rosenfeldt, E.; Wert, E. C. Delayed Release of Intracellular Microcystin Following Partial Oxidation of Cultured and Naturally Occurring Cyanobacteria. *Toxins.* **2020**, *12* (5), 335. https://doi.org/https://doi:10.3390/toxins12050335.

(84) Novoa, A. F.; Vrouwenvelder, J. S.; Fortunato, L. Membrane Fouling in Algal Separation Processes: A Review of Influencing Factors and Mechanisms. *Front. Chem. Eng.* **2021**, *3* (May), 1–18. https://doi.org/10.3389/fceng.2021.687422.

(85) Rodríguez, E.; Majado, M. E.; Meriluoto, J.; Acero, J. L. Oxidation of Microcystins by Permanganate: Reaction Kinetics and Implications for Water Treatment. *Water Res.* **2007**, *41* (1), 102–110. https://doi.org/10.1016/j.watres.2006.10.004.

(86) Rodríguez, E.; Onstad, G. D.; Kull, T. P. J.; Metcalf, J. S.; Acero, J. L.; von Gunten, U. Oxidative Elimination of Cyanotoxins: Comparison of Ozone, Chlorine, Chlorine Dioxide and Permanganate. *Water Res.* **2007**, *41* (15), 3381–3393. https://doi.org/10.1016/j.watres.2007.03.033.

(87) Dong, F.; Lin, Q.; Li, C.; He, G.; Deng, Y. Impacts of Pre-Oxidation on the Formation of Disinfection Byproducts from Algal Organic Matter in Subsequent Chlor(Am)Ination: A Review. *Sci. Total Environ.* **2021**, *754*, 141955. https://doi.org/10.1016/j.scitotenv.2020.141955.

(88) Shi, X.; Bi, R.; Yuan, B.; Liao, X.; Zhou, Z.; Li, F.; Sun, W. A Comparison of Trichloromethane Formation from Two Algae Species during Two Pre-Oxidation-Coagulation-Chlorination Processes. *Sci. Total Environ.* **2019**, *656*, 1063–1070. https://doi.org/10.1016/j.scitotenv.2018.11.461.

(89) Sheng, D.; Bu, L.; Zhu, S.; Wu, Y.; Wang, J.; Li, N.; Zhou, S. Impact of Pre-Oxidation on the Formation of Byproducts in Algae-Laden Water Disinfection: Insights from Fluorescent and Molecular Weight. *J. Environ. Sci.* **2022**, *117*, 21–27. https://doi.org/10.1016/j.jes.2021.12.021.

(90) Hua, G.; Reckhow, D. A. DBP Formation during Chlorination and Chloramination: Effect of Reaction Time. PH, Dosage, and Temperature. *J. / Am. Water Work. Assoc.* **2008**, *100* (8). https://doi.org/10.1002/j.1551-8833.2008.tb09702.x.

(91) Yang, X.; Guo, W.; Lee, W. Formation of Disinfection Byproducts upon Chlorine Dioxide Preoxidation Followed by Chlorination or Chloramination of Natural Organic Matter. *Chemosphere* **2013**, *91* (11), 1477–1485. https://doi.org/10.1016/j.chemosphere.2012.12.014.

(92) Jiang, Y.; Goodwill, J. E.; Tobiason, J. E.; Reckhow, D. A. Comparison of the Effects of Ferrate, Ozone, and Permanganate Pre-Oxidation on Disinfection Byproduct Formation from Chlorination. *ACS Symp. Ser.* **2016**, *1238* (Vi), 421–437. https://doi.org/10.1021/bk-2016-1238.ch016.

(93) Jiang, Y.; Goodwill, J. E.; Tobiason, J. E.; Reckhow, D. A. Comparison of Ferrate and Ozone Pre-Oxidation on Disinfection Byproduct Formation from Chlorination and Chloramination. *Water Res.* **2019**, *156*, 110–124. https://doi.org/10.1016/j.watres.2019.02.051.

(94) Zhou, S.; Zhu, S.; Shao, Y.; Gao, N. Characteristics of C-, N-DBPs Formation from Algal Organic Matter: Role of Molecular Weight Fractions and Impacts of Pre-Ozonation. *Water Res.* **2015**, *72*, 381–390. https://doi.org/10.1016/j.watres.2014.11.023.

(95) Chien, I. C.; Wu, S. P.; Ke, H. C.; Lo, S. L.; Tung, H. H. Comparing Ozonation and Biofiltration Treatment of Source Water with High Cyanobacteria-Derived Organic Matter: The Case of a Water Treatment Plant Followed by a Small-Scale Water Distribution System. *Int. J. Environ. Res. Public Health* **2018**, *15* (12), 2633. https://doi.org/10.3390/ijerph15122633.

(96) Zhu, M.; Gao, N.; Chu, W.; Zhou, S.; Zhang, Z.; Xu, Y.; Dai, Q. Impact of Pre-Ozonation on Disinfection by-Product Formation and Speciation from Chlor(Am)Ination of Algal Organic Matter of Microcystis Aeruginosa. *Ecotoxicol. Environ. Saf.* **2015**, *120*, 256–262. https://doi.org/10.1016/j.ecoenv.2015.05.048.

(97) McCurry, D. L.; Quay, A. N.; Mitch, W. A. Ozone Promotes Chloropicrin Formation by Oxidizing Amines to Nitro Compounds. *Environ. Sci. Technol.* **2016**, *50* (3), 1209–1217. https://doi.org/10.1021/acs.est.5b04282.

(98) Pedersen, E. J.; Urbansky, E. T.; Mariñas, B. J.; Margerum, D. W. Formation of Cyanogen Chloride from the Reaction of Monochloramine with Formaldehyde. *Environ. Sci. Technol.* **1999**, *33* (23), 4239–4249. https://doi.org/10.1021/es990153q.

(99) Zeng, T.; Plewa, M. J.; Mitch, W. A. N-Nitrosamines and Halogenated Disinfection Byproducts in U.S. Full Advanced Treatment Trains for Potable Reuse. *Water Res.* **2016**, *101*, 176–186. https://doi.org/10.1016/j.watres.2016.03.062.

(100) Szczuka, A.; Parker, K. M.; Harvey, C.; Hayes, E.; Vengosh, A.; Mitch, W. A. Regulated and Unregulated Halogenated Disinfection Byproduct Formation from Chlorination of Saline Groundwater. *Water Res.* **2017**, *122*, 633–644. https://doi.org/10.1016/j.watres.2017.06.028.

(101) Wagner, E. D.; Plewa, M. J. CHO Cell Cytotoxicity and Genotoxicity Analyses of Disinfection By-Products: An Updated Review. *J. Environ. Sci.* **2017**, *58*, 64–76. https://doi.org/10.1016/j.jes.2017.04.021.

(102) Laszakovits, J. R.; Kerr, A.; Mackay, A. A. Permanganate Oxidation of Organic Contaminants and Model Compounds. *Environ. Sci. Technol.* **2022**, *56* (8), 4728–4748. https://doi.org/10.1021/acs.est.1c03621.

(103) McKenna, E.; Thompson, K. A.; Taylor-Edmonds, L.; McCurry, D. L.; Hanigan, D. Summation of Disinfection By-Product CHO Cell Relative Toxicity Indices: Sampling Bias, Uncertainty, and a Path Forward. *Environ. Sci. Process. Impacts* **2020**, *22* (3), 708–718. https://doi.org/10.1039/c9em00468h.

(104) Wert, E. C.; Rosario-Ortiz, F. L. Intracellular Organic Matter from Cyanobacteria as a Precursor for Carbonaceous and Nitrogenous Disinfection Byproducts. *Environ. Sci. Technol.* **2013**, *47* (12), 6332–6340. https://doi.org/10.1021/es400834k.

(105) Yang, X.; Guo, W.; Shen, Q. Formation of Disinfection Byproducts from Chlor(Am)Ination of Algal Organic Matter. *J. Hazard. Mater.* **2011**, *197*, 378–388. https://doi.org/10.1016/j.jhazmat.2011.09.098.

(106) Zhang, Q.; Liu, B.; Liu, Y. Effect of Ozone on Algal Organic Matters as Precursors for Disinfection By-Products Production. *Environ. Technol.* **2014**, *35* (14), 1753–1759.

(107) Plummer, J. D.; Edzwald, J. K. Effect of Ozone on Algae as Precursors for Trihalomethane and Haloacetic Acid Production. *Environ. Sci. Technol.* **2001**, *35* (18), 3661–3668. https://doi.org/10.1021/es0106570.

(108) Gu, X.; Zhai, H.; Zhou, Y. Formation of Disinfection Byproducts from Algal Organic Matter Exposed to Monochloramine : Effects of Monochloramine Dosages, PH, and Bromide Concentrations. *Water, Air, Soil Pollut.* **2020**, *231*, 207.

(109) Zhang, T. Y.; Lin, Y. L.; Xu, B.; Cheng, T.; Xia, S. J.; Chu, W. H.; Gao, N. Y. Formation of Organic Chloramines during Chlor(Am)Ination and UV/Chlor(Am)Ination of Algae Organic Matter in Drinking Water. *Water Res.* **2016**, *103*, 189–196. https://doi.org/10.1016/j.watres.2016.07.036.

(110) Hua, L. C.; Lin, J. L.; Chen, P. C.; Huang, C. Chemical Structures of Extra- and Intra-Cellular Algogenic Organic Matters as Precursors to the Formation of Carbonaceous Disinfection Byproducts. *Chem. Eng. J.* **2017**, *328* (April), 1022–1030.

https://doi.org/10.1016/j.cej.2017.07.123.

(111) Kralles, Z. T.; Ikuma, K.; Dai, N. Assessing Disinfection Byproduct Risks for Algal Impacted Surface Waters and the Effects of Peracetic Acid Pre-Oxidation. *Environ. Sci. Water Res. Technol.* **2020**, *6*, 2365–2381. https://doi.org/10.1039/d0ew00237b.

(112) Li, L.; Gao, N.; Deng, Y.; Yao, J.; Zhang, K. Characterization of Intracellular & Extracellular Algae Organic Matters (AOM) of M*icrocystic aeruginosa* and Formation of AOM-Associated Disinfection Byproducts and Odor & Taste Compounds. *Water Res.* **2012**, *46* (4), 1233–1240. https://doi.org/10.1016/j.watres.2011.12.026.

(113) Huang, H.; Chen, B. Y.; Zhu, Z. R. Formation and Speciation of Haloacetamides and Haloacetonitriles for Chlorination, Chloramination, and Chlorination Followed by Chloramination. *Chemosphere* **2017**, *166*, 126–134. https://doi.org/10.1016/j.chemosphere.2016.09.047.

(114) Hua, G.; Reckhow, D. A.; Abusallout, I. Correlation between SUVA and DBP Formation during Chlorination and Chloramination of NOM Fractions from Different Sources. *Chemosphere* **2015**, *130*, 82–89. https://doi.org/10.1016/j.chemosphere.2015.03.039.

(115) Liang, L.; Singer, P. C. Factors Influencing the Formation and Relative Distribution of Haloacetic Acids and Trihalomethanes in Drinking Water. *Environ. Sci. Technol.* **2003**, *37* (13), 2920–2928. https://doi.org/10.1021/es026230q.

(116) Xu, B.; Ye, T.; Li, D. P.; Hu, C. Y.; Lin, Y. L.; Xia, S. J.; Tian, F. X.; Gao, N. Y. Measurement of Dissolved Organic Nitrogen in a Drinking Water Treatment Plant: Size Fraction, Fate, and Relation to Water Quality Parameters. *Sci. Total Environ.* **2011**, *409* (6), 1116–1122. https://doi.org/10.1016/j.scitotenv.2010.12.016.

(117) Zhang, X.; Chen, Z.; Shen, J.; Zhao, S.; Kang, J.; Chu, W.; Zhou, Y.; Wang, B. Formation and Interdependence of Disinfection Byproducts during Chlorination of Natural Organic Matter in a Conventional Drinking Water Treatment Plant. *Chemosphere* **2020**, *242*, 125227. https://doi.org/10.1016/j.chemosphere.2019.125227.

(118) Lu, J.; Zhang, T.; Ma, J.; Chen, Z. Evaluation of Disinfection By-Products Formation during Chlorination and Chloramination of Dissolved Natural Organic Matter Fractions Isolated from a Filtered River Water. *J. Hazard. Mater.* **2009**, *162* (1), 140–145. https://doi.org/10.1016/j.jhazmat.2008.05.058.

(119) Gallard, H.; Von Gunten, U. Chlorination of Natural Organic Matter: Kinetics of Chlorination and of THM Formation. *Water Res.* **2002**, *36* (1), 65–74. https://doi.org/10.1016/S0043-1354(01)00187-7.

(120) Reckhow, D. A.; Singer, P. C.; Malcolm, R. L. Chlorination of Humic Materials: Byproduct Formation and Chemical Interpretations. *Environ. Sci. Technol.* **1990**, *24* (11), 1655–1664. https://doi.org/10.1021/es00081a005.

(121) Kumar, K.; Margerum, D. W. Kinetics and Mechanism of General-Acid-Assisted Oxidation of Bromide by Hypochlorite and Hypochlorous Acid. *Inorg. Chem.* **1987**, *26* (16), 2706–2711. https://doi.org/10.1021/ic00263a030.

(122) Sivey, J. D.; Arey, J. S.; Tentscher, P. R.; Roberts, A. L. Reactivity of BrCl, Br_2, BrOCl, Br_2O and HOBr toward Dimethenamid in Solutions of Bromide + Aqueous Free Chlorine.

Environ. Sci. Technol. **2013**, *47* (15), 8990. https://doi.org/10.1021/es402917a.

(123) Broadwater, M. A.; Swanson, T. L.; Sivey, J. D. Emerging Investigators Series: Comparing the Inherent Reactivity of Often-Overlooked Aqueous Chlorinating and Brominating Agents toward Salicylic Acid. *Environ. Sci. Water Res. Technol.* **2018**, *4* (3), 369–384. https://doi.org/10.1039/c7ew00491e.

(124) Sivey, J. D.; Bickley, M. A.; Victor, D. A. Contributions of BrCl, Br_2, BrOCl, Br_2O, and HOBr to Regiospecific Bromination Rates of Anisole and Bromoanisoles in Aqueous Solution. *Environ. Sci. Technol.* **2015**, *49* (8), 4937–4945. https://doi.org/10.1021/acs.est.5b00205.

(125) Li, J.; Pang, S. Y.; Wang, Z.; Guo, Q.; Duan, J.; Sun, S.; Wang, L.; Cao, Y.; Jiang, J. Oxidative Transformation of Emerging Organic Contaminants by Aqueous Permanganate: Kinetics, Products, Toxicity Changes, and Effects of Manganese Products. *Water Res.* **2021**, *203* (January), 117513. https://doi.org/10.1016/j.watres.2021.117513.

(126) Wei, M. A Study of the Mechanism of the Permanganate Oxidation of Amines, The University of British Columbia, 1965.

(127) Jia, A.; Wu, C.; Duan, Y. Precursors and Factors Affecting Formation of Haloacetonitriles and Chloropicrin during Chlor(Am)Ination of Nitrogenous Organic Compounds in Drinking Water. *J. Hazard. Mater.* **2016**, *308*, 411–418. https://doi.org/10.1016/j.jhazmat.2016.01.037.

(128) Yang, X.; Shen, Q.; Guo, W.; Peng, J.; Liang, Y. Precursors and Nitrogen Origins of Trichloronitromethane and Dichloroacetonitrile during Chlorination/Chloramination. *Chemosphere* **2012**, *88* (1), 25–32. https://doi.org/10.1016/j.chemosphere.2012.02.035.

(129) Hureiki, L.; Croué, J. P.; Legube, B.; Doré, M. Ozonation of Amino Acids: Ozone Demand and Aldehyde Formation. *Ozone Sci. Eng.* **1998**, *20* (5), 381–402. https://doi.org/10.1080/01919519809480349.

(130) Wang, R.; Ji, M.; Zhai, H.; Liang, Y. Electron Donating Capacities of DOM Model Compounds and Their Relationships with Chlorine Demand, Byproduct Formation, and Other Properties in Chlorination. *Chemosphere* **2020**, *261*, 127764. https://doi.org/10.1016/j.chemosphere.2020.127764.

(131) Wang, A.; Lin, C.; Shen, Z.; Liu, Z.; Xu, H.; Cheng, J.; Wen, X. Effects of Pre-Oxidation on Haloacetonitrile and Trichloronitromethane Formation during Subsequent Chlorination of Nitrogenous Organic Compounds. *Int. J. Environ. Res. Public Health* **2020**, *17* (3), 1046. https://doi.org/10.3390/ijerph17031046.

(132) Rawalay, S. S.; Shechter, H. Oxidation of Primary, Secondary, and Tertiary Amines with Neutral Permanganate. A Simple Method for Degrading Amines to Aldehydes and Ketones. *J. Org. Chem.* **1967**, *32* (10), 3129–3131. https://doi.org/10.1021/jo01285a042.

(133) Shechter, H.; Rawalay, S. singh. Oxidation of Primary, Secondary, and Tertiary Amines with Neutral Potassium Permanganate. II. *J. Am. Chem. SOC.* **1964**, *86* (9), 1706–1709.

(134) Shaabani, A.; Tavasoli-Rad, F.; Lee, D. G. Potassium Permanganate Oxidation of Organic Compounds. *Synth. Commun.* **2005**, *35* (4), 571–580. https://doi.org/10.1081/SCC-200049792.

(135) Lau, S. S.; Wei, X.; Bokenkamp, K.; Wagner, E. D.; Plewa, M. J.; Mitch, W. A. Assessing Additivity of Cytotoxicity Associated with Disinfection Byproducts in Potable Reuse and Conventional Drinking Waters. *Environ. Sci. Technol.* **2020**, *54* (9), 5729–5736. https://doi.org/10.1021/acs.est.0c00958.

(136) Plewa, M. J.; Wagner, E. D.; Richardson, S. D. TIC-Tox: A Preliminary Discussion on Identifying the Forcing Agents of DBP-Mediated Toxicity of Disinfected Water. *J. Environ. Sci.* **2017**, *58*, 208–216. https://doi.org/10.1016/j.jes.2017.04.014.

(137) Muellner, M. G.; Wagner, E. D.; Mccalla, K.; Richardson, S. D.; Woo, Y. T.; Plewa, M. J. Haloacetonitriles vs. Regulated Haloacetic Acids: Are Nitrogen-Containing DBPs More Toxic? *Environ. Sci. Technol.* **2007**, *41* (2), 645–651. https://doi.org/10.1021/es0617441.

(138) Feng, Y.; Smith, D. W.; Bolton, J. R. Photolysis of Aqueous Free Chlorine Species (HOCl and OCl^-) with 254 Nm Ultraviolet Light. *J. Environ. Eng. Sci.* **2007**, *6* (3), 277–284. https://doi.org/10.1139/s06-052.

(139) Schreiber, I. M.; Mitch, W. A. Influence of the Order of Reagent Addition on NDMA Formation during Chloramination. *Environ. Sci. Technol.* **2005**, *39* (10), 3811–3818. https://doi.org/10.1021/es0483286.

(140) Lee, D. G.; Perez-Benito, J. F. Oxidation of Hydrocarbons.14.Autocatalysis during the Oxidation of 1-Tetradecene by Methyltributylammonium Permanganate. *Can. J. Chem.* **1985**, *63* (6), 1275–1279.

(141) Verdouw, H.; Van Echteld, C. J. A.; Dekkers, E. M. J. Ammonia Determination Based on Indophenol Formation with Sodium Salicylate. *Water Res.* **1978**, *12* (6), 399–402. https://doi.org/10.1016/0043-1354(78)90107-0.

(142) Baird, R. B.; Eaton, A. D.; Clesceri, L. S. *Standard Methods for the Examination of Water and Wastewater*, 23rd ed.; Rice, E. W., Ed.; American Public Health Association, American Water Works Association, Water Environment Federation, 2017; Vol. 10.

(143) Zhu, Y.; Yang, X.; Qiao, J.; Zhang, X.; Guan, X. Effects of $KMnO_4$/$NaHSO_3$ Pre-Oxidation on the Formation Potential of Disinfection by-Products during Subsequent Chlorination. *Chem. Eng. J.* **2019**, *372*, 825–835. https://doi.org/10.1016/j.cej.2019.04.210.

(144) Gordon, G.; Sweetin, D. L.; Smith, K.; Pacey, G. E. Improvements in the Method for the Determination of Free and Combined Residual Chlorine Through the Use of FIA. *Talanta* **1991**, *38* (2), 145–149.

(145) U.S. EIA. Annual Energy Outlook 2019 with Projections to 2050. *Annu. Energy Outlook 2019 with Proj. to 2050* **2019**, *44* (8), 1–64. https://doi.org/DOE/EIA-0383(2012) U.S.

(146) U.S. Environmental Protection Agency. Hydraulic Fracturing for Oil and Gas: Impacts from the Hydraulic Fracturing Water Cycle on Drinking Water Resources in the United States; **2016**.

(147) Clark, C. E.; Veil, J. A. Produced Water Volumes and Management Practices in the United States; **2009**.

(148) Lutz, B. D.; Lewis, A. N.; Doyle, M. W. Generation, Transport, and Disposal of Wastewater Associated with Marcellus Shale Gas Development. *Water Resour. Res.* **2013**,

49 (2), 647–656. https://doi.org/10.1002/wrcr.20096.

(149) Elsner, M.; Hoelzer, K. Quantitative Survey and Structural Classification of Hydraulic Fracturing Chemicals Reported in Unconventional Gas Production. *Environ. Sci. Technol.* **2016**, *50* (7), 3290–3314. https://doi.org/10.1021/acs.est.5b02818.

(150) Kodavanti, P. R. S.; Loganathan, B. G. Organohalogen Pollutants and Human Health. *Int. Encycl. Public Heal.* **2016**, No. October 2016, 359–366. https://doi.org/10.1016/B978-0-12-803678-5.00318-0.

(151) Parker, K. M.; Zeng, T.; Harkness, J.; Vengosh, A.; Mitch, W. A. Enhanced Formation of Disinfection Byproducts in Shale Gas Wastewater-Impacted Drinking Water Supplies. *Environ. Sci. Technol.* **2014**, *48* (19), 11161–11169. https://doi.org/10.1021/es5028184.

(152) Echigo, S.; Itoh, S.; Natsui, T.; Araki, T.; Ando, R. Contribution of Brominated Organic Disinfection By-Products to the Mutagenicity of Drinking Water. *Water Sci. Technol.* **2004**, *50* (5), 321–328. https://doi.org/10.2166/wst.2004.0344.

(153) Sharma, V. K.; Zboril, R.; McDonald, T. J. Formation and Toxicity of Brominated Disinfection Byproducts during Chlorination and Chloramination of Water: A Review. *J. Environ. Sci. Heal. - Part B Pestic. Food Contam. Agric. Wastes* **2014**, *49* (3), 212–228. https://doi.org/10.1080/03601234.2014.858576.

(154) Luek, J. L.; Harir, M.; Schmitt-Kopplin, P.; Mouser, P. J.; Gonsior, M. Temporal Dynamics of Halogenated Organic Compounds in Marcellus Shale Flowback. *Water Res.* **2018**, *136*, 200–206. https://doi.org/10.1016/j.watres.2018.02.055.

(155) Maguire-Boyle, S. J.; Barron, A. R. Organic Compounds in Produced Waters from Shale Gas Wells. *Environ. Sci. Process. Impacts* **2014**, *16* (10), 2237–2248. https://doi.org/10.1039/c4em00376d.

(156) Luek, J. L.; Schmitt-Kopplin, P.; Mouser, P. J.; Petty, W. T.; Richardson, S. D.; Gonsior, M. Halogenated Organic Compounds Identified in Hydraulic Fracturing Wastewaters Using Ultrahigh Resolution Mass Spectrometry. *Environ. Sci. Technol.* **2017**, *51* (10), 5377–5385. https://doi.org/10.1021/acs.est.6b06213.

(157) Hoelzer, K.; Sumner, A. J.; Karatum, O.; Nelson, R. K.; Drollette, B. D.; O'Connor, M. P.; D'Ambro, E. L.; Getzinger, G. J.; Ferguson, P. L.; Reddy, C. M.; et al. Indications of Transformation Products from Hydraulic Fracturing Additives in Shale-Gas Wastewater. *Environ. Sci. Technol.* **2016**, *50* (15), 8036–8048. https://doi.org/10.1021/acs.est.6b00430.

(158) Sumner, A. J.; Plata, D. L. Halogenation Chemistry of Hydraulic Fracturing Additives under Highly Saline Simulated Subsurface Conditions. *Environ. Sci. Technol.* **2018**, *52* (16), 9097–9107. https://doi.org/10.1021/acs.est.8b01591.

(159) Sumner, A. J.; Plata, D. L. Oxidative Breakers Can Stimulate Halogenation and Competitive Oxidation in Guar-Gelled Hydraulic Fracturing Fluids. *Environ. Sci. Technol.* **2019**, *53*, 8216–8226. https://doi.org/10.1021/acs.est.9b01896.

(160) Larson, R. A.; Rockwell, A. L. Chloroform and Chlorophenol Production by Decarboxylation of Natural Acids during Aqueous Chlorination. *Environ. Sci. Technol.* **1979**, *13* (3), 325–329. https://doi.org/10.1021/es60151a014.

(161) Dickenson, E. R. V.; Summers, R. S.; Croué, J. P.; Gallard, H. Haloacetic Acid and

Trihalomethane Formation from the Chlorination and Bromination of Aliphatic β-Dicarbonyl Acid Model Compounds. *Environ. Sci. Technol.* **2008**, *42* (9), 3226–3233. https://doi.org/10.1021/es0711866.

(162) Devon Energy Production. Hydraulic Fracturing Fluid Product Component Information Disclosure: State Richfield 1-34HD http://www.utlands.utsystem.edu/WellLibrary/WellDocument/4200347209/457767 (accessed Sep 21, 2020).

(163) Sun, P.; Lee, W.-N. N.; Zhang, R.; Huang, C.-H. H. Degradation of DEET and Caffeine under UV/Chlorine and Simulated Sunlight/Chlorine Conditions. *Environ. Sci. Technol.* **2016**, *50* (24), 13265–13273. https://doi.org/10.1021/acs.est.6b02287.

(164) Yang, Y.; Pignatello, J. J.; Ma, J.; Mitch, W. A. Comparison of Halide Impacts on the Efficiency of Contaminant Degradation by Sulfate and Hydroxyl Radical-Based Advanced Oxidation Processes (AOPs). *Environ. Sci. Technol.* **2014**. https://doi.org/10.1021/es404118q.

(165) Grebel, J. E.; Pignatello, J. J.; Mitch, W. A. Effect of Halide Ions and Carbonates on Organic Contaminant Degradation by Hydroxyl Radical-Based Advanced Oxidation Processes in Saline Waters. *Environ. Sci. Technol.* **2010**, *44* (17), 6822–6828. https://doi.org/10.1021/es1010225.

(166) Fan, Y.; Ji, Y.; Kong, D.; Lu, J.; Zhou, Q. Kinetic and Mechanistic Investigations of the Degradation of Sulfamethazine in Heat-Activated Persulfate Oxidation Process. *J. Hazard. Mater.* **2015**, *300*, 39–47. https://doi.org/10.1016/j.jhazmat.2015.06.058.

(167) Yang, Y.; Pignatello, J. J.; Ma, J.; Mitch, W. A. Effect of Matrix Components on UV/H_2O_2 and UV/$S_2O_8^{2-}$ Advanced Oxidation Processes for Trace Organic Degradation in Reverse Osmosis Brines from Municipal Wastewater Reuse Facilities. *Water Res.* **2016**, *89*, 192–200. https://doi.org/10.1016/j.watres.2015.11.049.

(168) Sivey, J. D.; McCullough, C. E.; Roberts, A. L. Chlorine Monoxide (Cl_2O) and Molecular Chlorine (Cl_2) as Active Chlorinating Agents in Reaction of Dimethenamid with Aqueous Free Chlorine. *Environ. Sci. Technol.* **2010**, *44* (9), 3357–3362. https://doi.org/10.1021/es9038903.

(169) Sivey, J. D.; Roberts, A. L. Assessing the Reactivity of Free Chlorine Constituents Cl_2, Cl_2O, and HOCl toward Aromatic Ethers. *Environ. Sci. Technol.* **2012**, *46* (4), 2141–2147. https://doi.org/10.1021/es203094z.

(170) Sumner, A. J.; Plata, D. L. Exploring the Hydraulic Fracturing Parameter Space: A Novel High-Pressure, High-Throughput Reactor System for Investigating Subsurface Chemical Transformations. *Environ. Sci. Process. Impacts* **2018**, *20* (2), 318–331. https://doi.org/10.1039/c7em00470b.

(171) Anipsitakis, G. P.; Dionysiou, D. D.; Gonzalez, M. A. Cobalt-Mediated Activation of Peroxymonosulfate and Sulfate Radical Attack on Phenolic Compounds. Implications of Chloride Ions. *Environ. Sci. Technol.* **2006**, *40* (3), 1000–1007. https://doi.org/10.1021/es050634b.

(172) Fang, G. D.; Dionysiou, D. D.; Wang, Y.; Al-Abed, S. R.; Zhou, D. M. Sulfate Radical-Based Degradation of Polychlorinated Biphenyls: Effects of Chloride Ion and Reaction

Kinetics. *J. Hazard. Mater.* **2012**, *227–228*, 394–401. https://doi.org/10.1016/j.jhazmat.2012.05.074.

(173) Waldemer, R. H.; Tratnyek, P. G.; Johnson, R. L.; Nurmi, J. T. Oxidation of Chlorinated Ethenes by Heat-Activated Persulfate: Kinetics and Products. *Environ. Sci. Technol.* **2007**, *41* (3), 1010–1015. https://doi.org/10.1021/es062237m.

(174) Wang, Z.; Shao, Y.; Gao, N.; Xu, B.; An, N.; Lu, X. Comprehensive Study on the Formation of Brominated Byproducts during Heat-Activated Persulfate Degradation. *Chem. Eng. J.* **2020**, *381*. https://doi.org/10.1016/j.cej.2019.122660.

(175) Huie, R. E.; Clifton, C. L. Temperature Dependence of the Rate Constants for Reactions of the Sulfate Radical, SO_4^-, with Anions. *J. Phys. Chem.* **1990**, *94* (23), 8561–8567. https://doi.org/10.1021/j100386a015.

(176) Peyton, G. R. The Free-Radical Chemistry of Persulfate-Based Total Organic Carbon Analyzers. *Mar. Chem.* **1993**, *41* (1–3), 91–103. https://doi.org/10.1016/0304-4203(93)90108-Z.

(177) Jayson, G. G.; Parsons, B. J.; Swallow, A. J. Some Simple, Highly Reactive, Inorganic Chlorine Derivatives in Aqueous Solution. Their Formation Using Pulses of Radiation and Their Role in the Mechanism of the Fricke Dosimeter. *J. Chem. Soc. Faraday Trans* **1973**, *69* (9), 1597–1607.

(178) Zehavi, D.; Rabani, J. The Oxidation of Aqueous Bromide Ions by Hydroxyl Radicals. A Pulse Radiolytic Investigation. *J. Phys. Chem.* **1972**, *76* (3), 312–319. https://doi.org/10.1021/j100647a006.

(179) Merényi, G.; Lind, J. Reaction Mechanism of Hydrogen Abstraction by the Bromine Atom in Water. *J. Am. Chem. Soc.* **1994**, *116* (17), 7872–7876. https://doi.org/10.1021/ja00096a050.

(180) Kläning, U. K.; Wolff, T. Laser Flash Photolysis of HClO, ClO−, HBrO, and BrO− in Aqueous Solution. Reactions of Cl- and Br-Atoms. *Berichte der Bunsengesellschaft für Phys. Chemie* **1985**, *89* (3), 243–245.

(181) Liang, C.; Huang, C.; Mohanty, N.; Mohan, R. A Rapid Spectrophotometric Determination of Persulfate Anion in ISCO. *Chemosphere* **2008**, *73* (9), 1540–1543. https://doi.org/10.1016/j.chemosphere.2008.08.043.

(182) Perlmutter-Hayman, B.; Weissmann, Y. The Oxidation of 2-Propanol by Bromine and by Hypobromous Acid in Aqueous Solution. *J. Am. Chem. Soc.* **1969**, *91* (3), 668–672. https://doi.org/10.1021/ja01031a025.

(183) Matzek, L. W.; Carter, K. E. Activated Persulfate for Organic Chemical Degradation: A Review. *Chemosphere* **2016**, *151*, 178–188. https://doi.org/10.1016/j.amjmed.2015.10.002.This.

(184) Zrinyi, N.; Pham, A. L. T. Oxidation of Benzoic Acid by Heat-Activated Persulfate: Effect of Temperature on Transformation Pathway and Product Distribution. *Water Res.* **2017**, *120*, 43–51. https://doi.org/10.1016/j.watres.2017.04.066.

(185) Manz, K. E.; Carter, K. E. Investigating the Effects of Heat Activated Persulfate on the Degradation of Furfural, a Component of Hydraulic Fracturing Fluid Chemical Additives.

Chem. Eng. J. **2017**, *327*, 1021–1032. https://doi.org/10.1016/j.cej.2017.06.168.

(186) Kolthoff, I. M.; Miller, I. K. The Chemistry of Persulfate. I. The Kinetics and Mechanism of the Decomposition of the Persulfate Ion in Aqueous Medium. *J. Am. Chem. Soc.* **1951**, *73* (7), 3055–3059. https://doi.org/10.1021/ja01151a024.

(187) Furman, O. S.; Teel, A. L.; Watts, R. J. Mechanism of Base Activation of Persulfate. *Environ. Sci. Technol.* **2010**, *44* (16), 6423–6428. https://doi.org/10.1021/es1013714.

(188) McElory, W. J.; Waygood, S. J. Kinetics of the Reactions of the SO_4^- Radical with SO_4^-, $S_2O_8^{2-}$, H_2O and Fe^{2+}. *J. Chem. Soc. Faraday Trans.* **1990**, *86* (14), 2557–2564.

(189) Jiang, P. Y.; Katsumura, Y.; Domae, M.; Ishikawa, K.; Nagaishi, R.; Ishigure, K.; Yoshida, Y. Pulse Radiolysis Study of Concentrated Phosphoric Acid Solutions. *J. Chem. Soc. Faraday Trans.* **1992**, *88* (22), 3319–3322. https://doi.org/10.1039/FT9928803319.

(190) Herrmann, H.; Reese, A.; Zellner, R. Time-Resolved UV/VIS Diode Array Absorption Spectroscopy of SO_x^- (x=3, 4, 5) Radical Anions in Aqueous Solution. *J. Mol. Struct.* **1995**, *348*, 183–186. https://doi.org/10.1016/0022-2860(95)08619-7.

(191) House, D. A. Kinetics and Mechanism of Oxidations by Peroxydisulfate. *Chem. Rev.* **1962**, *62* (3), 185–203. https://doi.org/10.1021/cr60217a001.

(192) Neta, P.; Madhavan, V.; Zemel, H.; Fessenden, R. W. Rate Constants and Mechanism of Reaction of $SO_4^{\bullet-}$ with Aromatic Compounds. **1976**, 163–164. https://doi.org/10.1021/ja00443a030.

(193) Liang, C.; Su, H. W. Identification of Sulfate and Hydroxyl Radicals in Thermally Activated Persulfate. *Ind. Eng. Chem. Res.* **2009**, *48* (11), 5558–5562. https://doi.org/10.1021/ie9002848.

(194) Huang, K. C.; Couttenye, R. A.; Hoag, G. E. Kinetics of Heat-Assisted Persulfate Oxidation of Methyl Tert-Butyl Ether (MTBE). *Chemosphere* **2002**, *49* (4), 413–420. https://doi.org/10.1016/S0045-6535(02)00330-2.

(195) Fang, G.; Gao, J.; Dionysiou, D. D.; Liu, C.; Zhou, D. Activation of Persulfate by Quinones: Free Radical Reactions and Implication for the Degradation of PCBs. *Environ. Sci. Technol.* **2013**, *47* (9), 4605–4611. https://doi.org/10.1021/es400262n.

(196) Kemsley, K.; Moore, J. S.; Phillip, G. O.; Sosnowski, A. Reaction of Radical Probes with Substituted Phenols as Models for the Investigation of Tyrosine in Aldolase and Chemically Modified Aldolase. *Acta Vitaminol. Enzym.* **1974**, *28* (6), 263–267.

(197) Fel'dman, V. I. I.; Belevskii, V. N. N.; Bugaenko, L. T. T.; Moralev, V. M. M.; Popov, V. I. I. Early Ionic Processes in the Radiolysis of Liquid Methanol. *High Energy Chem.* **1986**, *20* (2), 102–107.

(198) U.S. Environmental Protection Agency. Analysis of Hydraulic Fracturing Fluid Data from the FracFocus Chemical. **2015**, No. March, 1–153.

(199) Feng, Y.; Smith, D. W.; Bolton, J. R. Photolysis of Aqueous Free Chlorine Species (HOCl and OCl^-) with 254 nm Ultraviolet Light. *J. Environ. Eng. Sci.* **2007**, *6* (3), 277–284. https://doi.org/10.1139/s06-052.

(200) Troy, R. C.; Margerum, D. W. Non-Metal Redox Kinetics: Hypobromite and

Hypobromous Acid Reactions with Iodide and with Sulfite and the Hydrolysis of Bromosulfate. **1991**, No. 30, 3538–3543. https://doi.org/10.1021/ic00018a028.

(201) Rezaei, F.; Vanraes, P.; Nikiforov, A.; Morent, R.; Geyter, N. De. Applications of Plasma-Liquid Systems : A Review. *Materials.* **2019**, *12* (17), 2751. https://doi.org/https://doi.org/10.3390/ma12172751.

(202) Foster, J. E. Plasma-Based Water Purification: Challenges and Prospects for the Future. *Phys. Plasmas* **2017**, *24* (5), 055501. https://doi.org/10.1063/1.4977921.

(203) Wang, X.; Zhou, M.; Jin, X. Application of Glow Discharge Plasma for Wastewater Treatment. *Electrochim. Acta* **2012**, *83*, 501–512. https://doi.org/10.1016/j.electacta.2012.06.131.

(204) Zeghioud, H.; Nguyen-Tri, P.; Khezami, L.; Amrane, A.; Assadi, A. A. Review on Discharge Plasma for Water Treatment: Mechanism, Reactor Geometries, Active Species and Combined Processes. *J. Water Process Eng.* **2020**, *38*, 101664. https://doi.org/10.1016/j.jwpe.2020.101664.

(205) Foster, J.; Sommers, B. S.; Gucker, S. N.; Blankson, I. M.; Adamovsky, G. Perspectives on the Interaction of Plasmas with Liquid Water for Water Purification. *IEEE Trans. Plasma Sci.* **2012**, *40* (5), 1311–1323. https://doi.org/10.1109/TPS.2011.2180028.

(206) Tachibana, K.; Nakamura, T. Comparative Study of Discharge Schemes for Production Rates and Ratios of Reactive Oxygen and Nitrogen Species in Plasma Activated Water. *J. Phys. D. Appl. Phys.* **2019**, *52* (38), 385202. https://doi.org/10.1088/1361-6463/ab2529.

(207) Zhang, X.; Zhou, R.; Bazaka, K.; Liu, Y.; Zhou, R.; Chen, G.; Chen, Z.; Liu, Q.; Yang, S.; Ostrikov, K. Quantification of Plasma Produced OH Radical Density for Water Sterilization. *Plasma Process. Polym.* **2018**, *15* (6), 1700241. https://doi.org/10.1002/ppap.201700241.

(208) Franclemont, J.; Fan, X.; Thagard, S. M. Physicochemical Mechanisms of Plasma-Liquid Interactions within Plasma Channels in Liquid. *J. Phys. D. Appl. Phys.* **2015**, *48* (42), 424004. https://doi.org/10.1088/0022-3727/48/42/424004.

(209) Buxton, G. V.; Greenstock, C. L.; Helman, W. P.; Ross, A. B. Critical Review of Rate Constants for Reactions of Hydrated Electrons, Hydrogen Atoms and Hydroxyl Radicals (•OH/•O⁻ in Aqueous Solution. *J. Phys. Chem. Ref. Data* **1988**, *17* (2), 513–886. https://doi.org/10.1063/1.555805.

(210) Magureanu, M.; Bradu, C.; Parvulescu, V. I. Plasma Processes for the Treatment of Water Contaminated with Harmful Organic Compounds. *J. Phys. D. Appl. Phys.* **2018**, *51* (31), 313002. https://doi.org/10.1088/1361-6463/aacd9c.

(211) Sarangapani, C.; Misra, N. N.; Milosavljevic, V.; Bourke, P.; O'Regan, F.; Cullen, P. J. Pesticide Degradation in Water Using Atmospheric Air Cold Plasma. *J. Water Process Eng.* **2016**, *9*, 225–232. https://doi.org/10.1016/j.jwpe.2016.01.003.

(212) Banaschik, R.; Jablonowski, H.; Bednarski, P. J.; Kolb, J. F. Degradation and Intermediates of Diclofenac as Instructive Example for Decomposition of Recalcitrant Pharmaceuticals by Hydroxyl Radicals Generated with Pulsed Corona Plasma in Water. *J. Hazard. Mater.* **2018**, *342*, 651–660. https://doi.org/10.1016/j.jhazmat.2017.08.058.

(213) Magureanu, M.; Piroi, D.; Mandache, N. B.; David, V.; Medvedovici, A.; Bradu, C.; Parvulescu, V. I. Degradation of Antibiotics in Water by Non-Thermal Plasma Treatment. *Water Res.* **2011**, *45* (11), 3407–3416. https://doi.org/10.1016/j.watres.2011.03.057.

(214) Wang, R.; Wang, T.; Qu, G.; Zhang, Y.; Guo, X.; Jia, H.; Zhu, L. Insights into the Underlying Mechanisms for Integrated Inactivation of A. Spiroides and Depression of Disinfection Byproducts by Plasma Oxidation. *Water Res.* **2021**, *196*, 117027. https://doi.org/10.1016/j.watres.2021.117027.

(215) Xin, Q.; Zhang, Y.; Wu, K. Degradation of Microcystin-LR by Gas-Liquid Interfacial Discharge Plasma. *Plasma Sci. Technol.* **2013**, *15* (12), 1221–1225. https://doi.org/10.1088/1009-0630/15/12/11.

(216) Rumbach, P.; Bartels, D. M.; Sankaran, R. M.; Go, D. B. The Solvation of Electrons by an Atmospheric-Pressure Plasma. *Nat. Commun.* **2015**, *6*, 7248. https://doi.org/10.1038/ncomms8248.

(217) Richmonds, C.; Witzke, M.; Bartling, B.; Lee, S. W.; Wainright, J.; Liu, C.; Sankaran, R. M. Electron-Transfer Reactions at the Plasma À Liquid Interface. *J. Am. Chem. Soc.* **2011**, *133*, 17582–17585.

(218) Ilich, P. P.; McCormick, K. R.; Atkins, A. D.; Mell, G. J.; Flaherty, T. J.; Bruck, M. J.; Goodrich, H. A.; Hefel, A. L.; Juranić, N.; Seleem, S. Solvated Electrons in Organic Chemistry Laboratory. *J. Chem. Educ.* **2010**, *87* (4), 419–422. https://doi.org/10.1021/ed800093n.

(219) Abel, B.; Buck, U.; Sobolewski, A. L.; Domcke, W. On the Nature and Signatures of the Solvated Electron in Water. *Phys. Chem. Chem. Phys.* **2012**, *14* (1), 22–34. https://doi.org/10.1039/c1cp21803d.

(220) Zhao, Y.; Zhang, C.; Chu, L.; Zhou, Q.; Huang, B. Hydrated Electron Based Photochemical Processes for Water Treatment. *Water Res.* **2022**, *225*, 119212. https://doi.org/10.1016/j.watres.2022.119212.

(221) Bentel, M. J.; Yu, Y.; Xu, L.; Li, Z.; Wong, B. M.; Men, Y.; Liu, J. Defluorination of Per- and Polyfluoroalkyl Substances (PFASs) with Hydrated Electrons: Structural Dependence and Implications to PFAS Remediation and Management. *Environ. Sci. Technol.* **2019**, *53* (7), 3718–3728. https://doi.org/10.1021/acs.est.8b06648.

(222) Singh, R. K.; Multari, N.; Nau-Hix, C.; Anderson, R. H.; Richardson, S. D.; Holsen, T. M.; Mededovic Thagard, S. Rapid Removal of Poly- and Perfluorinated Compounds from Investigation-Derived Waste (IDW) in a Pilot-Scale Plasma Reactor. *Environ. Sci. Technol.* **2019**. https://doi.org/10.1021/acs.est.9b02964.

(223) Li, X.; Fang, J.; Liu, G.; Zhang, S.; Pan, B.; Ma, J. Kinetics and Efficiency of the Hydrated Electron-Induced Dehalogenation by the Sulfite/UV Process. *Water Res.* **2014**, *62* (2), 220–228. https://doi.org/10.1016/j.watres.2014.05.051.

(224) Wu, Z.; Shang, C.; Wang, D.; Zheng, S.; Wang, Y.; Fang, J. Rapid Degradation of Dichloroacetonitrile by Hydrated Electron (Eaq–) Produced in Vacuum Ultraviolet Photolysis. *Chemosphere* **2020**, *256*, 126994. https://doi.org/10.1016/j.chemosphere.2020.126994.

(225) Cole, S. K.; Cooper, W. J.; Fox, R. V.; Gardinali, P. R.; Mezyk, S. P.; Mincher, B. J.; O'Shea, K. E. Free Radical Chemistry of Disinfection Byproducts. 2. Rate Constants and Degradation Mechanisms of Trichloronitromethane (Chloropicrin). *Environ. Sci. Technol.* **2007**, *41* (3), 863–869. https://doi.org/10.1021/es061410b.

(226) Liu, Z.; Haddad, M.; Sauvé, S.; Barbeau, B. Alleviating the Burden of Ion Exchange Brine in Water Treatment: From Operational Strategies to Brine Management. *Water Res.* **2021**, *205*, 117728. https://doi.org/10.1016/j.watres.2021.117728.

(227) Singh, R. K.; Multari, N.; Nau-Hix, C.; Woodard, S.; Nickelsen, M.; Mededovic Thagard, S.; Holsen, T. M. Removal of Poly- And Per-Fluorinated Compounds from Ion Exchange Regenerant Still Bottom Samples in a Plasma Reactor. *Environ. Sci. Technol.* **2020**, *54* (21), 13973–13980. https://doi.org/10.1021/acs.est.0c02158.

(228) Giwa, A.; Dufour, V.; Al Marzooqi, F.; Al Kaabi, M.; Hasan, S. W. Brine Management Methods: Recent Innovations and Current Status. *Desalination* **2017**, *407*, 1–23. https://doi.org/10.1016/j.desal.2016.12.008.

(229) Tow, E. W.; Ersan, M. S.; Kum, S.; Lee, T.; Speth, T. F.; Owen, C.; Bellona, C.; Nadagouda, M. N.; Mikelonis, A. M.; Westerhoff, P.; et al. Managing and Treating Per- and Polyfluoroalkyl Substances (Pfas) in Membrane Concentrates. *AWWA Water Sci.* **2021**, *3* (5), 1–23. https://doi.org/10.1002/aws2.1233.

(230) Azerrad, S. P.; Lütke Eversloh, C.; Gilboa, M.; Schulz, M.; Ternes, T.; Dosoretz, C. G. Identification of Transformation Products during Advanced Oxidation of Diatrizoate: Effect of Water Matrix and Oxidation Process. *Water Res.* **2016**, *103*, 424–434. https://doi.org/10.1016/j.watres.2016.07.066.

(231) Jose, J.; Philip, L. Continuous Flow Pulsed Power Plasma Reactor for the Treatment of Aqueous Solution Containing Volatile Organic Compounds and Real Pharmaceutical Wastewater. *J. Environ. Manage.* **2021**, *286* (February), 112202. https://doi.org/10.1016/j.jenvman.2021.112202.

(232) Manakhov, A.; Orlov, M.; Grokhovsky, V.; Alghunaimi, F. I.; Ayirala, S. Functionalized Nanomembranes and Plasma Technologies for Produced Water Treatment a Review. *Polymers (Basel).* **2022**, *14* (9). https://doi.org/10.3390/polym14091785.

(233) Sun, M.; Lowry, G. V.; Gregory, K. B. Selective Oxidation of Bromide in Wastewater Brines from Hydraulic Fracturing. *Water Res.* **2013**, *47* (11), 3723–3731. https://doi.org/10.1016/j.watres.2013.04.041.

(234) Singh, R. K.; Brown, E.; Mededovic Thagard, S.; Holsen, T. M. Treatment of PFAS-Containing Landfill Leachate Using an Enhanced Contact Plasma Reactor. *J. Hazard. Mater.* **2021**, *408* (October 2020), 124452. https://doi.org/10.1016/j.jhazmat.2020.124452.

(235) Sathiyaraj, G.; Chellappan Ravindran, K.; Hussain Malik, Z. Physico-Chemical Characteristics of Textile Effluent Collected from Erode, Pallipalayam and Bhavani Polluted Regions, Tamilnadu, India. *J. Ecobiotechnology* **2017**, *9*, 1–4. https://doi.org/10.19071/jebt.2017.v9.3191.

(236) Rodriguez, E. E.; Tarpeh, W. A.; Wigginton, K. R.; Love, N. G. Application of Plasma for the Removal of Pharmaceuticals in Synthetic Urine. *Environ. Sci. Water Res. Technol.* **2022**, *8* (3), 523–533. https://doi.org/10.1039/d1ew00863c.

(237) Nau-Hix, C.; Holsen, T. M.; Thagard, S. M. Influence of Solution Electrical Conductivity and Ionic Composition on the Performance of a Gas-Liquid Pulsed Spark Discharge Reactor for Water Treatment. *J. Appl. Phys.* **2021**, *130* (12), 123301. https://doi.org/10.1063/5.0054327.

(238) Mededovic Thagard, S.; Stratton, G. R.; Dai, F.; Bellona, C. L.; Holsen, T. M.; Bohl, D. G.; Paek, E.; Dickenson, E. R. V. Plasma-Based Water Treatment: Development of a General Mechanistic Model to Estimate the Treatability of Different Types of Contaminants. *J. Phys. D. Appl. Phys.* **2017**, *50* (1). https://doi.org/10.1088/1361-6463/50/1/014003.

(239) Li, Z.; Lyu, X.; Gao, B.; Xu, H.; Wu, J.; Sun, Y. Effects of Ionic Strength and Cation Type on the Transport of Perfluorooctanoic Acid (PFOA) in Unsaturated Sand Porous Media. *J. Hazard. Mater.* **2021**, *403* (November 2019), 123688. https://doi.org/10.1016/j.jhazmat.2020.123688.

(240) Lyu, Y.; Brusseau, M. L. The Influence of Solution Chemistry on Air-Water Interfacial Adsorption and Transport of PFOA in Unsaturated Porous Media. *Sci. Total Environ.* **2020**, *713*, 136744. https://doi.org/10.1016/j.scitotenv.2020.136744.

(241) Le, S. T.; Gao, Y.; Kibbey, T. C. G.; Glamore, W. C.; O'Carroll, D. M. Predicting the Impact of Salt Mixtures on the Air-Water Interfacial Behavior of PFAS. *Sci. Total Environ.* **2022**, *819*, 151987. https://doi.org/10.1016/j.scitotenv.2021.151987.

(242) Shih, K. Y.; Locke, B. R. Optical and Electrical Diagnostics of the Effects of Conductivity on Liquid Phase Electrical Discharge. *IEEE Trans. Plasma Sci.* **2011**, *39* (3), 883–892. https://doi.org/10.1109/TPS.2010.2098052.

(243) Thagard, S. M.; Takashima, K.; Mizuno, A. Chemistry of the Positive and Negative Electrical Discharges Formed in Liquid Water and above a Gas-Liquid Surface. *Plasma Chem. Plasma Process.* **2009**, *29* (6), 455–473. https://doi.org/10.1007/s11090-009-9195-x.

(244) El-Tayeb, A.; El-Shazly, A. H.; Elkady, M. F. Investigation the Influence of Different Salts on the Degradation of Organic Dyes Using Non-Thermal Plasma. *Energies* **2016**, *9* (11), 874. https://doi.org/10.3390/en9110874.

(245) Zhu, D.; Sun, Z.; Zhang, H.; Zhang, A.; Zhang, Y.; Miruka, A. C.; Zhu, L.; Li, R.; Guo, Y.; Liu, Y. Reactive Nitrogen Species Generated by Gas–Liquid Dielectric Barrier Discharge for Efficient Degradation of Perfluorooctanoic Acid from Water. *Environ. Sci. Technol.* **2022**, *56* (1), 349–360. https://doi.org/10.1021/acs.est.1c06342.

(246) Yi, R.; Yi, C.; Du, D.; Zhang, Q.; Yu, H.; Yang, L. Research on Quinoline Degradation in Drinking Water by a Large Volume Strong Ionization Dielectric Barrier Discharge Reaction System. *Plasma Sci. Technol.* **2021**, *23* (8), 085505.

(247) Haghighat, G.; Sohrabi, A.; Shaibani, P. M.; Van Neste, C. W.; Naicker, S.; Thundat, T. The Role of Chloride Ions in Plasma-Activated Water Treatment Processes. *Environ. Sci. Water Res. Technol.* **2017**, *3* (1), 156–168. https://doi.org/10.1039/c6ew00308g.

(248) Wang, L. Aqueous Organic Dye Discoloration Induced by Contact Glow Discharge Electrolysis. *J. Hazard. Mater.* **2009**, *171* (1–3), 577–581. https://doi.org/10.1016/j.jhazmat.2009.06.037.

(249) Wang, L.; Jiang, X.; Liu, Y. Degradation of Bisphenol A and Formation of Hydrogen Peroxide Induced by Glow Discharge Plasma in Aqueous Solutions. *J. Hazard. Mater.* **2008**, *154* (1–3), 1106–1114. https://doi.org/10.1016/j.jhazmat.2007.11.016.

(250) Jirásek, V.; Lukeš, P. Formation of Reactive Chlorine Species in Saline Solution Treated by Non-Equilibrium Atmospheric Pressure He/O2 Plasma Jet. *Plasma Sources Sci. Technol.* **2019**, *28* (3). https://doi.org/10.1088/1361-6595/ab0930.

(251) Jirásek, V.; Lukeš, P. Competitive Reactions in Cl− Solutions Treated by Plasma-Supplied O Atoms. *J. Phys. D. Appl. Phys.* **2020**, *53*, 505206. https://doi.org/10.1088/1361-6463/abb5d6.

(252) Gorbanev, Y.; Van Der Paal, J.; Van Boxem, W.; Dewilde, S.; Bogaerts, A. Reaction of Chloride Anion with Atomic Oxygen in Aqueous Solutions: Can Cold Plasma Help in Chemistry Research? *Phys. Chem. Chem. Phys.* **2019**, *21* (8), 4117–4121. https://doi.org/10.1039/c8cp07550f.

(253) Magazinovic, R. S.; Nicholson, B. C.; Mulcahy, D. E.; Davey, D. E. Bromide Levels in Natural Waters: Its Relationship to Levels of Both Chloride and Total Dissolved Solids and the Implications for Water Treatment. *Chemosphere* **2004**, *57* (4), 329–335. https://doi.org/10.1016/j.chemosphere.2004.04.056.

(254) Justo, A.; González, O.; Aceña, J.; Pérez, S.; Barceló, D.; Sans, C.; Esplugas, S. Pharmaceuticals and Organic Pollution Mitigation in Reclamation Osmosis Brines by UV/H_2O_2 and Ozone. *J. Hazard. Mater.* **2013**, *263*, 268–274. https://doi.org/10.1016/j.jhazmat.2013.05.030.

(255) Westerhoff, P.; Chao, P.; Mash, H. Reactivity of Natural Organic Matter with Aqueous Chlorine and Bromine. *Water Res.* **2004**, *38* (6), 1502–1513. https://doi.org/10.1016/j.watres.2003.12.014.

(256) Zeng, T.; Wilson, C. J.; Mitch, W. A. Effect of Chemical Oxidation on the Sorption Tendency of Dissolved Organic Matter to a Model Hydrophobic Surface. *Environ. Sci. Technol.* **2014**, *48* (9), 5118–5126. https://doi.org/10.1021/es405257b.

(257) Sun, B.; Sato, M.; Clements, J. S. Optical Study of Active Species Produced by a Pulsed Streamer Corona Discharge in Water. *J. Electrostat.* **1997**, *39* (3), 189–202. https://doi.org/10.1016/S0304-3886(97)00002-8.

(258) Clifford, D.; Liu, X. Biological Denitrification of Spent Regenerant Brine Using a Sequencing Batch Reactor. *Water Res.* **1993**, *27* (9), 1477–1484. https://doi.org/10.1016/0043-1354(93)90028-G.

(259) Haddad, M.; Bazinet, L.; Barbeau, B. Eco-Efficient Treatment of Ion Exchange Spent Brine via Electrodialysis to Recover NaCl and Minimize Waste Disposal. *Sci. Total Environ.* **2019**, *690*, 400–409. https://doi.org/10.1016/j.scitotenv.2019.06.539.

(260) Haddad, M.; Bazinet, L.; Barbeau, B. Towards Water, Sodium Chloride and Natural Organic Matter Recovery from Ion Exchange Spent Brine. *Membranes (Basel).* **2021**, *11* (4), 1–13. https://doi.org/10.3390/membranes11040262.

(261) Hiremath, T.; Roberts, D. J.; Lin, X.; Clifford, D. A.; Gillogly, T. E. T.; Lehman, S. G. Biological Treatment of Perchlorate in Spent ISEP Ion-Exchange Brine. *Environ. Eng.*

Sci. **2006**, *23* (6), 1009–1016. https://doi.org/10.1089/ees.2006.23.1009.

(262) Homan, N. P.; Green, P. G.; Young, T. M. Evaluating Ferrous Chloride for Removal of Chromium From Ion-Exchange Waste Brines. *J. Am. Water Works Assoc.* **2018**, *110* (4), E43–E54. https://doi.org/10.5942/jawwa.2018.110.0022.

(263) Hutchison, J. M.; Zilles, J. L. Biocatalytic Removal of Perchlorate and Nitrate in Ion-Exchange Waste Brine. *Environ. Sci. Water Res. Technol.* **2018**, *4* (8), 1181–1189. https://doi.org/10.1039/c8ew00178b.

(264) Korak, J. A.; Huggins, R. G.; Arias-Paić, M. S. Nanofiltration to Improve Process Efficiency of Hexavalent Chromium Treatment Using Ion Exchange. *J. Am. Water Works Assoc.* **2018**, *110* (6), E13–E26. https://doi.org/10.1002/awwa.1051.

(265) Leong, J.; Tan, J.; Heitz, A.; Ladewig, B. P. Performance of a Vibratory Shear Membrane Filtration System during the Treatment of Magnetic Ion Exchange Process Concentrate. *Desalination* **2015**, *365*, 196–203. https://doi.org/10.1016/j.desal.2015.02.042.

(266) Liu, J.; Choe, J. K.; Sasnow, Z.; Werth, C. J.; Strathmann, T. J. Application of a Re-Pd Bimetallic Catalyst for Treatment of Perchlorate in Waste Ion-Exchange Regenerant Brine. *Water Res.* **2013**, *47* (1), 91–101. https://doi.org/10.1016/j.watres.2012.09.031.

(267) McAdam, E. J.; Judd, S. J. Biological Treatment of Ion-Exchange Brine Regenerant for Re-Use: A Review. *Sep. Purif. Technol.* **2008**, *62* (2), 264–272. https://doi.org/10.1016/j.seppur.2008.01.007.

(268) Pakzadeh, B.; Batista, J. R. Chromium Removal from Ion-Exchange Waste Brines with Calcium Polysulfide. *Water Res.* **2011**, *45* (10), 3055–3064. https://doi.org/10.1016/j.watres.2011.03.006.

(269) Plummer, S.; Gorman, C.; Henrie, T.; Shimabuku, K.; Thompson, R.; Seidel, C. Optimization of Strong-Base Anion Exchange OandM Costs for Hexavalent Chromium Treatment. *Water Res.* **2018**, *139*, 420–433. https://doi.org/10.1016/j.watres.2018.04.011.

(270) Schaefer, C. E.; Tran, D.; Fang, Y.; Choi, Y. J.; Higgins, C. P.; Strathmann, T. J. Electrochemical Treatment of Poly- and Perfluoroalkyl Substances in Brines. *Environ. Sci. Water Res. Technol.* **2020**, *6* (10), 2704–2712. https://doi.org/10.1039/d0ew00377h.

(271) Vaudevire, E.; Radmanesh, F.; Kolkman, A.; Vughs, D.; Cornelissen, E.; Post, J.; van der Meer, W. Fate and Removal of Trace Pollutants from an Anion Exchange Spent Brine during the Recovery Process of Natural Organic Matter and Salts. *Water Res.* **2019**, *154*, 34–44. https://doi.org/10.1016/j.watres.2019.01.042.

(272) Yang, T.; Doudrick, K.; Westerhoff, P. Photocatalytic Reduction of Nitrate Using Titanium Dioxide for Regeneration of Ion Exchange Brine. *Water Res.* **2013**, *47* (3), 1299–1307. https://doi.org/10.1016/j.watres.2012.11.047.

(273) Hajbi, F.; Hammi, H.; M'Nif, A. Reuse of RO Desalination Plant Reject Brine. *J. Phase Equilibria Diffus.* **2010**, *31* (4), 341–347. https://doi.org/10.1007/s11669-010-9727-3.

(274) Ji, X.; Curcio, E.; Al Obaidani, S.; Di Profio, G.; Fontananova, E.; Drioli, E. Membrane Distillation-Crystallization of Seawater Reverse Osmosis Brines. *Sep. Purif. Technol.* **2010**, *71* (1), 76–82. https://doi.org/10.1016/j.seppur.2009.11.004.

(275) Lior, N.; Kim, D. Quantitative Sustainability Analysis of Water Desalination – A Didactic Example for Reverse Osmosis. *Desalination* **2018**, *431* (December 2017), 157–170. https://doi.org/10.1016/j.desal.2017.12.061.

(276) Opong, R. W.; Nsiah-Baafi, E.; Andrews, A.; Koomson, B. Preliminary Study on the Use of Reverse Osmosis Brine and Mine Tailings as Cement Paste Mixtures for Mine Backfilling Application. *Water. Air. Soil Pollut.* **2022**, *233* (12), 1–15. https://doi.org/10.1007/s11270-022-05959-1.

(277) Walker, W. S.; Kim, Y.; Lawler, D. F. Treatment of Model Inland Brackish Groundwater Reverse Osmosis Concentrate with Electrodialysis - Part II: Sensitivity to Voltage Application and Membranes. *Desalination* **2014**, *345*, 128–135. https://doi.org/10.1016/j.desal.2014.04.026.

(278) Eeso, K. Non-Thermal Plasma Degradation of Per- and Polyfluoroalkyl Substances from Landfill Leachate. **2022**.

(279) Ma, X.; Li, M.; Feng, C.; He, Z. Electrochemical Nitrate Removal with Simultaneous Magnesium Recovery from a Mimicked RO Brine Assisted by in Situ Chloride Ions. *J. Hazard. Mater.* **2020**, *388* (January), 122085. https://doi.org/10.1016/j.jhazmat.2020.122085.

(280) An, B.; Steinwinder, T. R.; Zhao, D. Selective Removal of Arsenate from Drinking Water Using a Polymeric Ligand Exchanger. *Water Res.* **2005**, *39* (20), 4993–5004. https://doi.org/10.1016/j.watres.2005.10.014.

(281) An, B.; Liang, Q.; Zhao, D. Removal of Arsenic(V) from Spent Ion Exchange Brine Using a New Class of Starch-Bridged Magnetite Nanoparticles. *Water Res.* **2011**, *45* (5), 1961–1972. https://doi.org/10.1016/j.watres.2011.01.004.

(282) Arias-Paić, M. S.; Korak, J. A. Forward Osmosis for Ion Exchange Waste Brine Management. *Environ. Sci. Technol. Lett.* **2020**, *7* (2), 111–117. https://doi.org/10.1021/acs.estlett.9b00733.

(283) Bergquist, A. M.; Choe, J. K.; Strathmann, T. J.; Werth, C. J. Evaluation of a Hybrid Ion Exchange-Catalyst Treatment Technology for Nitrate Removal from Drinking Water. *Water Res.* **2016**, *96*, 177–187. https://doi.org/10.1016/j.watres.2016.03.054.

(284) De Geyter, N.; Morent, R.; Leys, C.; Gengembre, L.; Payen, E. Treatment of Polymer Films with a Dielectric Barrier Discharge in Air, Helium and Argon at Medium Pressure. *Surf. Coatings Technol.* **2007**, *201* (16–17), 7066–7075. https://doi.org/10.1016/j.surfcoat.2007.01.008.

(285) Jiang, J.; Han, J.; Zhang, X. Nonhalogenated Aromatic DBPs in Drinking Water Chlorination: A Gap between NOM and Halogenated Aromatic DBPs. *Environ. Sci. Technol.* **2020**, *54* (3), 1646–1656. https://doi.org/10.1021/acs.est.9b06403.

(286) Lei, Y.; Lei, X.; Yu, Y.; Li, K.; Li, Z.; Cheng, S.; Ouyang, G.; Yang, X. Rate Constants and Mechanisms for Reactions of Bromine Radicals with Trace Organic Contaminants. *Environ. Sci. Technol.* **2021**, *55* (15), 10502–10513. https://doi.org/10.1021/acs.est.1c02313.

(287) Heeb, M. B.; Criquet, J.; Zimmermann-Steffens, S. G.; Von Gunten, U. Oxidative

Treatment of Bromide-Containing Waters: Formation of Bromine and Its Reactions with Inorganic and Organic Compounds - A Critical Review. *Water Res.* **2014**, *48* (1), 15–42. https://doi.org/10.1016/j.watres.2013.08.030.

(288) Lei, Y.; Cheng, S.; Luo, N.; Yang, X.; An, T. Rate Constants and Mechanisms of the Reactions of $Cl^{\bullet}$ and $Cl_2^{\bullet-}$ with Trace Organic Contaminants. *Environ. Sci. Technol.* **2019**, *53* (19), 11170-11182. https://doi.org/10.1021/acs.est.9b02462.

(289) Barazesh, J. M.; Prasse, C.; Sedlak, D. L. Electrochemical Transformation of Trace Organic Contaminants in the Presence of Halide and Carbonate Ions. *Environ. Sci. Technol.* **2016**, *50* (18), 10143–10152. https://doi.org/10.1021/acs.est.6b02232.

(290) Mertens, R.; von Sonntag, C. Photolysis (λ=254 nm) of Tetrachloroethene in Aqueous Solutions. *J. Photochem. Photobiol. A Chem.* **1995**, *85* (1–2), 1–9. https://doi.org/10.1016/1010-6030(94)03903-8.

(291) Huie, R. E.; Clifton, C. L.; Neta, P. Electron Trasnfer Reaction Rates and Equilibria of the Carbonate and Sulfate Radical Anions. *Radiat. Phys. Chem. Int. J. Radiat. Appl. lnstrum., Part C* **1991**, *38* (5), 477–481.

(292) Jiang, P.-Y.; Katsumura, Y.; Nagaishi, R.; Domae, M.; Ishikawa, K.; Ishigure, K.; Yoshia, Y. Pulse Radiolysis Study of Concentrated Sufiric Acid Solutions. *J. Chem. Soc. Faraday Trans.* **1992**, *88* (22), 3319–3322. https://doi.org/10.1039/FT9928803319.

(293) Katsumura, Y.; Jiang, P. Y.; Nagaishi, R.; Oishi, T.; Ishigure, K.; Yoshida, Y. Pulse Radiolysis Study of Aqueous Nitric Acid Solutions. Formation Mechanism, Yield, and Reactivity of NO3 Radical. *J. Phys. Chem.* **1991**, *95* (11), 4435–4439. https://doi.org/10.1021/j100164a050.

(294) Buxton, G. V.; Elliot, A. J. Rate Constant for Reaction of Hydroxyl Radicals with Bicarbonate Ions. *Int. J. Radiat. Appl. Instrumentation. Part* **1986**, *27* (3), 241–243. https://doi.org/10.1016/1359-0197(86)90059-7.

(295) Westerhoff, P.; Mezyk, S. P.; Cooper, W. J.; Minakata, D. Electron Pulse Radiolysis Determination of Hydroxyl Radical Rate Constants with Suwannee River Fulvic Acid and Other Dissolved Organic Matter Isolates. *Environ. Sci. Technol.* **2007**, *41* (13), 4640–4646. https://doi.org/10.1021/es062529n.

(296) Chen, R.; Avotinsh, Y.; Freenman, G. R. Solvent Effects on Reactivity of Solvated Electrons with Ions in Isobutanol/Water Mixed Solvents. *Can. J. Chem.* **1994**, *72* (4), 1083–1093. https://doi.org/10.1016/j.jiec.2008.03.002.

(297) Thomas, J. K.; Gordon, S.; Hart, E. J. The Rates of Reaction of the Hydrated Electron in Aqueous Inorganic Solutions. *J. Phys. Chem.* **1964**, *68* (6), 1524–1527. https://doi.org/10.1021/j100788a043.

(298) Nash, K.; Mulac, W.; Noon, M.; Fried, S.; Sullivan, J. C. Pulse Radiolysis Studies of U(VI) Complexes in Aqueous Media. *J. Inorg. Nucl. Chem.* **1981**, *43* (5), 897–899. https://doi.org/10.1016/0022-1902(81)80146-7.

(299) Huang, Y. C.; Rao, A.; Huang, S. J.; Chang, C. Y.; Drechsler, M.; Knaus, J.; Chan, J. C. C.; Raiteri, P.; Gale, J. D.; Gebauer, D. Uncovering the Role of Bicarbonate in Calcium Carbonate Formation at Near-Neutral PH. *Angew. Chemie - Int. Ed.* **2021**, *60* (30), 16707–

16713. https://doi.org/10.1002/anie.202104002.

(300) Van Driessche, A. E. S.; Stawski, T. M.; Kellermeier, M. Calcium Sulfate Precipitation Pathways in Natural and Engineered Environments. *Chem. Geol.* **2019**, *530* (August), 119274. https://doi.org/10.1016/j.chemgeo.2019.119274.

(301) Case, D. H.; Wang, F.; Giammar, D. E. Precipitation of Magnesium Carbonates as a Function of Temperature, Solution Composition, and Presence of a Silicate Mineral Substrate. *Environ. Eng. Sci.* **2011**, *28* (12), 881–889. https://doi.org/10.1089/ees.2010.0341.

(302) American Public Health Association. *Standard Methods for the Examination of Water and Wastewater*; 1998.

(303) Pearse, R. W. B.; Gaydon, A. G. *The Identification of Molecular Spectra*; London Chapman & Hall LTD, 1941.

(304) NIST Physical Meas. Laboratory. Nist Atomic Spectra Database Lines Data https://physics.nist.gov/PhysRefData/ASD/lines_form.html.

(305) Hong, Y. J.; Nam, C. J.; Song, K. B.; Cho, G. S.; Uhm, H. S.; Choi, D. I.; Choi, E. H. Measurement of Hydroxyl Radical Density Generated from the Atmospheric Pressure Bioplasma Jet. *J. Instrum.* **2012**, *7* (3). https://doi.org/10.1088/1748-0221/7/03/C03046.

(306) Zhang, D. J.; Cai, Y.; Chen, M. L.; Yu, Y. L.; Wang, J. H. Dielectric Barrier Discharge-Optical Emission Spectrometry for the Simultaneous Determination of Halogens. *J. Anal. At. Spectrom.* **2016**, *31* (2), 398–405. https://doi.org/10.1039/c5ja00266d.

(307) Ashton, L.; Buxton, G. V.; Stuart, C. R. Temperature Dependence of the Rate of Reaction of OH with Some Aromatic Compounds in Aqueous Solution Evidence for the Formation of a Pi-Complex Intermediate? *J. Chem. Soc. Faraday Trans.* **1995**, *91* (11), 1631–1633. https://doi.org/10.1016/s0082-0784(00)80664-5.

(308) Anderson, R. F.; Patel, K. B.; Stratford, M. R. L. Radical Spectra and Product Distribution Following Electrophilic Attack by the OH. Radical on 4-Hydroxybenzoic Acid and Subsequent Oxidation. *J. Chem. Soc. Faraday Trans. 1 Phys. Chem. Condens. Phases* **1987**, *83* (10), 3177–3187. https://doi.org/10.1039/F19878303177.

(309) Anbar, M.; Alfassi, Z. B.; Bregman-Reisler, H. Hydrated Electron Reactions in View of Their Temperature Dependence. *J. Am. Chem. Soc.* **1967**, *89* (5), 1263–1264.

(310) Li, Y.; Song, W.; Fu, W.; Tsang, D. C. W.; Yang, X. The Roles of Halides in the Acetaminophen Degradation by UV/H_2O_2 Treatment: Kinetics, Mechanisms, and Products Analysis. *Chem. Eng. J.* **2015**, *271*, 214–222. https://doi.org/10.1016/j.cej.2015.02.090.

(311) Rebenne, L. M.; Gonzalez, A. C.; Olson, T. M. Aqueous Chlorination Kinetics and Mechanism of Substituted Dihydroxybenzenes. *Environ. Sci. Technol.* **1996**, *30* (7), 2235–2242. https://doi.org/10.1021/es950607t.

(312) Korshin, G. V. Chlorine Based Oxidants for Water Purification and Disinfection. In *Aquatic Redox Chemistry*; 2011; Vol. 1071, pp 223–245. https://doi.org/10.1021/bk-2011-1071.ch011.

(313) Liu, T.; Xiao, S.; Li, N.; Chen, J.; Xu, Y.; Yin, W.; Zhou, X.; Huang, C. H.; Zhang, Y.

Selective Transformation of Micropollutants in Saline Wastewater by Peracetic Acid: The Overlooked Brominating Agents. *Environ. Sci. Technol.* **2023**. https://doi.org/10.1021/acs.est.3c00835.

(314) Zhang, B.; Fang, Z.; Wang, S.; Shi, X.; Guo, B.; Gao, J.; Wang, D.; Zong, W. Effect of Bromide on Molecular Transformation of Dissolved Effluent Organic Matter during Ozonation, UV/H_2O_2, UV/Persulfate, and UV/Chlorine Treatments. *Sci. Total Environ.* **2022**, *811*, 152328. https://doi.org/10.1016/j.scitotenv.2021.152328.

(315) Shu, Z.; Wang, J.; Liu, H.; Liu, C. Improvement of Bromide Ions on the Degradation of Sulfamerazine by Horseradish Peroxidase-H_2O_2 System and Its Interaction Mechanisms. *Chem. Eng. J.* **2022**, *428* (April 2021), 131132. https://doi.org/10.1016/j.cej.2021.131132.

(316) Oum, K. W.; Lakin, M. J.; DeHaan, D. O.; Brauers, T.; Finlayson-Pitts, B. J. Formation of Molecular Chlorine from the Photolysis of Ozone and Aqueous Sea-Salt Particles. *Science* **1998**, *279* (5347), 74–77. https://doi.org/10.1126/science.279.5347.74.

(317) George, I. J.; Abbatt, J. P. D. Heterogeneous Oxidation of Atmospheric Aerosol Particles by Gas-Phase Radicals. *Nat. Chem.* **2010**, *2* (9), 713–722. https://doi.org/10.1038/nchem.806.

(318) Enami, S.; Hoffmann, M. R.; Colussi, A. J. Halogen Radical Chemistry at Aqueous Interfaces. *J. Phys. Chem. A* **2016**, *120* (31), 6242–6248. https://doi.org/10.1021/acs.jpca.6b04219.

(319) Amphlett, C. B.; Adams, G. E.; Michael, B. D. Pulse Radiolysis Studies of Deaerated Aqeuous Salicylate Solutions. In *Radiation Chemistry*; 1968; pp 231–250. https://doi.org/10.1021/ba-1968-0081.ch016.

(320) Bisby, R. H.; Tabassum, N. Properties of the Radicals Formed by One-Electron Oxidation of Acetaminophen-A Pulse Radiolysis Study. *Biochem. Pharmacol.* **1988**, *37* (14), 2731–2738. https://doi.org/10.1016/0006-2952(88)90035-4.

(321) Mezyk, S. P.; Neubauer, T. J.; Cooper, W. J.; Peller, J. R. Free-Radical-Induced Oxidative and Reductive Degradation of Sulfa Drugs in Water: Absolute Kinetics and Efficiencies of Hydroxyl Radical and Hydrated Electron Reactions. *J. Phys. Chem. A* **2007**, *111* (37), 9019–9024. https://doi.org/10.1021/jp073990k.

(322) Prutz, W. A.; Land, E. J. Chemiluminescent Reactions after Pulse Radiolysis of Aqeuous Dye Solutions. Absolute Yields. *J. Phys. Chem.* **1974**, *78* (13), 1251–1253.

(323) Wojnárovits, L.; Tóth, T.; Takács, E. Rate Constants of Carbonate Radical Anion Reactions with Molecules of Environmental Interest in Aqueous Solution: A Review. *Sci. Total Environ.* **2020**, *717*. https://doi.org/10.1016/j.scitotenv.2020.137219.

(324) Olszowy, H. A.; Rossiter, J.; Hegarty, J.; Geoghegan, P.; Haswell-Elkins, M. Background Levels of Bromide in Human Blood. *J. Anal. Toxicol.* **1998**, *22* (3), 225–230. https://doi.org/10.1093/jat/22.3.225.

(325) Kaushik, N.; Lee, S. J.; Choi, T. G.; Baik, K. Y.; Uhm, H. S.; Kim, C. H.; Kaushik, N. K.; Choi, E. H. Non-Thermal Plasma with 2-Deoxy-D-Glucose Synergistically Induces Cell Death by Targeting Glycolysis in Blood Cancer Cells. *Sci. Rep.* **2015**, *5*, 1–11. https://doi.org/10.1038/srep08726.

(326) Scholtz, V.; Pazlarova, J.; Souskova, H.; Khun, J.; Julak, J. Nonthermal Plasma - A Tool for Decontamination and Disinfection. *Biotechnol. Adv.* **2015**, *33* (6), 1108–1119. https://doi.org/10.1016/j.biotechadv.2015.01.002.

(327) Guesmi, A.; Cherif, M. M.; Baaloudj, O.; Kenfoud, H.; Badawi, A. K.; Elfalleh, W.; Hamadi, N. Ben; Khezami, L.; Assadi, A. A. Disinfection of Corona and Myriad Viruses in Water by Non-Thermal Plasma: A Review. *Environ. Sci. Pollut. Res.* **2022**, *29* (37), 55321–55335. https://doi.org/10.1007/s11356-022-21160-7.

(328) Patange, A.; Boehm, D.; Giltrap, M.; Lu, P.; Cullen, P. J.; Bourke, P. Assessment of the Disinfection Capacity and Eco-Toxicological Impact of Atmospheric Cold Plasma for Treatment of Food Industry Effluents. *Sci. Total Environ.* **2018**, *631–632*, 298–307. https://doi.org/10.1016/j.scitotenv.2018.02.269.

(329) Hua, G.; Reckhow, D. A. Evaluation of Bromine Substitution Factors of DBPs during Chlorination and Chloramination. *Water Res.* **2012**, *46* (13), 4208–4216. https://doi.org/10.1016/j.watres.2012.05.031.

(330) Silvio, C.; Kohn, T.; Mac, M.; Real, F. J.; Wirz, J.; Gunten, U. von. Photosensitizer Method to Determine Rate Constants for the Reaction of Carbonate Radical with Organic Compounds. *Environ. Sci. Technol.* **2005**, *39* (23), 9182–9188. https://doi.org/10.1021/es051236b.

(331) Bolton, J. R.; Bircher, K. G.; Tumas, W.; Tolman, C. A. Figures-of-Merit for the Technical Development and Application of Advanced Oxidation Technologies for Both Electric- and Solar-Driven Systems. *Pure Appl. Chem.* **2001**, *73* (4), 627–637. https://doi.org/10.1351/pac200173040627.